Advances in Colloid and Interface Science 314 (2023) 102864

Contents lists available at ScienceDirect

Advances in Colloid and Interface Science

journal homepage: www.elsevier.com/locate/cis

Historical Perspective

Morphology control through the synthesis of metal-organic frameworks

Justyna Łuczak [a], Malwina Kroczewska [a], Mateusz Baluk [b], Jakub Sowik [b], Paweł Mazierski [b], Adriana Zaleska-Medynska [b,*]

[a] Department of Process Engineering and Chemical Technology, Faculty of Chemistry, Gdańsk University of Technology, 80-233 Gdańsk, Poland
[b] Faculty of Chemistry, University of Gdańsk, Wita Stwosza 63, 80-308 Gdansk, Poland

ARTICLE INFO

Keywords:
Metal-organic frameworks
Morphology control
Modulators
Coordination modulation
Deprotonation
Surfactants adsorption
Reaction conditions
pH
Temperature
Solvent

ABSTRACT

Designable morphology and predictable properties are the most challenging goals in material engineering. Features such as shape, size, porosity, agglomeration ratio significantly affect the final properties of metal-organic frameworks (MOFs) and can be regulated throughout synthesis parameters but require a deep understanding of the mechanisms of MOFs formation. Herein, we systematically summarize the effects of the individual synthesis factors, such as pH of reaction mixture, including acidic or basic character of modulators, temperature, solvents types, surfactants type and content and ionic liquids on the morphology of growing MOFs. We identified main mechanisms of MOFs' growth leading to different morphology of final particles and next systematically discuss the effect of miscellaneous parameters on MOFs morphology based on the main mechanisms related to the nucleation, growth and formation of final MOFs structure, including coordination modulation, protonation/deprotonation acting and modulation by surfactants or capping agents. The effect of microwaves and ultrasound employment during synthesis is also considered due to their affecting especially nucleation and particles growing steps during MOFs formation.

1. Introduction and scope

Constructed of inorganic and organic components, metal-organic frameworks (MOF) form interesting porous crystalline hybrid materials. Polydenate organic linkers such as carboxylates, phosphates, pyrazolates, tetrazolates, catecholates, and imidazolates have been used to stitch inorganic building units together into extended framework structures [1]. MOFs linked by carboxylate functionalities comprise by far the largest group. Nevertheless, the great diversity of building blocks can provide an infinite number of two- or three-dimensional organic-inorganic hybrids. In 2017, approximately 70,000 MOF materials were identified using the Cambridge Crystallographic Data Centre (CCDC) [2]. In such structures, organic linkers form a support for metallic nodes (commonly referred to as secondary building units, SBUs) providing free voids easily created due to the rigidity and directionality of the components. Such porous constructions can be also further post-synthetically modified, adding new functionalities to the material.

Up today numerous MOF structures have been developed including highly ordered structures with densities as low as 0.13 g/cm^3, pore volumes up to 90% free volume, and Brunauer-Emmett-Teller (BET) surface area even 6240 and 7800 m^2/g for MOF-210 and DUT-60, respectively [3–5]. Adjustable composition is also an advantageous feature. Selection of constituents for the reticular synthesis provides products with high thermal (even 600 °C) [6] and chemical stability. The accessibility of the voids to guest molecules has led to tremendous scientific interest in MOFs due to their commercial utility in gas adsorption [7,8], catalysis [9,10], photocatalysis [11,12], separation [13,14], sensing [15,16], light harvesting and energy conversion [17,18] and drug delivery [19,20] *etc*.

One of the strategic goals in materials engineering is to synthesize materials with predictable morphologies and valuable properties. Although plenty of reports described the preparation of MOFs with a variety of compositions, there are fewer syntheses that are focused on the morphology control of MOFs exclusively. It is difficult to predict the shape and size of MOFs in the form of nanomaterials, even if the structure of a single MOF unit can be predicted, especially when one MOF structure can crystallize in many different ways. The ability to accurately control their shape, dimensions and porosity is highly required in developing and applying MOFs for specific applications.

Metal–organic frameworks may exist in several morphologically distinct forms. IUPAC defines morphology as "shape, optical appearance, or form of phase domains in substances, such as high polymers,

* Corresponding author.
E-mail address: adriana.zaleska-medynska@ug.edu.pl (A. Zaleska-Medynska).

https://doi.org/10.1016/j.cis.2023.102864
Received in revised form 20 February 2023;
Available online 26 February 2023

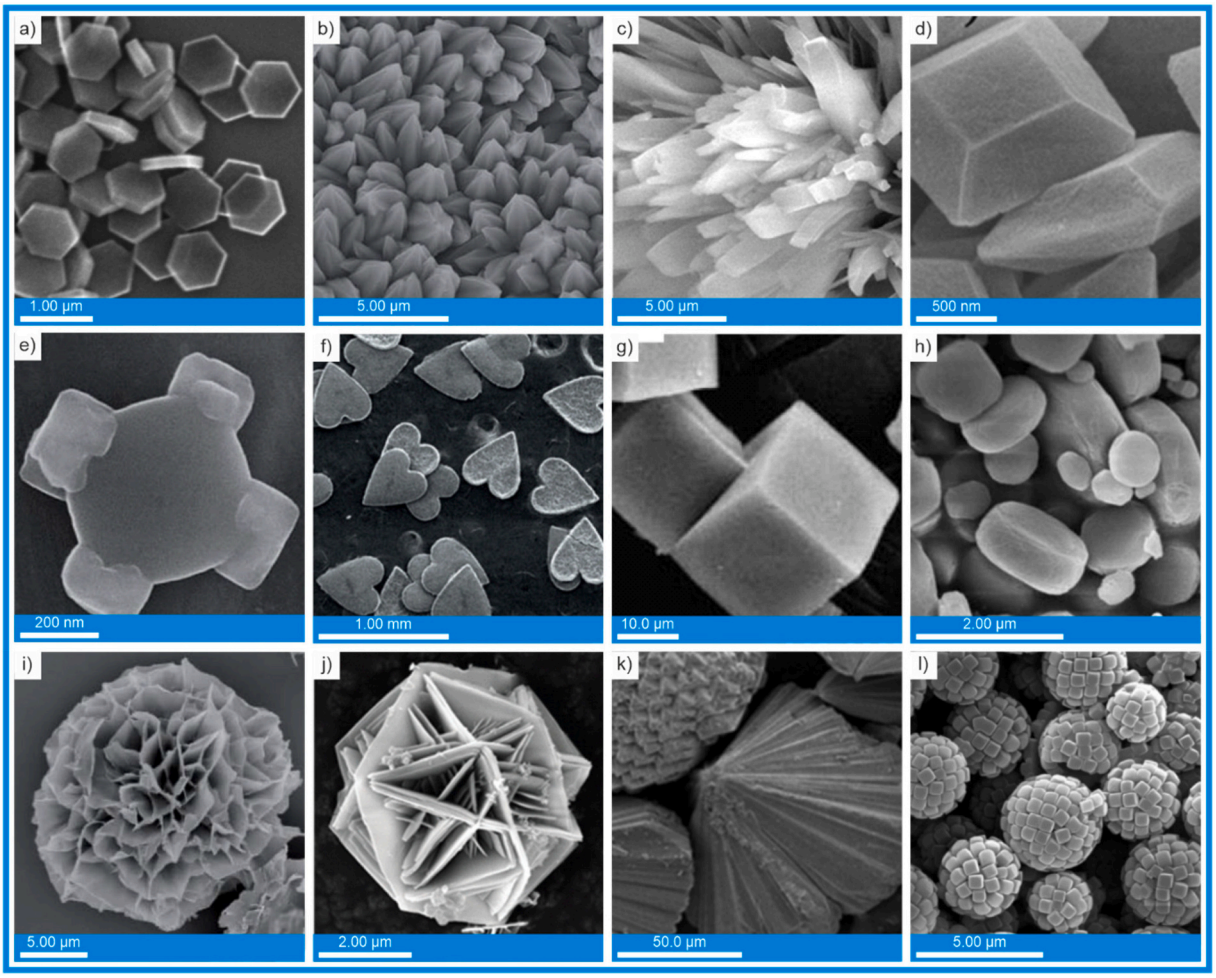

Fig. 1. Examples of MOF's morphologies: a) hexagonal nanodisks of $Ni_2(BDC)_2(DABCO)$ [24]; b) cone-like one-dimensional structure of Ni-MOF-74@CNTF [25]; c) sphere-organized rods of MIL-91(Ti) [26]; d) square disk-shaped NH_2-MIL-125 [27]; e) cake-like MIL-125 with epitaxially grown cubes of ZIF-8 [28]; f) heart-shaped HKUST-1 superstructure [29]; g) cubes of MOF-5 [30]; h) puck-shaped MIL-125 [31]; i) flower-like structure of Cu-TCPP [32]; j) interlaced structure of edba-MOF 4 [33]; k) Co-MOF-74 of bunched needle-like morphology [34]; l) Fe-soc-MOF hollow colloidosomes assembled from uniform cubes [35].

polymer blends, composites, and crystals" [21]. In this regard, the term morphology includes physical size, flatness, roundness, sphericity, appearance of fibers, aspect ratio of the particles, *etc*. Considering morphology, nanomaterials were classified as zero-dimensional (0D), one-dimensional (1D), two-dimensional (2D), and three-dimensional (3D) depending on their geometrical features [22]. Anisotropic nature of MOFs allows for controlled growth of specific crystal faces, which enables control of MOF crystal dimensions. To date, many structurally diverse MOFs have already been described in the literature, including spheres, cubes, cuboctahedra, octahedra, rods, filaments, sheets, and complicated hierarchical structures (e.g. flowers) [23], as shown in Fig. 1.

However, the syntheses are usually carried out by selecting specific building blocks aiming to obtain scaffold structures with unusually large surface areas or other specific properties. Therefore, these different shapes are usually random rather than planned. This is not surprising, as predicting the shape of a material is extremely difficult, as one MOF topology can crystallize into several different ones. The morphology control means a well-thought out strategy that accurately leads to a pre-selected MOF shape and size. In fact, achieving such control is extremely difficult, especially for complex structures. Therefore, the first step to control morphology is a thorough understanding of the chemical processes occurring at the molecular level.

The past decade have witnessed a huge growth in review papers approaching different aspects of MOFs, including structure and construction [36], general paths of fabrication [37], electronic structure [38], ferroelectro features [39], luminescent properties of MOFs [40], Brønsted acidity [41], proton conduction phenomena in MOFs [42], electroconductivity [43], interaction between water and MOFs [44], motion possibilities [45] and specific applications such as in biomedicine [46], as a materials used for capture, separation or degradation of molecules and toxic chemicals [14,47–51], photoswitch utilization [52], photoactivity [11,12,53] as well as, application in food industry [54]. Very recently the shaping of MOFs into monoliths as films, pellets, tablets, gels and honeycomb structure has been also recapitulated [55]. Nonetheless, previous papers did not address the problem of morphology control during synthesis. Thus, in the present review, we first introduce several different mechanisms for manipulating the morphology and next systematically discuss the effect of miscellaneous parameters on MOFs morphology. In addition, the basic concepts of MOF particles nucleation and growth are briefly summarized to better understand how these processes affect the size and morphology of MOF nanoparticles. While reviewing the literature, we found that the most important synthesis parameters influencing the morphology of MOFs are: acidic or basic character of modulators, temperature, solvents, surfactants and ionic liquids and the effect of those parameters is discussed in separate sections. We also found that application of microwaves and ultrasound could affect MOFs morphology, therefore the enforcement of these factors is also considered by us.

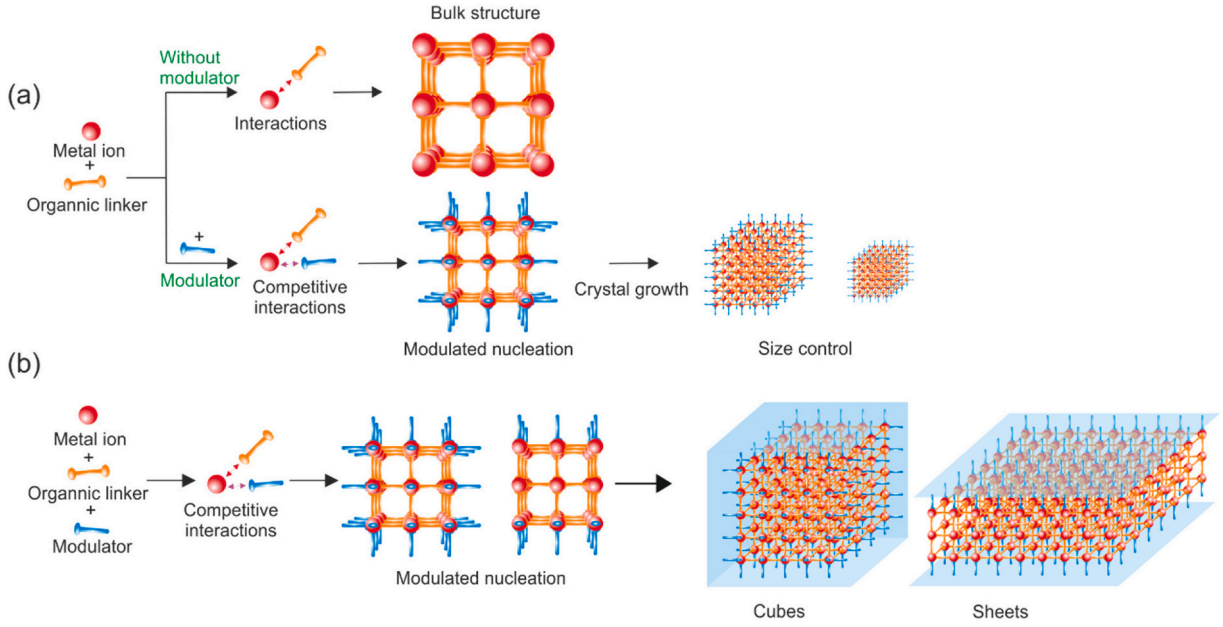

Fig. 2. Schematic showing the coordination modulation method used to obtain metal-organic frameworks. (a) Control of MOF's size and (b) morphology is usually achieved by adding a reagent with the same chemical functionality as the linker (Mechanism I).

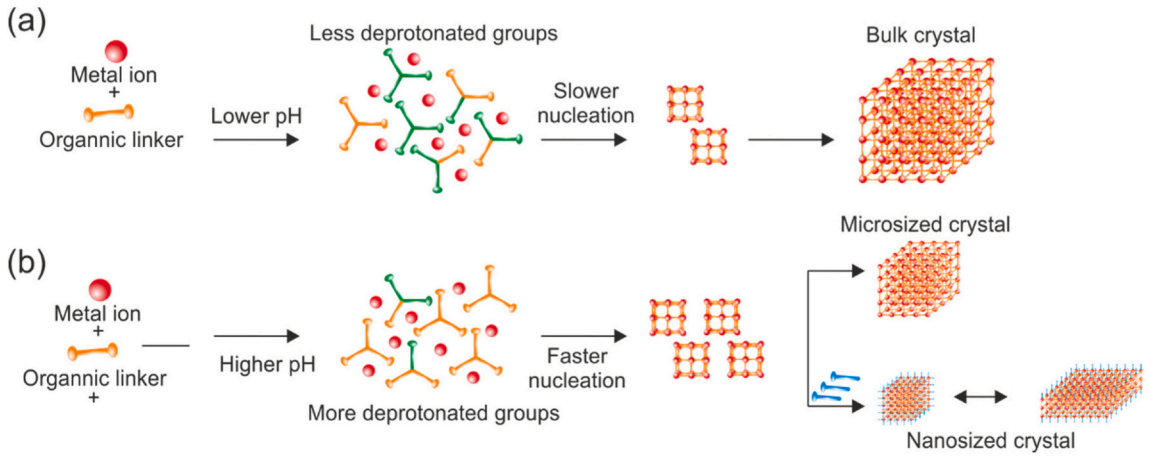

Fig. 3. Protonation/deprotonation mechanism used to control morphology of metal-organic frameworks (Mechanism II).

2. Mechanisms of achieving morphology control

MOFs structure could be received using a various range of preparation methods, but the most straightforward and widely used synthetic path is the solvothermal route, in which a metal precursor is mixed with an organic linker in a selected solvent and heated under specific conditions. Most of the structures presented and discussed in this review have been obtained using this approach. In addition to the nature of the precursors, various parameters can be selected/changed, including temperature and/or reaction time, type of solvent, concentration of reagents, pH, and type of modulators/additives [23]. Other commonly used synthetic routes include electrochemical, mechanochemical, sonochemical, and microwave assisted. For thin films of MOFs preparation, layer-by-layer deposition, liquid phase epitaxial growth, or seeded growth on a coated substrate were proposed [56].

A careful analysis of literature allowed us to distinguish that the achievement of morphology control can be described by a few main mechanisms. Among them, the most effective are:

(i) coordination modulation mechanism (known also as modulation of complex formation) – Mechanism I,
(ii) protonation/deprotonation mechanism (acid-base adjustment) – Mechanism II,
(iii) surfactants/capping agents' modulation – Mechanism III.

These approaches are directly related to the choice of: type of additives (capping agent/structuring agent/modulator), reaction conditions or type of solvent.

Mechanism I: The most popular approach to control the morphology of MOFs is the *coordination modulation method*, in which monodentate additives are used to modulate crystal growth by affecting the coordination equilibria between metal ions and organic linkers (Fig. 2). Modulators compete with the multidentate linkers for metal coordination sites during nucleation and crystal growth, thus regulating the rate of framework extension and crystal growth [57]. Competitive coordination of the modulating reagent can regulate (impede) the rate of crystal growth, allowing more nuclei to be formed [58]. In addition, modulators may also slow down the precipitation of amorphous material, thus improving the crystallinity of MOFs [57,59] and physically

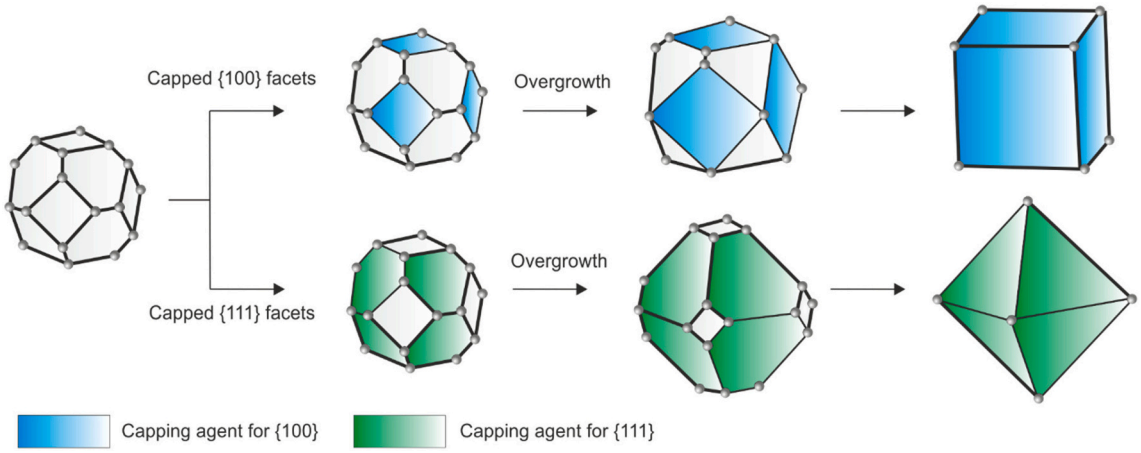

Fig. 4. Morphology control of metal-organic frameworks by adsorption of surfactants on specific facets (Mechanism III).

prevent crystal's aggregation, which leads to anisotropic growth [57]. This approach allows control over both the size (Fig. 2a) and morphology (Fig. 2b) of the resulting crystals. Consequently, smaller and relatively uniform nanoparticles with different shapes may be formed. Typically, the additive with the same chemical functionality as the linker is used to control the crystal size and morphology (e.g., monocarboxylic acids or salts) [58]. However, modulators with other functionalities were also used, such as triethylamine for carboxylate-based MOFs [60].

Mechanism II: Additives (also the same as mentioned above) can also determine the morphology of the final product by affecting the acid–base environment of the reaction system, thus *protonation/deprotonation* equilibria (Fig. 3). In this mechanism, the pH of the additive plays a key role; its structure is less important. Alkaline modulators increase the pH of the reaction system and facilitate linker deprotonation, providing more organic anions to coordinate the metal cation. These phenomena cause an acceleration of the crystal's nucleation rate. Consequently, the formation of smaller structures (even nanocrystals), sometimes with altered morphology, is possible, due to the rapid decrease of supersaturation of the reaction system [60]. Nevertheless, an adequate acid–base balance is essential to regulate the nucleation rate and to obtain a thermodynamically favored MOF single crystal.

Mechanism III: A particular type of additives used to modulate crystal morphology are surfactants. Adsorption of amphiphiles on crystal facets can play a key role in altering morphology and controlling particle size (Fig. 4). Depending on the affinity of the surfactant to a specific crystal facet (interaction energy), the adsorption of the additive is more or less pronounced. This causes the growth rate of one facet to accelerate and the growth rate of another facet to decelerate, making it more difficult or easier for reactants to attach to the surface. Thus, surfactant addition affects the shape and size distribution of the product. In addition, amphiphiles have the ability to aggregate in water and some other solvents to form a soft matrix for nanostructures.

Besides three mechanisms described above, the morphology of growing MOFs could be controlled by the way and form of energy supplied to the reaction system during synthesis, initiating reactions between components of the mixture. Energy could be provided to the reaction system as: (*i*) heat (gradually increasing the temperature of the reaction mixture); (*ii*) microwaves (temperature increase due to interaction of electromagnetic waves with polar solvent), or (iii) ultrasounds (locally increasing temperature and precure to extreme values) and amount/form of energy may affect the kinetics of MOFs' particles seeding and growing finally resulting in different size of MOFs particles and porosity. Control of particles size, porosity and surface imperfection (i.e. surface defects) regulated by kinetics of nucleation and growing process will be here described as Mechanism IV.

3. Bottom-up synthesis: mechanistic overview

The studies and thus understanding the MOFs crystallization, i.e., the formation of extended network structures from simple chemical precursors in solution, may provide many information on how to tune synthesis conditions to realize a particular design idea (polymorphic structure, topology, morphology, crystallinity, porosity, size).

According to the LaMer mechanism [61] (developed for solids), when combining dissolved reactants, it is necessary to supersaturate the solution until the critical concentration is achieved. On reaching this reproducible metastable condition, the system becomes heterogeneous due to a spontaneous nucleation of the product and the supersaturation partially relieves. Growth of the nuclei results in a further decrease of supersaturation of the solution to the value of equilibrium concentration. The process of nuclei growth to form discrete particles can proceed by diffusion of molecularly dissolved species to the nuclei. Smaller particles - due to their higher surface energy - exhibit greater solubility and deposit on the surface of the more energetically favored larger particles (Ostwald ripening [62]). The concentration of the dissolved material represents a balance between the rate of the material production by the chemical reaction and its removal from solution by diffusion to the nuclei.

The conventional description of nucleation is based on the classical theory of nucleation (CNT), which assumes, the spontaneous formation of stable crystal nuclei in the supersaturated solution, the size of which is increased by the attachment of single molecules and neglects collisions between two clusters [63]. However, theoretical calculations and experiments suggest that cluster-cluster interactions can have a significant effect on the nucleation process [64] and the nucleation rates are often many orders of magnitudes faster than those predicted by CNT. Therefore, nucleation of solids from solution often does not proceed classically, but follows more complex pathways.

Studies of the nucleation and growth of the MOF crystals still verify the widely accepted CNT model, according to which MOF crystals grow by adding monomers to spontaneously formed stable crystal nuclei. Most experimental studies show prenucleation of clusters/nanocrystals/species, which tends to confirm multi-step models [65]. According to them, ions in solution first form small clusters containing metals and linkers, which then aggregate into amorphous nanoparticles, followed by crystallization or crystallization is preceded by the formation of a metastable precursor [65].

An example of crystallization according to the CNT model may be HKUST-1, (Cu3(BTC)2, where BTC is benzene-1,3,5-tricarboxylate) which is mostly controlled by the formation of nucleation sites, rather than the diffusion of reactive species to sites or crystal growth itself at these sites [65] (slow nucleation and fast particle growth). The

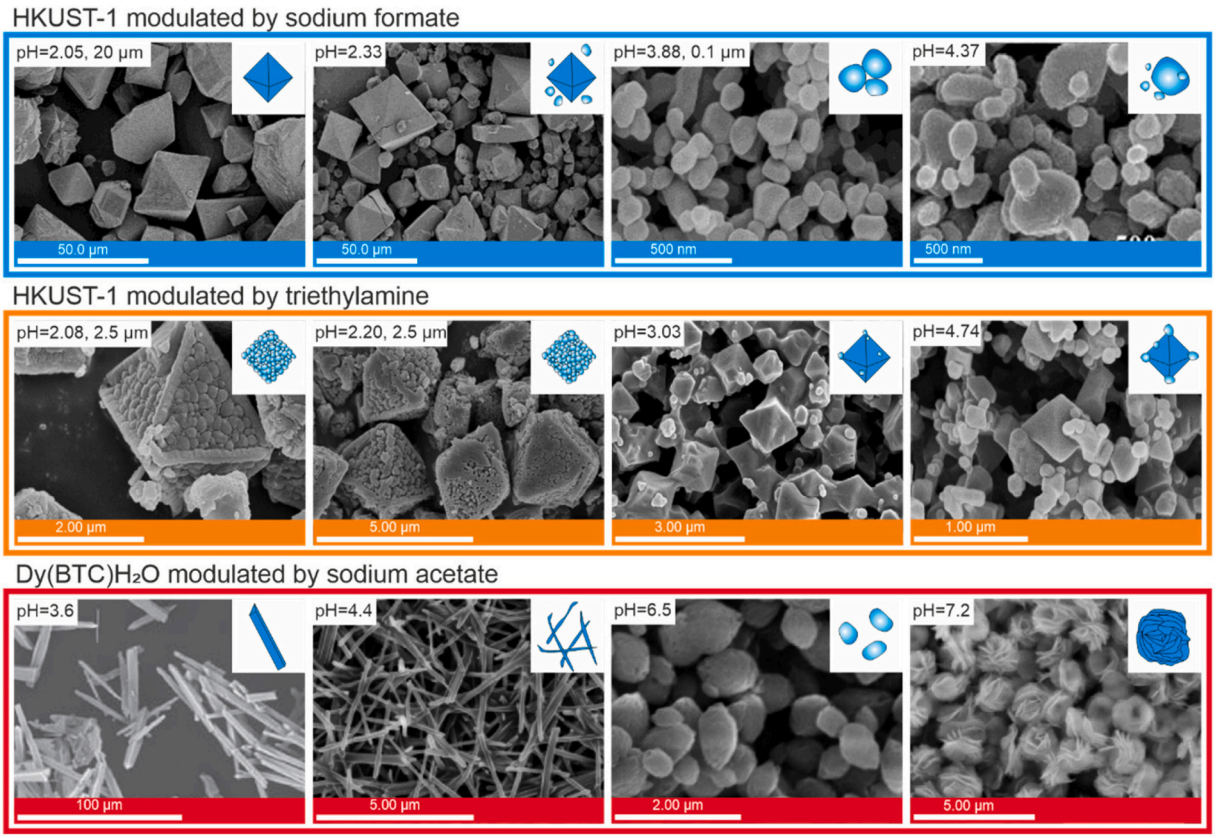

Fig. 5. Structures of HKUST-1 synthesized with different amounts of sodium formate and triethylamine (reproduced from [60]), first row from left: octahedrons, octahedrons, oval particles, oval particles; second row: octahedral crystals; SEM images of Dy(BTC)H_2O synthesized without and with different amounts of sodium acetate (reproduced from [58,59]) third row from left: pillar-like rods, rods, oval particles, rose-like structures.

formation of nucleation sites is immediate regardless of the temperature used [66]. By controlling the rate of nucleation and growth independently, the size of HKUST-1 crystals can be controlled. A higher feed rate of reactants during nucleation step increases the number of formed nuclei needed to reduce supersaturation to below critical degree of supersaturation for nucleation, thereby the average size of the product can be reduced. Increasing the reactant feed rate during the product growth stage can lead to "secondary nucleation," and may result in bimodal-sized products [67].

Multi-model crystallization was proposed for MIL-53 (Al^{3+}/BDC, where BDC is terephthalic acid), which was found to proceed by the appearance of a transient metastable crystalline MIL- 253 phase. Interestingly, the topology of MIL-235 is different of MIL-53, which may suggest that there is no conversion of one into the other only that the first phase dissolves, releasing reactive forms into solution to crystallize the final product [65]. On the other hand, the synthesis of MIL-89 (Cr^{3+} carboxylate), starts during the first hour by the formation a non-identified amorphous (or nano-crystalline) phase, and MIL-89 begin to appear only after 2 h [68]. For ZIF-8 Zn–2-MIM, where 2-MIM is 2-methylimidazole, the formation of clusters with a radius of about 1.1 nm was observed, and the first nanoparticles were detected after 15 s. The particles grow by attaching clusters or smaller particles [69]. Usage of direct time-resolved in situ TEM imaging allowed to distinguish three main steps of crystals formation in aqueous solution, i.e.: (*i*) phase separation (solute-rich and solute-poor regions), (*ii*) condensation of the solute-rich phases into dense aggregates, and (*iii*) crystallization of ZIF-8 nanocrystals [70]. For ZIF-71 ($Zn(DCIM)_2$, where DCIM is 4,5-dichloroimidazolate), even four step crystallization process was proposed: formation of small amorphous clusters by coagulation, growth of larger amorphous particles (via "monomer" addition), transformation into periodic structure of ZIF-71 (by reorganization of molecules) and aggregation of nanocrystals [71]. The works of Ferey *et al.* indicated that during Cr carboxylates synthesis in water SBUs form as a free species prior to MOF precipitation and crystallization, and can be retained during MOF synthesis. In case of Al carboxylates (MIL-96, MIL-100 and MIL-110) intermediate complexes called by Authors as PreNucleation Building Units (PNBU) were detected [68]. When the required concentration of zero charged PNBU is reached, nucleation occurs immediately.

4. Effect of various parameters on morphology of metal organic frameworks

4.1. Effect of pH of the reaction environment

MOFs morphology was mainly controlled by using alkaline modulators at different concentrations. Sodium formate [60], sodium acetate [60], triethylamine (TEA) [60], 1-methylimidazole [73], n-butylamine [73], pyridine [24,74], tetramethylammonium hydroxide (TMAOH) [75], among others, were used for this purpose. It is worth noting that the main purpose of using these alkaline compounds was not to change the pH of the reaction medium from acidic to basic. By using an alkaline modulator, the pH of the reaction mixture increases but does not necessarily enter the basic pH range. Obviously, the final effect relies upon the concentration of the modulator. Their function is mainly to affect the acid–base environment of the reaction system [58] and deprotonate the linker according to the protonation/deprotonation mechanism mentioned above (*Mechanism II* presented in Fig. 3). Reshaping of MOF's structure with acidic modulators is rather rare, but also possible, e.g., HF [76], HNO_3 [77,78] and acetic acid [57,72,74] were used for this purpose. Moreover, simultaneous modulation by acidic and basic species can be also applied when MOFs are constructed from two or more linkers with different coordination modes [74]. The

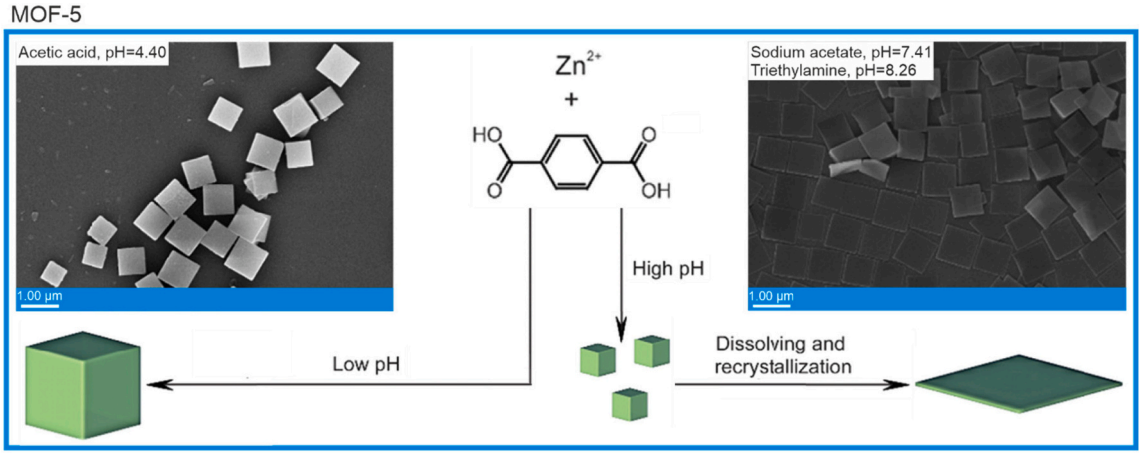

Fig. 6. Formation of the cubic MOF-5 structure in acidic solution and square sheets in basic pH (reproduced and adapted from [72]).

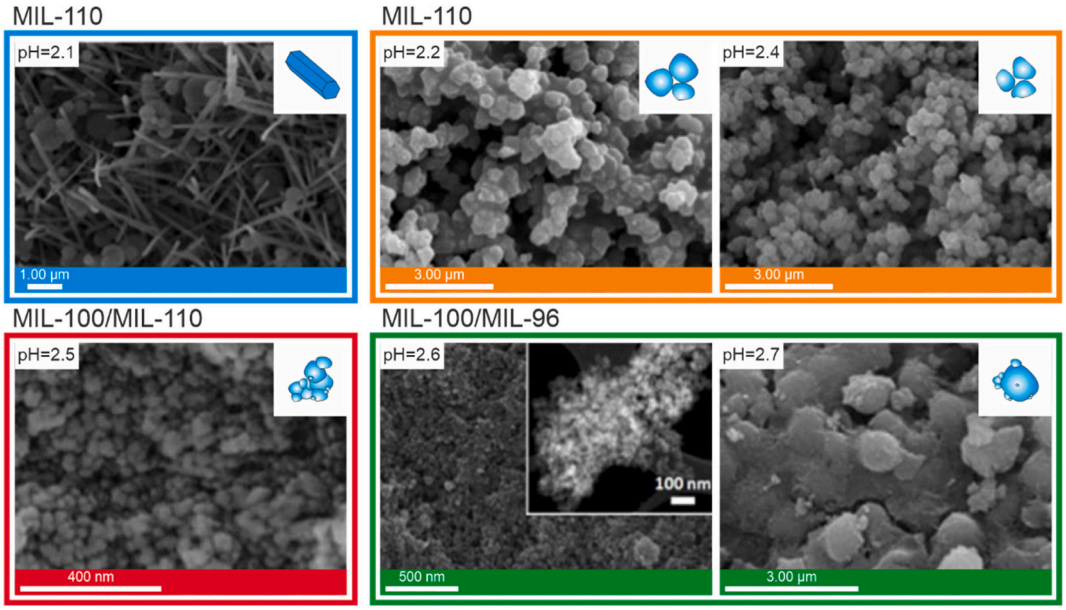

Fig. 7. Various Al-MOFs morphologies obtained at different pH of the reaction medium modulated by addition of TMAOH (reproduced from [75]). Obtained morphologies were described by authors as: pH = 2.1: elongated hexagonal crystals (MOF-100), pH = 2.2–2.4: small octahedra (MOF-100), pH = 2.5: small octahedra (mixture of MIL-100 and MIL-110), pH = 2.6 and pH = 2.7: a mixture of small octahedra and ill-defined hexagonal crystals (mixture of MIL-100 and MIL-96).

effect of acidity/alkalinity of the reaction environment on the morphology of MOFs was most often observed for structures prepared by hydro- and solvothermal methods or by simply heating the reactants.

Small amounts of modulator often do not affect the morphology of the crystals [60], however, may lead to formation of non-agglomerated, fully formed particles [79] with smaller dimension [59]. More alkaline modulator in the reaction system means its higher pH and therefore more linker molecules in the deprotonated form available for coordination with metal ions. It can cause a dramatic change in the shape of the crystal. For example, the octahedral HKUST-1 crystals ($Cu_3(BTC)_2$, where BTC is benzene-1,3,5-tricarboxylate), change to spherical and rod-like particles when exposed to more sodium formate ($pK_b = 10.25$), or to heterogeneous nanocrystals in the presence of TEA ($pK_b = 3.25$) (Fig. 5) [60]. A similar effect was also revealed for Eu-1,4-NDC-fcu-MOF (NDC stands for 1,4-naphtalene dicarboxylate) formed in the presence of methylamine [79]. When the modulator was absent, apart from aggregated, diverse in size octahedrons, plenty of irregularly shaped fine chunks were noticed. By increasing the amount of methylamine, uniform particles with rough, angular surface or smooth spheres respectively were collected [79].

Nevertheless, at relatively too high pH of the system (too much modulator), competition of the modulators and linkers for coordination to metal ions (*Mechanism I*), accompanied by an extremely fast nucleation rate, can prevent the assembly of small nuclei or clusters from the formation of ordered crystalline structures [59]. This observation was made by Guo *et al.* [59] for $Dy(BTC)H_2O$ modulated by sodium acetate (Fig. 5). The addition of 1 equivalent of sodium acetate (pH 4.4) resulted in shortened of rod-like crystals (from 60 μm to 3 μm), 3 equivalents (pH 5.8) led to the formation of spherical nanostructures (~71 nm), whereas at pH > 7.2 amorphous structures with elongated shape and increased size were formed (inverse relationship) [59]. In comparison, the use of TEA did not provide $Dy(BTC)H_2O$ nanocrystals, but micrometric stars. Spherical nanocrystals (50–85 nm) were obtained using TEA as a pH mediator in combination with acetic acid as a capping agent [59].

The above-mentioned change in the dimensions of the crystals may

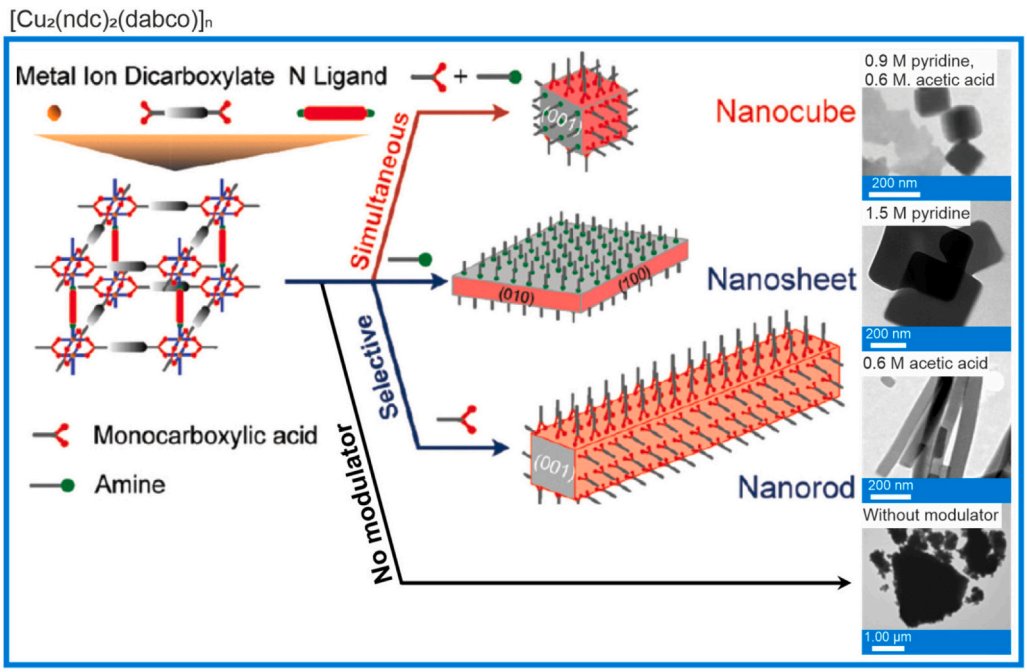

Fig. 8. Divers morphologies of [{$Cu_2(NDC)_2(DABCO)$}$_n$] formed at different pH (reproduced and adapted from [57,74]).

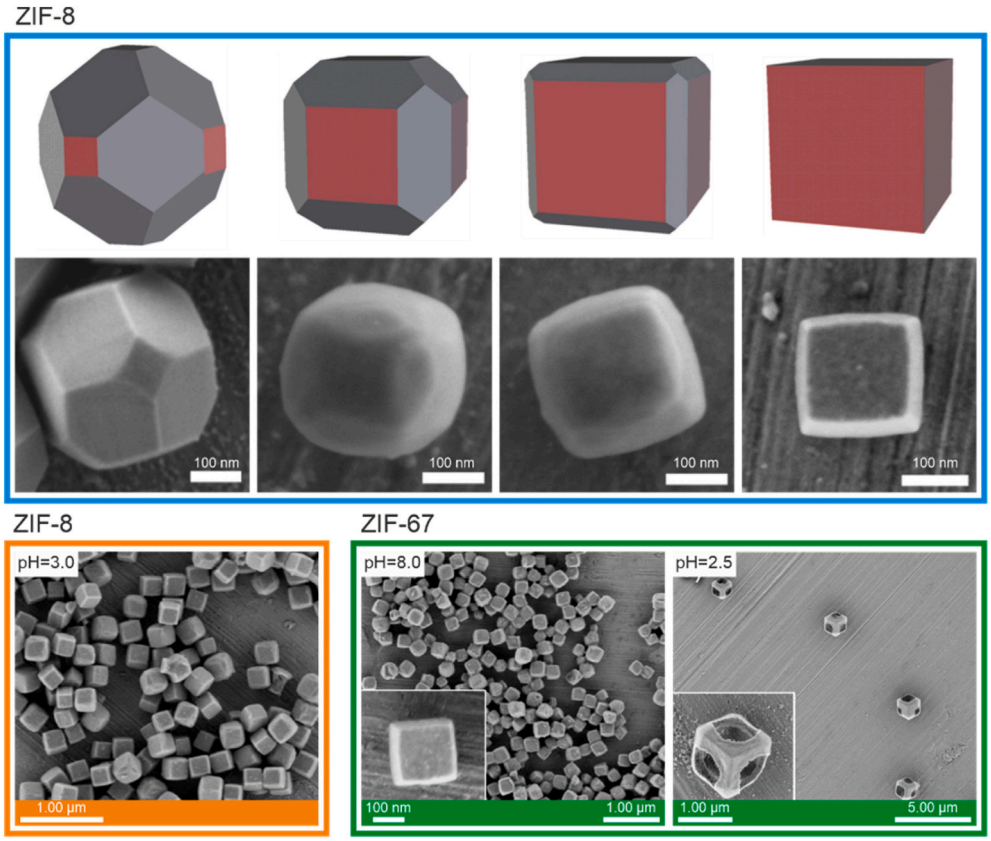

Fig. 9. Reshaping of the truncated rhombic dodecahedral crystals of ZIF-8 and ZIF-67 into cubes by post-synthetic etching, which occurs preferentially in the ⟨100⟩ direction. The etching solution was composed of xylenol orange, whose pH was adjusted by HCl or NaOH (reproduced from [80]).

be due to changes in the supersaturation of the reaction solution after the addition of the alkaline modulator. Taking into account HKUST-1 mentioned above, a relatively slow nucleation is followed by fast particle growth providing bigger crystals [59]. Addition of sodium formate increases the supersaturation of the solution, thus increasing the rate of nucleation, slowing the growth phase of the particles, thus leading to narrower size distribution. Gradual increase of the pH of the solution in the range of 2.05 (without modulator) and 4.18 (with sodium formate)

resulted in decrease of the HKUST-1 crystal size (from 20 μm to about 100 nm, respectively) [60].

The possibility of using an acidic modulator (acetic acid) was verified by Lv *et al.* [72] for MOF-5 ($Zn_4O(BDC)_3$. Acetic acid did not change the cubic morphology, but it did affect the size of the crystals due to capping ability (Fig. 6). A change in sheet morphology was, however, achieved by using the alkaline modulator - sodium acetate - which increased the pH of the system to 7.41 (Fig. 6). The alkaline pH-mediated relationship was also confirmed using TEA as modulator and zinc acetate as precursor (the pH of the reaction mixture was then 8.26). In both cases well-defined MOF-5 square sheets were formed [72].

Synthesis of Al-based MOFs with BTC as a linker also appeared to be very sensitive to pH conditions. In water, hexagonal rods of MIL-110 were formed at very acidic pH (pH ≈ 0–0.3), octahedral shaped MIL-100 crystals at 0.5 < pH < 0.7, ill-defined MIL-96 at pH 1–3, whereas at pH 4 again MIL-110 dominated on MIL-96 [76–78]. The complex structure of MIL-96 combines chains forming hexagonal 18-membered ring tunnels, in the center of which appears a trimeric cluster. This trimer is the basic building unit of mesoporous MIL-100, while MIL-110 is built from an association of Al8 octamers [68]. A slightly different pH relation was obtained by Seoane *et al.* [75] who applied TMAOH for pH modulation in the range of 2.1–2.7, plus cetyltrimethylammonium bromide (CTAB) as a capping agent (Fig. 7). In the absence of alkali (pH 2.1), elongated hexagonal crystals of MIL-110 were obtained, at higher pH values (2.2–2.5) small octahedra of MIL-100 began to form, and at pH 2.6 the product consisted of a mixture of MIL-100 and ill-defined hexagonal crystals of MIL-96 (Fig. 7). The pH conditions also determined the particle size of MIL-100, which decreased from 330 ± 70 nm to 30 ± 5 nm with an increase of TMAOH content [75].

Simultaneous modulation by additives with different functionalities (both acidic and basic) was applied, for example, for [{$Cu_2(NDC)_2$(-DABCO)}$_n$], where NDC is 1,4-naphtalene dicarboxylate, whereas DABCO is 1,4-diazabicyclo[2.2.2]octane. Acetic acid with the same functionality as the NCD linker hinders NDC–copper interaction (growth in the {100} direction), whereas pyridine, containing nitrogen with a lone pair analogously to DABCO, impedes the DABCO-copper interaction, thus the coordination mode in the {001} direction. Selective modulation by acetic acid at concentrations greater than 0.6 M led to the formation of oblong rods with a square cross-section of about 390 × 80 nm [57], by pyridine – nanosheets, while using both modulators nanocubes were achieved (Fig. 8) [74]. The observed lower reaction rate and the coating of the particle surface with acetic acid helped to reduce particle aggregation [57]. The nanorods had the highest surface area (1180 m^2/g), but the differences were not significant [74].

The pH-mediated morphology change of MOFs (e.g. zeolitic imidazolate frameworks, ZIF) can also be achieved by post-synthetic modification using a wet chemical etching strategy modulated by pH regulation of the etchant solution [80]. The proposed procedure, based on the acid–base reaction and subsequent sequestration of metal ions, enabled reshaping the truncated rhombic dodecahedrons into cubic, tetrahedral, and even hollow box structures of ZIF-8 (Zn–2-MIM, where 2-MIM, 2-methylimidazole) and ZIF-67 (Co–2-MIM), as shown in Fig. 9. The etching (breaking the Zn/Co-2-MIM bonds) was found to be pH dependent, surface-selective and preferentially favors crystallographic directions rich in metal–ligand bonds and crystal surfaces of higher dimensionality [80]. Well-defined ZIF 8 and ZIF-67 cubes were obtained especially at pH 3 and 8, respectively. The slightly higher surface area of the new structures was attributed to the formation of defects during etching.

Examples described above clearly demonstrate that alkaline pH-modulators can significantly change the shape [60,72] or type [75–78] of a formed MOF, often with an accompanying reduction in particle size [60]. The effectiveness of alkaline modulators is due to the acidic nature of the reaction mixtures. By increasing the pH of the reaction mixture with different alkaline compounds, MOFs of a certain shape can be obtained, but this is not the rule. For example, at acidic pH MOF-5 crystallizes as cubes, whereas at pH > 7 it crystallizes as nanosheets, despite the additives used (sodium acetate or TEA). The structure of the additive used, especially with or without capping ability, is important and may exert specific impact (affinity to crystal surfaces). For HKUST-1, a final morphology (rod-like particles or nanocrystals) depends on the type of modulator used. For some modulators, e.g., TEA, adjusting the alkalinity may only result in a change in morphology, but may not be effective in reducing the size of structures to nanometers. To form nanosized structures, not only the rate of deprotonation and the subsequent nucleation must be fast, but there must be a limiting factor (e.g. capping agent) for the crystal growth and ultimate assembly [59]. However, some modulators (e.g. sodium acetate) combine both factors in the molecule: alkaline properties and capping ability. What is more, two different modulators can be also utilized at once [74], which gives the additional possibility to obtain a variety of products by simply adjusting the amount of acidic or basic compounds added.

Overall, the addition of an alkaline modulator makes it possible to obtain particles of smaller size, due to the facilitation of the supersaturation of the system and increasing the rate of nucleation. However, the appropriate acid–base equilibrium is necessary to adjust the nucleation rate and prepare the MOF crystals of the desired shape. In this regard, reappearance of larger crystals [59], formation of amorphous materials [59], decrease of the crystal anisotropy [59], change of the specific MOF structure to other phase structures [60], formation of infinite coordination polymer particles (ICPs) due to aggregation of small nuclei or nanoparticles [81] may be caused by unsuitable alkalinity/acidity of the reaction system thus crystallization rate.

4.2. *Effect of temperature*

The morphology of HKUST-1 [82], Cu_3(BTC) [83–85] or Cu-BTC [86] was found to be strongly related *i.a.* to the temperature conditions of the sample preparation. Changes of the values, rate of temperature increase during the synthesis and rate of cooling were found to affect the morphology of the crystallites by controlling the kinetics of crystal growth. Changes of the temperature conditions can cause a gradual/smooth or sudden change of shape, thickness, size, the surface area, or affect the porosity of the structure [84,86–88].

The BET surface area of $Cu_3(BTC)_2$ varied from 692 to 1500 m^2/g since temperature was changes from 110 to 180 °C during solvothermal synthesis using ethanol (EtOH) and water (1:1 vol) as a solvent and benzene-1,3,5-tricarboxylic acid and cupric nitrate as precursors [89–91]. Despite the fact that these data came from various works, it could be found that elongation of heating of reagents in 110 °C from 15 h (formation of octahedral crystals with 1200 m^2/g) [90], to 18 h lead to development of surface area to ~1500 m^2/g [91], while increasing the heating temperature to 180 °C for 12 h caused the arising of crystals having 692 m^2/g [89]. Therefore, it could be stated that the lower temperature during solvothermal synthesis favors better development of the specific surface area and this is not consistent with typical mechanism describing correlation between temperature and nucleation, i.e. higher temperature favors faster nucleation step, resulting in formation of high number of small particles with well-developed surface area. Although the evidence for this statement is rather unsatisfactory due to lack of systematic studies for different MOFs, this is consistent with the effect observed for semiconductor materials obtained by sol-gel method followed by calcination, *i.e.* higher calcination temperature and longer duration causes surface area shrinkage due to sintering effect.

The effect of temperature (140, 150, 160 and 170 °C) on the morphology and levels of hydration of Cu-BTC was revealed by Seo *et al.* by using microwave synthesis [84]. The synthesis carried out at 140 °C led to the greatest extent to the formation of $Cu_3(BTC)_2(H_2O)_3$ as monocrystalline octahedra (>1 μm). The use of 150 °C resulted in the formation of $[Cu(BTC\text{-}H_2)_2(H_2O)_2] \times 3H_2O$, which transformed into $[Cu_2(OH)(BTC)(H_2O)] \times 2H_2O$ with plate shapes of about 5 μm with increasing temperature.

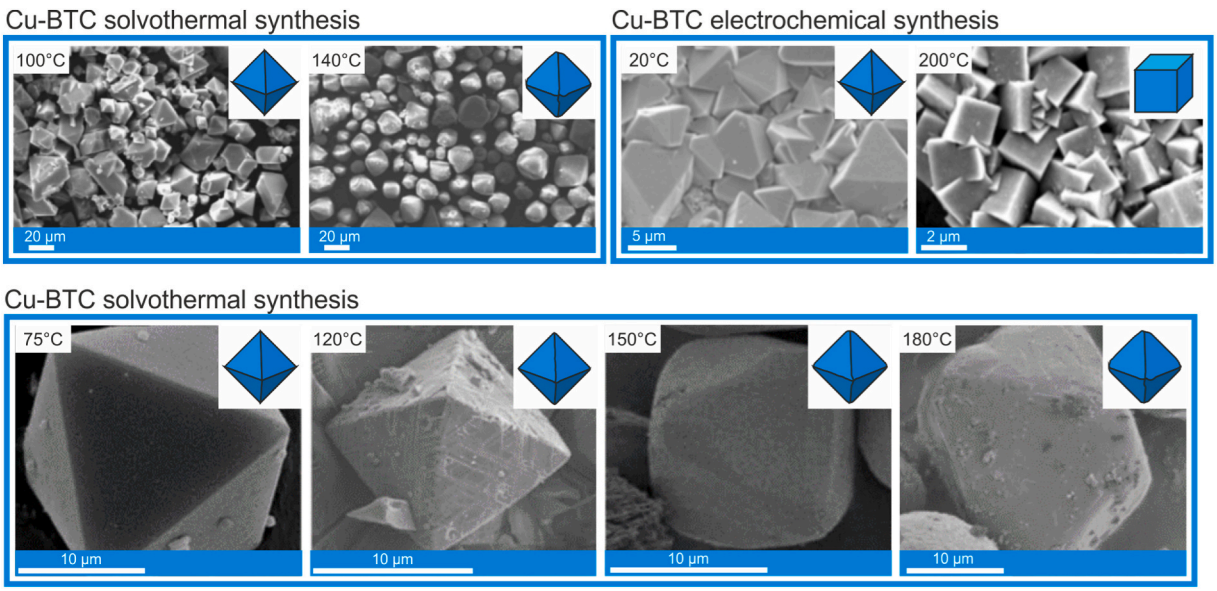

Fig. 10. SEM images of Cu-BTC prepared by solvothermal and electrochemical methods at different temperature conditions. First group of SEM images: left - sharp edges octahedra, right - smooth edges octahedra; second group: left - octahedra, right - cube; third group: left - sharp edges octahedra next ones smooth edges octahedra (reproduced from [82,85,86]).

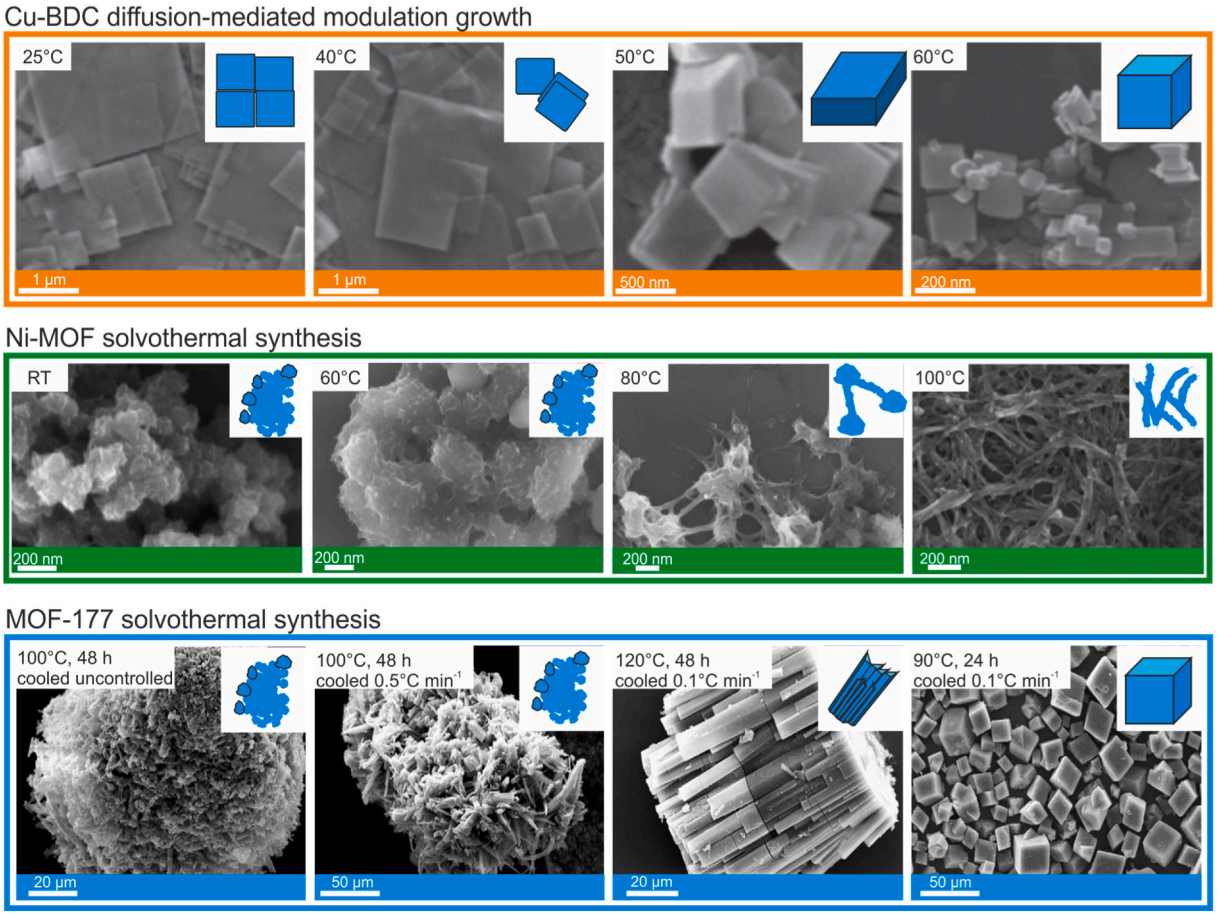

Fig. 11. Effect of heating temperature on morphology of Cu-BDC nanosheets - ultrathin nanosheets, thicker structures of platelets and cube-shaped structures respectively (reproduced from [88]), Ni-MOF - urchin-like structures, neuron-like structures and microwires, respectively (reproduced from [87]), and the combined effect of heating temperature and cooling rate of during formation of MOF-177 ($ZnO_4(BTB)_2$) - aggregated microfilaments, aggregated microfilaments and micro-needles and cubes, respectively (reproduced from [92]).

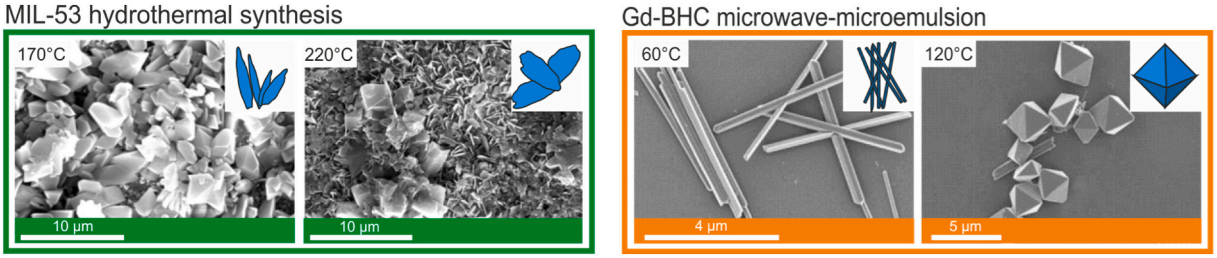

Fig. 12. Effect of temperature on morphology of $[Gd_2(BHC)(H_2O)_8](H_2O)_2$ - nanorods and octahedral/truncated octahedral (reproduced from [93]) and MIL-53 (Al^{3+}/BDC) structure with no defined shape and nanosheets (reproduced from [94]).

Temperature can also play an important role in the formation of sharp crystal edges. The Cu-BTC particles obtained by Chowdhury *et al.* [86] at lower temperature (100 °C, 10 h, EtOH/water) have an octahedral shape with sharp edges, while ones prepared at 140 °C (48 h, EtOH/dimethylformamide (DMF)/water) have rounded edges (Fig. 10). Despite the aforementioned differences in the course of Cu-BTC preparation, the differences between the MOF's morphologies were attributed to a different formation of the 3D polymeric network of Cu-BTC due to the temperature factor. Lowering the synthesis temperature resulted in relatively smaller particles (35.9 µm) with higher surface area 1482 m^2/g in comparison with 38.4 µm and 857 m^2/g detected for product obtained at 140 °C. Similarly, Biemmi *et al* [82], observed that with increasing temperature the edges of octahedra at 75, 120, 150, 180 °C become smoothed (Fig. 10), however the Authors did not observe significant change in the particle size. Attention was also paid to the structure of a single crystal, namely it changed from platelet shape for 120 °C to intergrown octahedrons for 180 °C. In both investigations [82,86], higher temperature promoted the formation of Cu_2O impurities.

Morphology transformation from octahedral structures (low-temperature process) toward cubes (higher temperature) was achieved by Campagnol *et al.* [85], who performed the electrodeposition of Cu-BTC on copper and iron foils at room temperature (RT) and 200 °C, using electrolyte containing H_3BTC, EtOH and water (Fig. 10). X-ray diffraction patterns showed a high similarity of the obtained structures under both temperature conditions. When comparing the signal locations of both samples, they overlap, the only difference between them is the higher intensity and sharpness of the signals, in the case of a sample obtained at 200 °C.

The same research group tried also to analyze the effect of temperature on the morphology of MIL-100(Fe) particles obtained by an analogous electrochemical method in the temperature range from 110 to 190 °C. Polydisperse crystals with a wide range of dimensions 50 nm - 1 µm were formed in the temperature range of 110–130 °C, whereas monodisperse crystals with small sizes at 170–190 °C. Based on the XRD analysis, it was concluded that the kinetics of MIL-100 formation is strongly related to temperature. Namely, nucleation is stimulated to a greater extent than the increase in crystal size with increasing temperature. Therefore, in the low-temperature process, a relatively small amount of large-sized crystals forming clusters was obtained, while at high temperature, a relatively large number of small-sized crystals were formed, separated from each other to a greater level than in the first case.

The morphology of the analogical to the abovementioned structure, namely, Cu-BDC was analyzed by Rodenas *et al.* [88] 25, 40, 50 or 60 °C. The use of 25 °C resulted in obtaining ultrathin nanosheets (approx. 10 nm), while at 50 °C, thicker structures of platelets were formed. On the other hand, at a higher temperature of 60 °C, a large amount of cube-shaped structures ranging in size from 30 to 500 nm were obtained, moreover, there were remains of platelets and larger crystals in the sample (Fig. 11). Increasing the temperature also reduced the dimensions of the particles obtained from initially micrometric (25 and 40 °C) to nanometric (50 and 60 °C), at the expense of transformation from two-dimensional to three-dimensional structures.

Changes in the Ni-MOF structure during solvothermal synthesis conducted at RT, 60, 80 and 100 °C were revealed by Yuan *et al.* [87] (Fig. 11). At room temperature and at 60 °C, a morphology without a strictly defined shape was obtained, which the Authors called "urchin-like", the diameter of which was determined to be approx. 200 nm. The Ni-MOF obtained at 80 °C was characterized by a more spindle-like shape compared to the previously described structures, which was termed "neuron-like". However, the synthesis carried out at 100 °C resulted in obtaining nanowires with a diameter of approx. 10 nm, several micrometers long. The viscosity of the solution in which the synthesis was carried out was indicated as the reason for the change in the morphology of the particles obtained at different temperatures. The increase in temperature lowered the viscosity of the solution, which abolished the mass transfer limitation.

Li *et al.* [92] pointed out that both the synthesis temperature and the cooling rate can affect the structure and morphology of MOFs using MOF-177 ($ZnO_4(BTB)_2$, where BTB 4,4′,4″- benzene-1,3,5-triyl-tribenzoate) as an example. A large aggregate consisting of microfilaments was obtained when synthesis was performed at 100 °C, whereas cooling at RT (Fig. 11). The controlled cooling (0.5 °C min^{-1}) resulted in the production of aggregated microfilaments and microneedles. Higher synthesis temperature (120 °C) and slower cooling 0.1 °C min^{-1} lead to formation of more geometric solids with clearly outlined edges, which consist of subunits with shapes similar to long cuboids. The most regular product, disaggregated cubes with smooth edges and relatively small dimensions were obtained at lower temperature, namely 90 °C, when the synthesis was shorter (24 h), and cooling controlled for 0.1 °C min^{-1}.

Two completely different morphologies of Gd-BHC MOF ($[Gd_2(BHC)(H_2O)_8](H_2O)_2$, where BHC is a benzenehexacarboxylate ligand), were obtained by Taylor *et al.* [93] by microwave-assisted microemulsion method. When the temperature of 60 °C was used, nanorods with a diameter of 100–300 nm and a length of several micrometers were obtained, while the temperature of 120 °C resulted in the formation of octahedral and truncated octahedral structures with a small amount of nanorods (Fig. 12). Despite the different morphology of the obtained samples, they had the same crystal phase. The difference between the morphologies obtained for the synthesis MOFs at different temperatures were related with differences in process kinetics. Namely, a higher temperature promotes faster nucleation and slower particle growth.

Significant reduction of the particle size with temperature was shown for MIL-53 by Hu *et al.* [94]. Namely, the synthesis carried out at 170 °C resulted in a smooth-walled morphology with a three-dimensional structure with no defined shape, while the process carried out at 220 °C resulted in the formation of nanosheets, densely located on the same surface (Fig. 12). This may be due to the duality of temperature influence on the seeding of crystallites and the process of crystal growth. Low temperature stimulates crystal growth, while high temperature stimulates their seeding. Optimization of the MIL-53(Al) synthesis temperature was described by Meshram *et al.* [95]. The authors obtained interesting results of their analyzes - namely, they synthesized MIL-53

Table 1
Examples of MOFs obtained by solvo- or hydrothermal reactions.

Type of reaction	Hydrothermal	Solvothermal
Main solvents	water, formic acid	DMF, DEF, EtOH, MeOH, DMSO
Examples of MOFs	MOF-808 (Hf^{4+}/BTC) [105] MIL-121 (Al^{3+}/BTEC) [106] EuY/Mel (Eu^{3+} and Y^{3+}/Mel) [107] Cu-BTC [108] MIL-96 [109] MIL-100 [109]	NH_2-UiO-66 (Zn^{4+}/NH_2-BDC) [110] UiO-66 (Zn^{4+}/BDC) [111] MOF-5 [112] MOF-74 (Ni^{2+}/DOT) [113] NH_2-MIL-125 (Ti^{4+}/NH_2-BDC) [114] Cu-TDPAT (Cu^{2+}/TDPAT) [115]

BTEC - 1,2,4,5-benzenetetracarboxylic acid (pyromellitic acid).
Mel – benzene-1,2,3,4,5,6-hexacarboxylic acid (mellitic acid).
NH_2-BDC – 2-amino-1,4-benzenedicarboxylic acid (2-amino terephthalic acid).
BDC - 1,4-benzenedicarboxylic acid (terephthalic acid).
DOT - 2,5-dihydroxy-1,4-benzenedicarboxylic acid (2,5-dihyroxyterephtalic acid).
TDPAT - 2,4,6-tris(3,5-dicarboxylphenylamino)-1,3,5-triazine.

(Al) at two different temperatures, 150 and 220 °C, using water or DMF as the solvent. In the case of hydrothermal synthesis, in both cases, geometric structures of undefined shape with smooth walls were obtained, showing a low tendency to agglomeration, which decreased in size from 1.402 to 0.713 μm with increasing temperature and surface area increased from 200.26 to 408.3 m^2/g. In the case of DMF, however, amorphous structures with a high tendency to agglomeration were obtained, the size of which increased from 66.3 to 105.2 nm and the surface area decreased from 1160.7 to 501.2 m^2/g. The authors explained the differences in morphology as a difference in the process of nucleation and crystal growth for different solvents, which is due to the better solubility of the used linker in DMF than in water, which facilitates deprotonation of the linker and stimulation of formation. Unfortunately, the effect of temperature has not been clearly explained [95].

The influence of temperature on the structure of the UiO-66 was one of the main topics of several research groups at that time. Namely, Jajko *et al.* [96] observed an increase in the size of particles that make up structures of undefined shape from about 0.1–0.3 μm to 0.5–0.9 μm for solvothermal synthesis at 100 °C and 220 °C, respectively. It was also noted that the increase in temperature affects the promotion of aggregate formation. Which was reflected in the BET surface area of 1646 and 1115 m^2/g, for 100 °C and 220 °C, respectively [96]. A similar relationship was also observed in the case of UiO-66(-NH_2, -NO_2 and —Br). An increase in the solvothermal synthesis temperature from 120 °C to 220 °C caused a decrease in BET from 1042 to 769 m^2/g, 836 to 542 m^2/g and 1161 to 167 m^2/g for the -NH_2, -NO_2 and —Br modifiers, respectively [97]. Morphologically similar structures were described in the manuscript of Ali *et al.* [98], for which the BET analysis did not show a clear trend. Namely, the researchers synthesized samples solvothermally at 120, 150 and 220 °C, for which the surface area was the lowest each time for structures obtained at 150 °C, while larger, similar to each other for 120 and 220 °C [98].

The influence of solvothermal synthesis temperatures (DMF) in the range of 100–220 °C on the Zn/Co(EtIM)$_2$ (EtIM - 2-ethylimidazole linker) structure was investigated by Ma *et al.* [99]. The researchers found that at temperatures of 150 °C or lower, the resulting structures were shaped like a rhombic dodecahedron, while at 170 °C a globate polyhedron with 24 faces and at 190 °C with 26 faces. From the SEM analyzes included in the manuscript, it can also be estimated that the size of the synthesized structures increased with the applied temperature [99].

Based on the information in the above articles, we can conclude that in the case of Cu-BTC obtained in the solvothermal process, along with the temperature increase, there is a tendency to increase the size of the obtained particles [86], increase the amount of impurities (Cu_2O) [82,86] round the edges [82,86] and decrease the surface area [86]. A similar dependence was also observed for MOF-177 [92], namely a lower synthesis temperature and controlled, mild cooling favored the formation of crystallites with a defined shape of smaller sizes than during the synthesis at higher temperature and rapid cooling.

An interesting observation worth noting is that, depending on the type of MOF, the temperature effect can be completely reversed. Namely, by comparing Ni-MOF [87] and Cu-BTC [86] obtained with the solvothermal method, and even at the same temperature, two completely different morphologies were obtained and a different effect of temperature changes on the crystallites was observed. In the case of Ni-MOF, the increase in temperature caused the formation of nanowires ($T = 100$ °C) of smaller sizes than in the case of the lower temperature of large amorphous clusters [87]. In the case of Cu-BTC, the increase in temperature caused an increase in size and smoothing the edges of the initially octahedrons, which were obtained for T = 100 °C [86].

However, a clearly marked tendency toward a decrease in particle size and an increase in the number of crystallites with increasing temperature was observed in the case of MIL-100 (Fe) [85], Cu-BDC [88], Ni-MOF [87] and [Gd_2(BHC)(H_2O)$_8$](H_2O)$_2$] [93].

An increase in temperature stimulates nucleation at the expense of lower particle growth, and thus, with increasing temperature, a larger amount of smaller crystallites may be obtained [94]. On the other hand, too high a temperature may favor shape deformation by smoothing the edges, which are sharp in the case of lower temperature syntheses. In addition, often too high a temperature promotes the formation of impurities such as metal oxides forming a given MOF structure [82]. By means of XRD analysis, no significant differences were shown between the samples obtained in the series, only, in some cases, the samples synthesized at a higher temperature showed higher crystallinity than those obtained at a lower temperature [86,87]. In the case of Ni-MOF, the BET surface increases from 246, through 257 to 295 m^2/g, when temperature rises from 60, through 80 to 100 °C, respectively [87]. It is an individual feature of each type of MOF structures and the method of their purification and activation. The differences in the formation of MOF particles are explained by the compensation of the activation energy of the product formation or a decrease in the viscosity of the solution [87], and thus an increase in mass transfer and pressure in the solution with increasing temperature [100]. All above-mentioned reasons are consistent with the general propensity of the acting of temperature on the obtained crystallites. Generally, higher temperature promotes the seeding process, so can result in formation of smaller particles, but suppresses surface area development (*Mechanism IV*). Additionally, higher temperature makes it easier to exceed the activation energy of product formation and lowers the viscosity of the solution, this causes the possibility of more effective collisions of molecules with each other, which leads to a larger amount of smaller product formed, due to the increase in the speed of particle movement with increasing temperature.

4.3. *Effect of solvent, concentration of reagents and components type*

One of the determinants for the morphology of MOFs, their polymorphic structures or properties is the type of solvent in which the synthesis is carried out - its composition, properties (especially polarity and ability to form hydrogen bonds, thus solubility of the precursors and product), and volume (precursor concentration). It is a common fact that the first step in the synthesis of MOFs is to dissolve the metal precursor (the corresponding salt) and linker in a solvent or mixture of solvents [1], although recent scientific reports suggest that solvent-free synthesis of these materials is also possible [101]. When synthesizing materials in solvents in which the solubility of the addressed compounds is low, nuclei formation and particle growth occur on a very short time scale, because the consumption of dissolved building blocks occurs very quickly.

By controlling the initial concentration of the precursors, the period

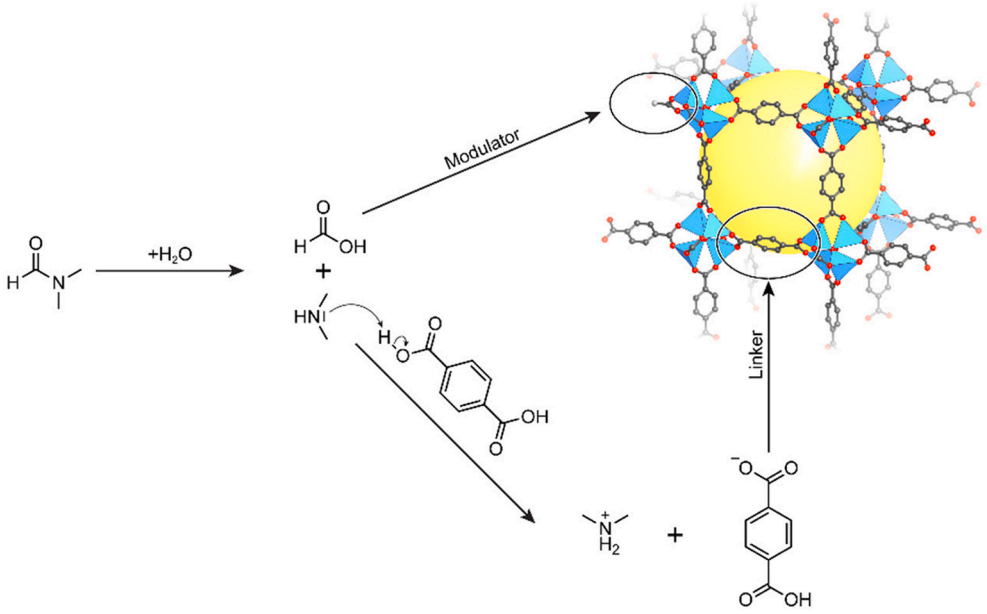

Fig. 13. DMF function in the creation of MOFs (reproduced from [1]).

in which repetitive nucleation can occur can be made so short that a monodispersed colloid results by the subsequent uniform growth on the existing nuclei [102]. The most common reaction medium used in the synthesis of MOFs is a mixture of solvents, which are commonly the DMF, diethylformamide (DEF), dimethyl sulfoxide (DMSO), 1-metylo-2-pirolidon (NMP), water, EtOH, methanol (MeOH) and other alcohols, TMAOH, acetone and organic acids. In hydrothermal reactions, the ground is water, but in this environment most MOFs are unstable (loss in crystallinity and structural decomposition) [103]. In this situation, organic solvents can be used (solvothermal reaction) or the addition of alcohols, which can prevent the destructive properties of water, as described later for Cu-BTC [104]. Examples of MOFs obtained by solvo- or hydrothermal reactions are shown in Table 1.

The solvent in which the linker is often dissolved is DMF (polar aprotic solvent) or a compound from the amide group, while a suitable fairly polar solvent is used to dissolve the metal salt. Additionally, a co-solvent is added to assist the mutual dissolution of the compounds. During heating, DMF decomposes to dimethylamine, through which linker acids are deprotonated to form anions (*Mechanism II*), which interact with metal ions to form SBUs and bonds between these MOFs fragments (Fig. 13). The second product of DMF decomposition in the time of heating is formic acid, which acts as a modulator of the resulting backbone (*Mechanism I*) [1]. Thereby, the solvents may play a role of a secondary structuring and modulating agent. In addition, the solvent molecules can take part in the coordination of metal ions [116] and be guests in the pores [117].

The experimental data indicate that the volume of solvents used in the synthesis plays an important role in controlling the morphology of MOFs. ZIF-67 or NH_2-MIL-125(Ti) have been well studied in terms of the effect of these conditions on the structural appearance of MOFs, which are shown in Fig. 14. With increasing solvent (MeOH) volume, ZIF-67 changes from a flower-like nanostructure to a multi-walled wafer with a concomitant increase in specific surface area (BET) from 800 to 2037 m^2/g [118]. In contrast, NH_2-MIL-125(Ti) particle (composed of titanium ions and 2-aminoterephtalic acid) changes its structure with increasing solvent from circular platelets through multi-walled platelets to octahedral particles, resulting in a decrease in specific surface area from 1268 to 1041 m^2/g, respectively [114].

Very related to the volume of the solvent is the concentration of the reactants in the reaction mixture. The more a solution is concentrated with the reactants involved in the synthesis, the larger crystals are obtained. In addition, at high concentrations defects may appear in the crystals, which is due to very rapid crystallization - this is well illustrated in Fig. 14 for Cu-BTC MOFs [119]. An excess of metal or ligand during nucleation of this MOF leads to the formation of more nuclei, thereby reducing the average size of nanoparticles obtained when adding the same amount of reactants [67]. Analogously for ZIF-71, it was shown that the kinetics of the reaction accelerates as the linker to metal concentration ratio increases, yielding nanocrystals of decreasing size, while the lifetimes of the amorphous intermediates become short and difficult to observe experimentally [71].

The shape of MOFs can be controlled by changing the type of solvent or mixed solvents with different properties. The Cu-BTC frameworks, presented in Fig. 15, obtained using a water-DMF mixture, have a porous irregular structure [120], while the use of a water-ethanol environment provides octahedral structures [119]. The synthesis performed in alcoholic solution without water resulted in spherical shaped particles [121], whereas in water, without organic co-solvent, a tagliatelle-like structure with low porosity (BET surface area - 15.6 m^2/g) was obtained [119]. Addition of DMF to an alcoholic solution (water-EtOH) increases the amount of pure MOFs obtained as well as the uniformity and fineness of the particles and increases the specific surface area. On the other hand, an excessive amount of DMF in the solution (optimum - up to 14% by volume) causes aggregation of crystals and reduction of the surface area [122]. A similar effect of water as a solvent is evident in the synthesis of NH_2-MIL-88B (Fe) [123]. MOFs obtained from pure DMFs form aggregates of crystals composed of many small crystals (due to the relatively high surface energy of the small MOFs crystals). When the volume of water is 4% of the total solvent volume, small whorls form. With increasing water to DMF ratio, MOFs are obtained in the form of a monocrystalline spindle (which increases in volume as more water is used in the synthesis).

The solubility of the precursors in the solvent is one of the factors determining the achievement of a certain MOF dimensionality. Morphology of Mg-BDC can be controlled by the EtOH/H_2O ratio in the reaction mixture. Using only water for the synthesis, a zero-dimensional molecular structure is obtained, while using EtOH as a co-solvent, 1D or 2D crystals (25% and 45% molar EtOH/H_2O, respectively) are produced. In contrast, using pure ethanol resulted in a 3D structure, as shown in Fig. 15. The change in morphology was related, among other factors, to the solubility of BDC, which increases with increasing amount of ethanol in the reaction medium, facilitating coordination of carboxyl

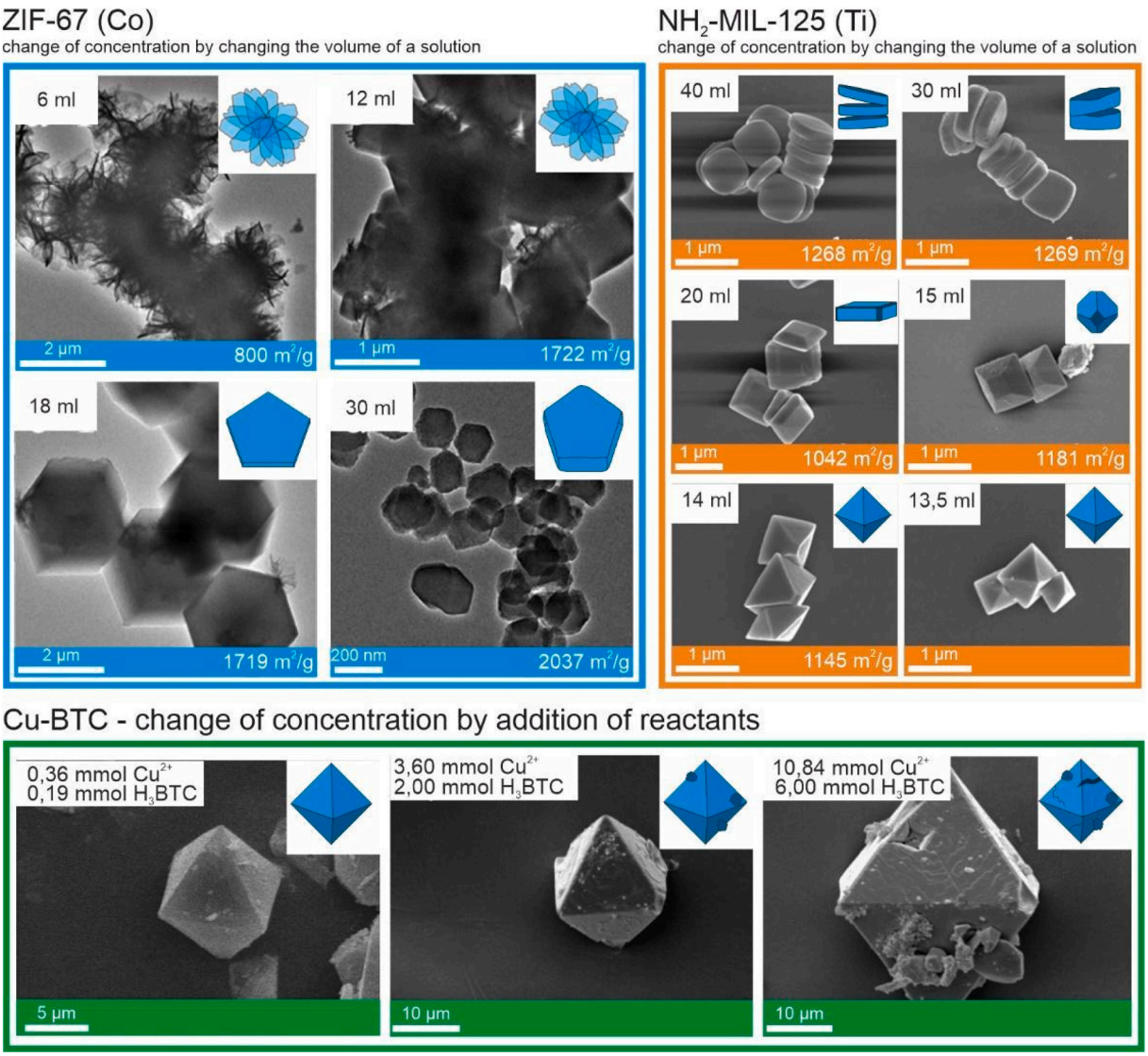

Fig. 14. Effect of solvent amount on the morphology of NH_2-MIL-125(Ti): 40 ml – circular plates, 30/20 ml – multi-walled plates, 15 ml – spherical octahedra, 14/13.5 ml – octahedra and ZIF-67: 6 ml - flower like, 30 ml – multi-walled wafer (reproduced from [114,118]). Dependence of Cu-BTC morphology (octahedra and octahedra with defects))on the amount of reactants in the reaction mixture, mixture volume is 24 ml (reproduced from [119]).

group with Mg^{2+} leading to the more thermodynamically stable structure of higher dimensionality [124].

Another example, where the type of co-solvent used made it possible to obtain structures with different aspect ratios is Cu-BDC. Very high aspect ratio crystals with a preferential orientation in the {201} direction were obtained when acetonitrile or propionitrile (polar aprotic solvents) were added to DMF (Fig. 16). However, the employment of propionitrile resulted in more rounded edges, indicating the effect of the co-solvent on crystal growth along the basal plane. Using polar protic co-solvents (m.in. methanol, 2-propanol) causes the aspect ratio of the nanoplates to decrease and the material begins to take on a 3D form. The alcohol probably adsorbs more strongly on the metal nodes (different coordination ability of the solvent) which leads to the displacement of DMF molecules, facilitating the formation of a three-dimensional crystal structure. Moreover, the different kinetics of linker deprotonation by the solvent can also affect the crystal growth rate and morphology (*Mechanism II*) [88].

The effect of solvent on the shape of MOFs was also related with their ability to form hydrogen bonds (acceptor/donor), and thus to disturb the internal forces in the crystal structure of MOF [125]. The Cu-PYDC structures, shown in Fig. 16, obtained in ethanol were described by Authors as small size nanorods, in acetonitrile as large-sized flakes, while changing the solvent to water resulted in the formation of clomerized rods, flakes and particles. Of interest are the materials formed in the ethanol-water mixture, which form flower-like nanosheets. Hydrogen bonds between the solvent molecules (here acetonitrile, ethanol) and water in which the MOFs precursors are dissolved can hinder coordination interactions in Cu-PYDCs. There are weaker interactions between acetonitrile-water because acetonitrile can only be a bond acceptor, thereby its impact on the final structure is lower. However, with the use of water, the hydrogen interactions increase dramatically which results in the formation of a heterogeneous Cu-PYDC nanocomposite [125]. Similar observations were made for Cu-BTC. Using water as a reaction medium may not lead to cluster formation because the water molecules form hydrogen bonds with the linker, preventing the -COOH groups from approaching the copper ions. Increasing the amount of alcohol in solution results in the formation of water clusters surrounded by alcohol, which facilitates the coordination of H_3BTC carboxyl groups to Cu^{2+} (Fig. 17) [104].

The effect of the solvent type on the size distribution of MOFs can be illustrated by an example of ZIF-8 synthesis. In DMF, the material forms hexagonal particles with sizes of 150–200 µm, while changing the

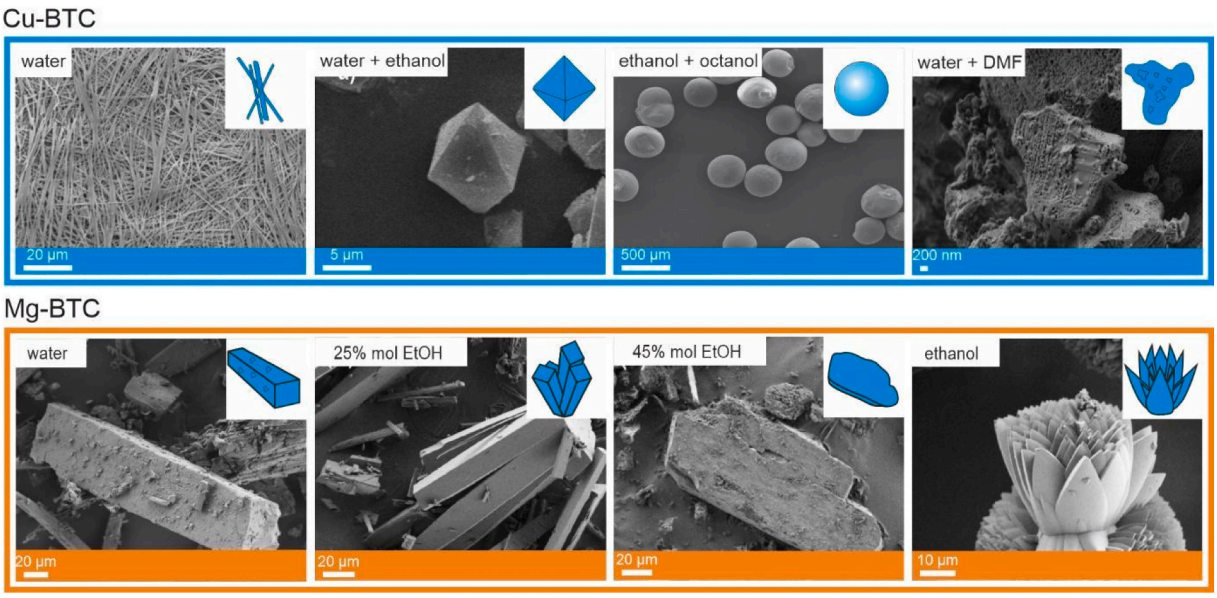

Fig. 15. Dependence of Cu-BTC morphology on the composition of the reaction solution; from left: water – tagliatelle-like structure, water + ethanol – octahedra, ethanol + octanol – sphere, water + DMF – irregular (reproduced from [119 to 121]). Different morphology of Mg/BTC (SEM images and chain model) depending on the amount of ethanol; from left: water – 1D structure, 25%, 45% mol EtOH – 2D structure, ethanol – 3D structure, flower-like structure (reproduced from [124]).

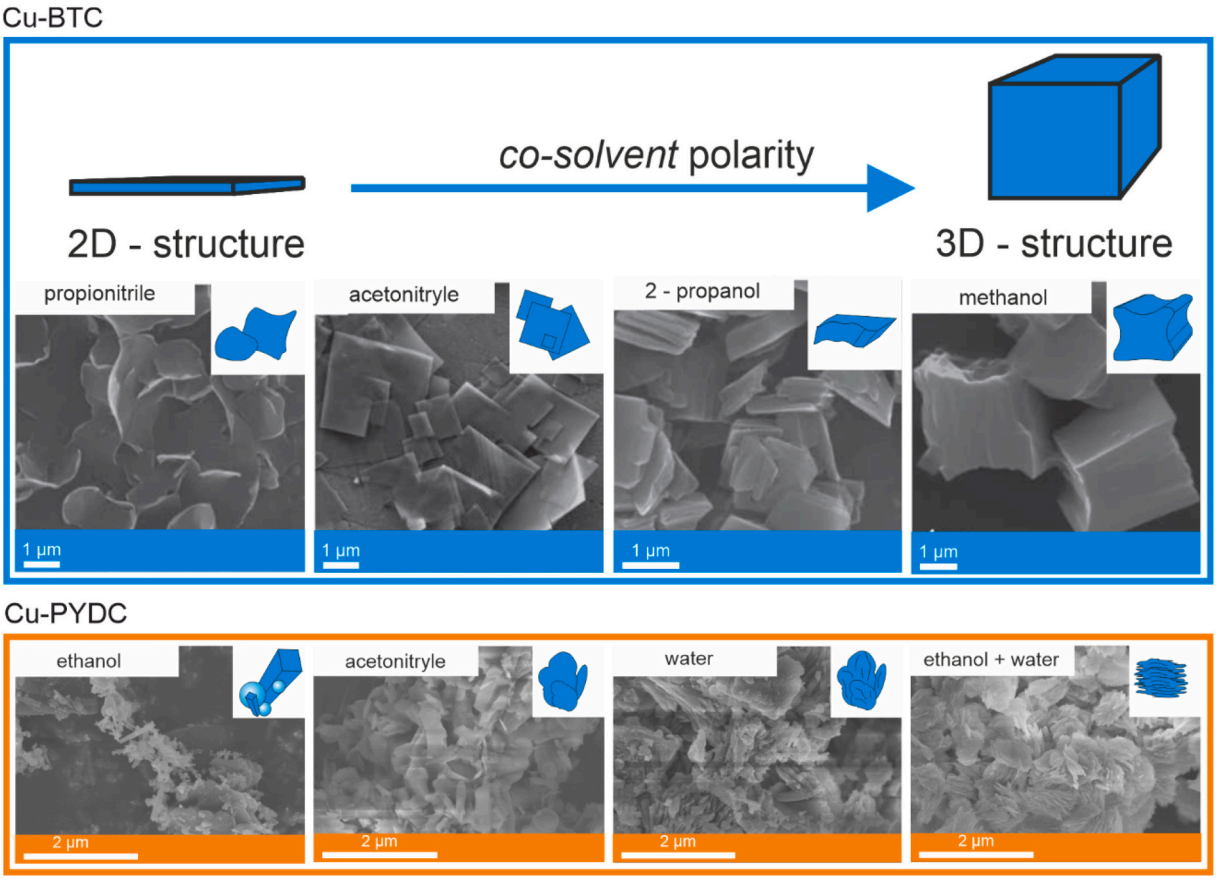

Fig. 16. Shape dependence of Cu-BDC on the solvent used in the synthesis; from left: propionitrile and acetonitrile – 2D nanoplates, 2-propanol and methanol – 3D structure).Shape dependence of Cu-PYDC crystals on solvent composition, PYDC is pyridine-2,5-dicarboxylic acid; ethanol – nanorods, acetonitrile – flakes, water and ethanol + water – irregular, agglomerated particles (reproduced from [88,125]).

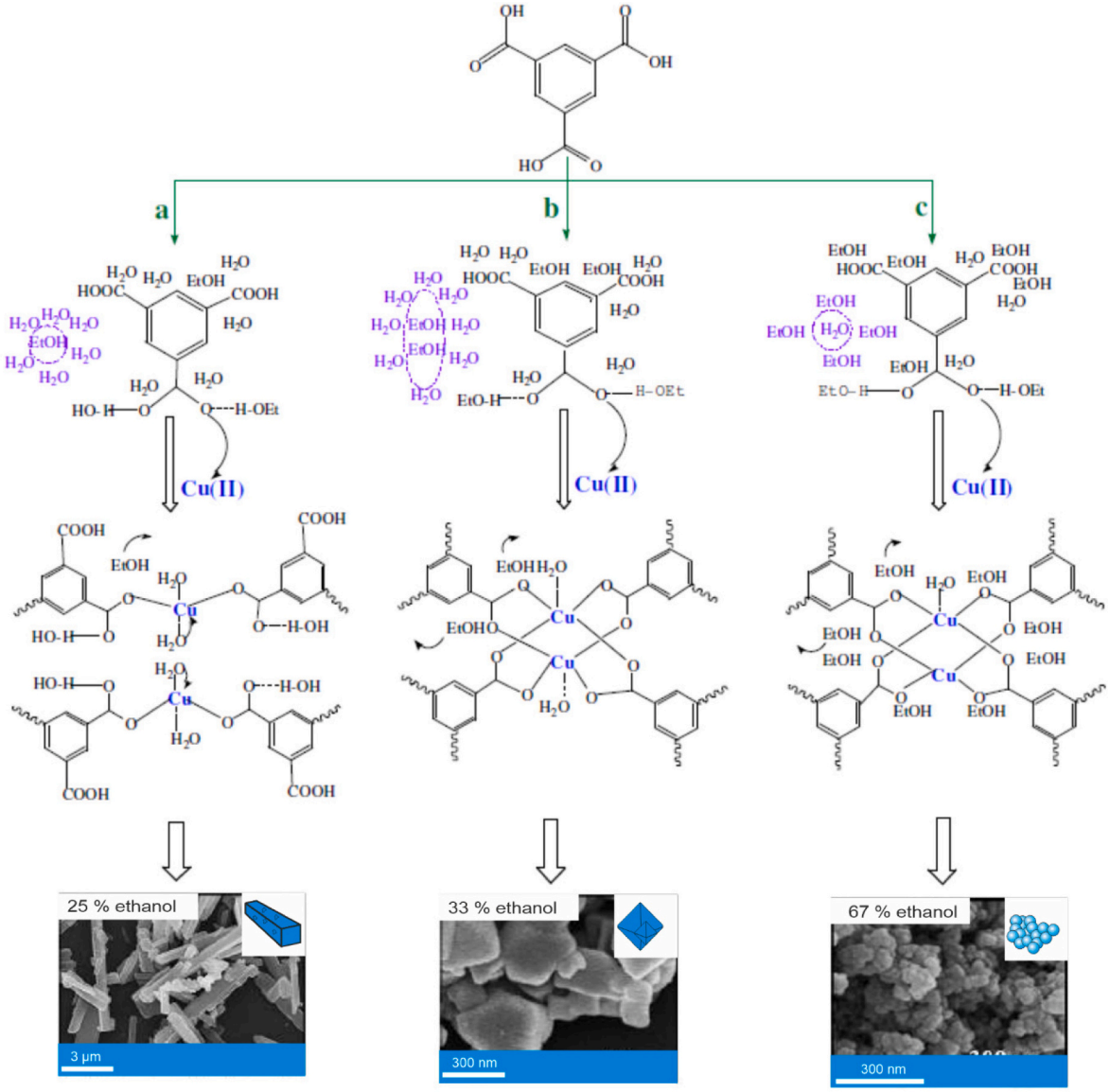

Fig. 17. Schematic illustration for the formation of Cu-BTC depending on the amount of ethanol and water (25% vol. ethanol – beams, 33% – octaedr, 67%-agglomerated particles (reproduced from [104]).

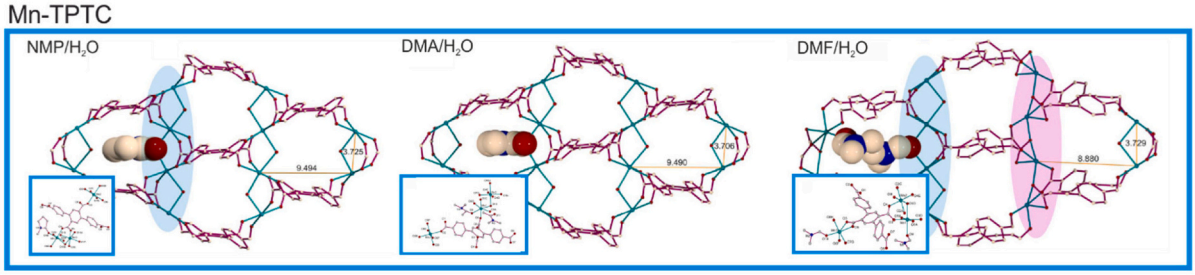

Fig. 18. Models of 1 D channels in Mn-TPTC, deposited by H_2O and NMP/DMA/DMF solvent molecules and the coordination environment of Mn(II) ion MOFs (in boxes), gray C, red O, blue N, cyan Mn (reproduced from [128]).

environment to MeOH or water increases the particle fineness (to 3–5 μm and 0.3–0.4 μm, respectively) [126]. In other studies, the particle diameter of ZIF-8 varied as follows: 134 nm for methanol; 324 nm for ethanol; 212 nm for propan-2-ol; 372 nm for butan-2-ol, 421 nm for *n*-propanol; and 324 nm for *n*-butanol [127]. In both cases, the dependence of the particle size on the polarity of the solvent became apparent. The more polar the solvent, the smaller the particles that can be obtained.

The type of solvent can also affect the pore and channel size and topology of MOFs. An example is Mn-TPTC (where TPTC is terphenyl-3,3′,5,5′-tetracarboxylate) obtained using three different solvents: NMP, *N*,*N*-dimethylacetamide (DMA) and DMF. The size of the channels in

Table 2
Structural parameters of MOFs – Mn-TPTC [128].

Mn-TPTC in	NMP	DMA	DMF
Size of channels	35.37 A^2	35.17 A^2	33.11 A^2
Pore volume	1242.4 A^3	1205.9 A^3	1005.3 A^3
Void ratio	41.4%	40.5%	37.0%

MOF is related to the molecular size of the solvent used (Fig. 18, Table 2). Using DMF, the structure with the smallest channel size, pore size and void ratio was formed. As the size of the solvent molecules increases, the channels formed in the structures become larger. Small DMF does not support the entire channel so that the Mn/TPTC obtained in DMF is somewhat distorted. DMF adopts different solvent coordination modes: bridging and monodentate compared to NMP and DMA, which adopt only bridging mode [128].

A similar relationship between the size of the voids in MOFs and the size of the coordinated solvents (the larger the solvent, the larger the pores of DMA > DMF > MeOH>H_2O) was also noticed for Mn-CPBDA (where CPBDA is 4,4′-((5-carboxy-1,3-phenylene)bis(oxy))dibenzoate). It was also noticed that the solvent can affect the way the linker is coordinated with the metal. In the case of Mn-CPBDA, the application of an appropriate solvent causes the coordination of two $CPBDA^{3-}$ anions with three Mn^{2+} anions to take the form of a T or Y (for T - DMF, Y - MeOH and DMA, respectively) - which directly impacts the formation of the corresponding isomer [129].

Another parameter affecting the shape of MOFs crystals can be the type of precursor salt used for synthesis (type of anion, acidic residue). The importance of this factor will be discussed with the example of ZIF-8 prepared using different zinc salts, 2-methylimidazole and methanol as solvent (Fig. 19). The ZIF-8 crystals obtained from $Zn(acac)_2$ (where acac is acetylacetone) were irregular and poorly developed (size about 45 nm). The use of inorganic salts yielded other shapes: truncated dodecahedral rhombus (141 nm) and undulating spheres (244 nm) were observed for $Zn(NO_3)_2$ and $Zn(ClO_4)_2$, respectively. Large crystals (300 nm) and many smaller ones (150 nm) - with cubic and rhombic shapes - were formed when zinc chloride was applied as a precursor. The usage of $Zn(OAc)_2$ and ZnI_2 gave ZIF-8 with the shape of a typical rhombic dodecahedron, and the particle size was 500 nm. The largest particle sizes were obtained after using $ZnBr_2$ - cubes and rhombic dodecahedrons (1050 nm) - which were characterized by sharp edges and corners. The small particle size and its anisotropy are attributed to the high reactivity of the precursors (soft acid Zn^{2+} and hard bases) - which creates a large number of crystal nuclei. Conversely, the large particle size can be attributed to the low reactivity of the $ZnBr_2$ precursor (soft acid Zn^{2+} with soft base Br^-), which is associated with limited crystal nuclei formation [130].

There is a similar effect when synthesizing MOF-74 (Co), which is obtained as monodisperse crystals of different sizes depending on the counterion of the cobalt(II) salt [131]. The MOFs obtained had the smallest sizes with cobalt(II) acetate and the largest sizes with cobalt(II) trichloroacetate - but all materials showed high crystallinity and high specific surface area (the crystal aspect ratio increases in the order acetate < formate < chloroacetate < trichloroacetate).

In addition to the type of precursor, the morphology of the crystals can also be determined by the number of cations that make up the MOFs. In the case of Ni-BDC, which can form bimetallic MOFs with cobalt, the particle shape is highly dependent on the Ni/Co molar ratio (see Fig. 20).

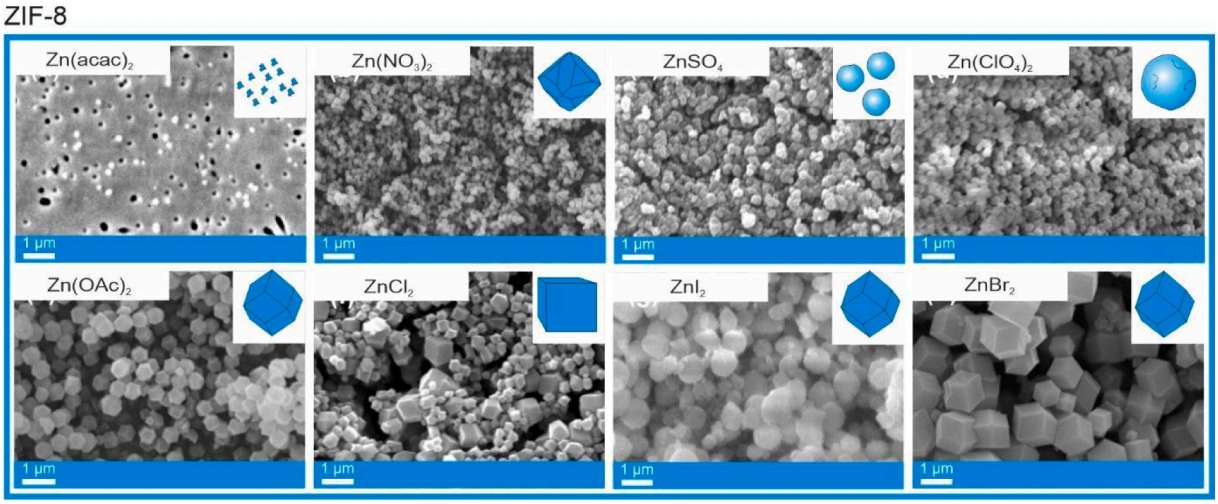

Fig. 19. Morphology of ZIF-8 depending on the salt used for synthesis; $Zn(acac)_2$ – irregular small particles, $Zn(NO_3)_2$ – truncated dodecahedral rhombus, $ZnSO_4$ – truncated nanoparticles, $Zn(ClO_4)_2$ – undulating spheres, $Zn(OAc)_2$, ZnI_2, $ZnBr_2$, – rhombic dodecahedrons, $ZnCl_2$ – cubic and rhombic, (reproduced from [130]).

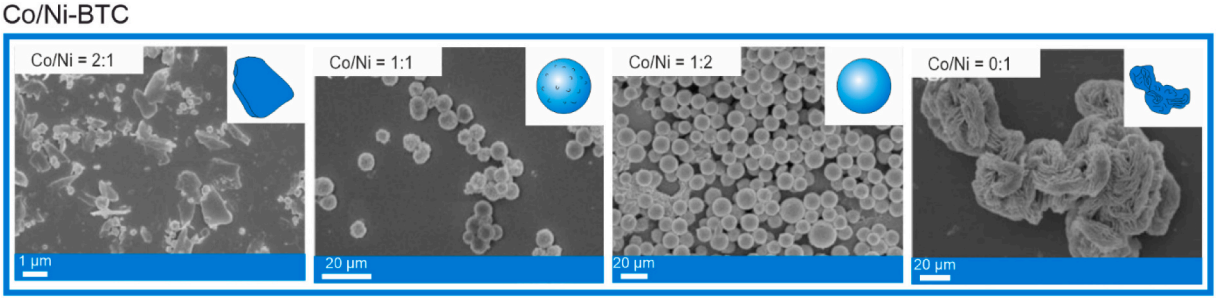

Fig. 20. Morphology of Co/Ni-BDC depending on the ratio molar of salt used for synthesis; Co/Ni = 2:1 – irregular, 1:1 – nanosphere, 1:2 – nanosphere, 0:1 – nanosheets (reproduced from [132]).

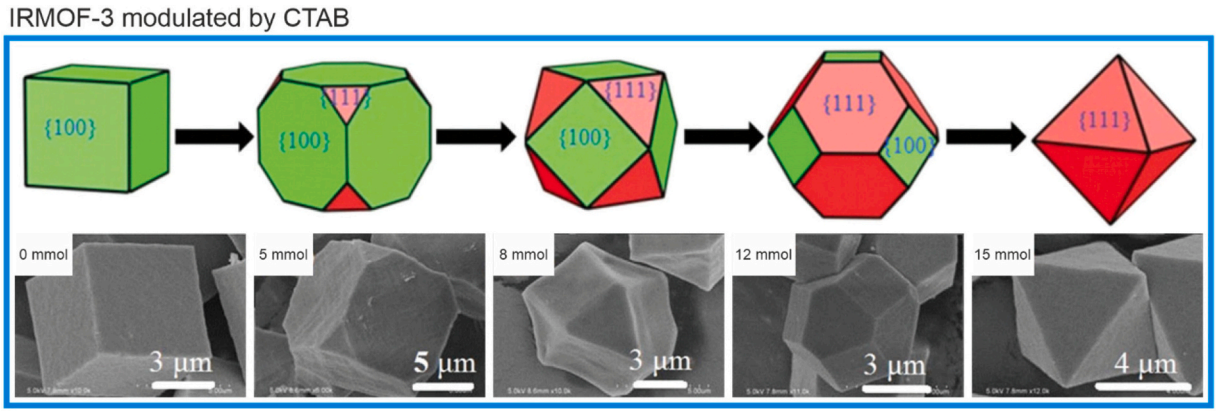

Fig. 21. Schematic and SEM images of the morphology evolution of the IRMOF-3 polyhedral crystals from cubes through truncated cube, cuboctahedron, truncated octahedron to octahedron prepared in the presence of different amounts of CTAB: green facets represent {100}, red facets represent {111} (reproduced from [143]).

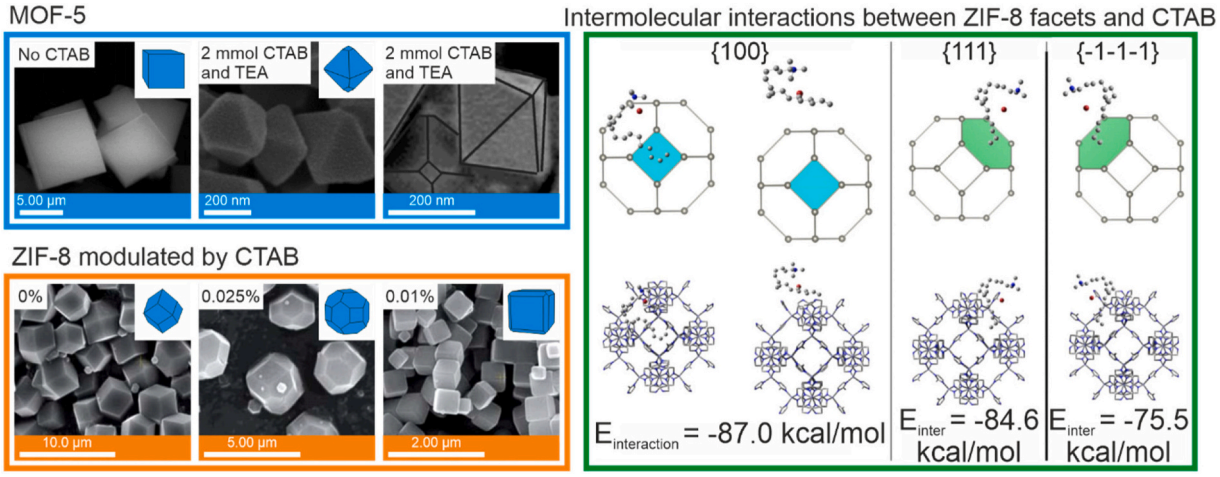

Fig. 22. Different morphologies of MOF-5 (cubes [144] prepared without any modulator and octahedral nanocrystals in a presence of CTAB [145]) and ZIF-8 (rhombic dodecahedrons prepared without any additives, (cubes prepared in the presence of CTAB), (reproduced from [138]); intermolecular interactions between the ZIF-8 facets of and CTAB obtained by semiempirical methods PM6 and PM7 methods included in MOPAC2012 (reproduced from [146]).

The crystals obtained by solvothermal method with Co/Ni in 2:1 M ratio are characterized by irregularity, for 1:1 and 1:2 by nanospheric shape, while MOFs of monometallic type - Ni-BDC can be obtained as nanosheets [132].

Compounds present in solution that have a direct effect on morphology can be co-ordinating compounds (co-ordinating modulators or foreign co-ordinating competitive ions). Co-ordinating modulators can also be salts of organic acids, e.g. *m*-terephenyl-4,4′ dicarvoxylate. In the work of Suresh *et al.* [133], its dadate was investigated on the morphology of MOF-5. Pristine MOF-5 was characterized by a cubic structure, where crystal control occurs by blocking growth along the {100} facet direction. The addition of *m*-terephenyl-4,4′ dicarvoxylate, which co-ordinates adjacent SBUs, causes blocking of the {111} facet resulting in a cuboctahedral structure (when the control is along the {100} facet and {111} facet) or an octahedral structure (when the control is along the {111} facet only). In later work by Suresh *et al.* [134], they described a similar effect of the addition of coordination compounds to the synthesis of IRMOF-8. Under the influence of these compounds, the crystal morphology of IRMOF-8 can be changed from cubic to rhombic dodecahedral, truncated octahedral and octahedral. Another modulating factor could be inorganic salts min. Aluminium nitrate. In a study by Gao *et al.* [135], the effect of a co-competitive coordination strategy in the synthesis of HKUST-1 was investigated. In the study, pristine MOFs retained the orginal octahedral morphology (with {111} facets), and upon addition of the modulator ($Al(NO_3)_3$), the morphology changed to a cubic structure. Al^{3+} competed with Cu^{2+} ions to react with linker anions during synthesis facilitating growth with orientation (100).

Concluding, both type of solvent and type of metal precursor strongly influence the shape, structure, particle size and fineness of MOFs. The solvent can act as only the reaction medium, but in the most cases the solvent alters the modulation of the structure through interactions with the linker. These interactions may involve deprotonation of the linker-carboxylic acid (which facilitates its coordination with metal ions) (*Mechanism II*) or hydrogen bonds (water-linker) which often prevents the formation of MOFs. Moreover, solvent molecules can affect the size of pores and channels - acting as a guest. The second important component of the reaction solution are dissolved salt anions, the reactivity of which affects the shape, size and crystallinity of MOFs.

4.4. *Effect of surfactants*

The main characteristic of surfactants is their amphiphilic structure consisting of a long hydrocarbon chain and a hydrophilic functional group (ionic or nonionic). Because of this structure, surfactants are often used as structure directing agents or capping agents for the preparation of materials, inducing many interesting effects such as formation of high-index facets, transformation of crystal shape, affecting the crystal size [136]. The amphiphilic properties of the surfactants also induce the ability to self-assemble in the solution and form micellar aggregates,

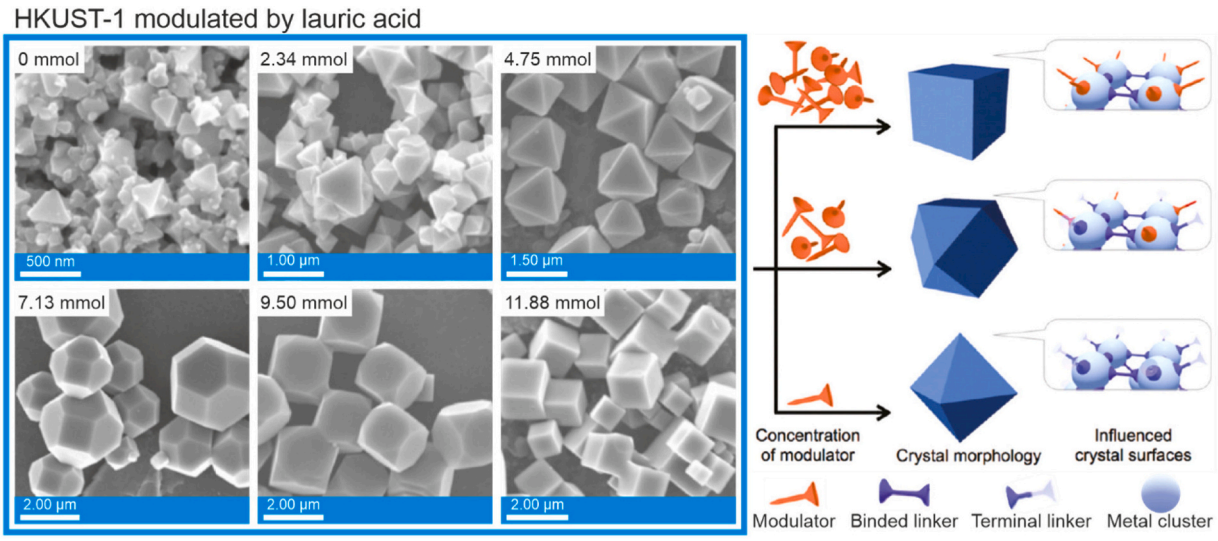

Fig. 23. On the left: morphology transition of $[Cu_3(BTC)_2]_n$ synthesized in a presence of increasing amount of lauric acid (reproduced from [149]); first row from left: deformed octahedrons, deformed octahedrons, octahedrons; second row: cuboctahedron, truncated cubes, cubes; On the right: schematic illustration of the effect of different modulator (orange symbols) amounts on the coordination process to the MOFs network. The growing concentration of modulator is consequently replacing the terminal linkers (white-blue symbols) and preventing from further growth in specific directions.

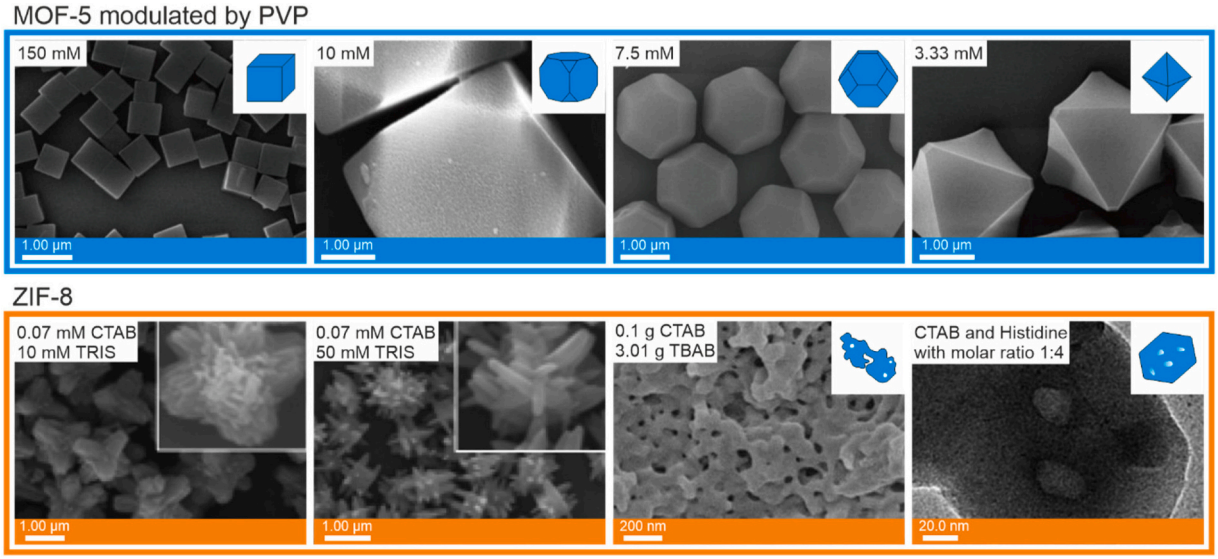

Fig. 24. Morphologies of MOF-5 crystals synthesized with 20-fold diluted synthetic solutions with different concentrations of PVP [150], from left: cubes, truncated cubes, truncated cuboctahedrons, octahedrons; ZIF-8 obtained in the presence of CTAB and various additives (reproduced from [146,152,153]), from left hexapod morphology, sort of burr puzzle, stackable particles, hierarchically structured hexagons.

allowing them to provide a soft template for morphology-defined nanocrystals (structure directing ability). On the other hand, surfactants can selectively adsorb on specific crystal surfaces via diverse interactions, such as dipole−dipole, van der Waals forces, *etc*. (*Mechanism III*). Thereby, surfactants can control the crystal growth, facilitate the formation of different morphologies, prevent the aggregation of crystals to larger and intergrown ones during synthesis and storage, and promote the formation of the uniform structure [136]. The final shape of the crystal is determined by both thermodynamic and kinetic factors. Thermodynamics of crystal formation can be affected by the affinity of the surfactant to a particular facet through selective binding. Thus, surfactants stabilize surface atoms and lower their surface energy. Additionally, the formation of a physical barrier to atom's deposition/diffusion affects the kinetics of crystal growth [137].

The most common surface active additive used to modulate the morphology of MOF is an ionic representative of quaternary ammonium compounds (QAC), namely CTAB. This surfactant was used for synthesis of ZIF-8 [138], isoreticular metal-organic frameworks (IRMOFs) [139], HKUST-1 [140], Fe-MIL-88B (Fe^{3+} combined with BDC) [141], CAU-17 (Bi^{3+} combined with BTC) [142] among others. The effect of a surfactant concentration on the morphology of MOF was clearly explained by Yang *et al.* [143] through the use of IRMOF-3 ($Zn_4O(BDC\text{-}NH_2)_3$) modulated by CTAB. In the absence of the surfactant, IRMOF-3 crystallizes as a cube with six exposed {100} facets (Fig. 21). The addition of CTAB resulted in the formation of truncated cubes due to the appearance of eight small triangular {111} facets. More CTAB promotes further growth of {111}, so that instead of octagonal {100} facets under these conditions, square {100} ones are formed giving cuboctahedrons. Further increase in CTAB content ensures that triangular {111} facets turned into larger hexagonal {111} facets (truncated octahedrons) and the final disappearance of

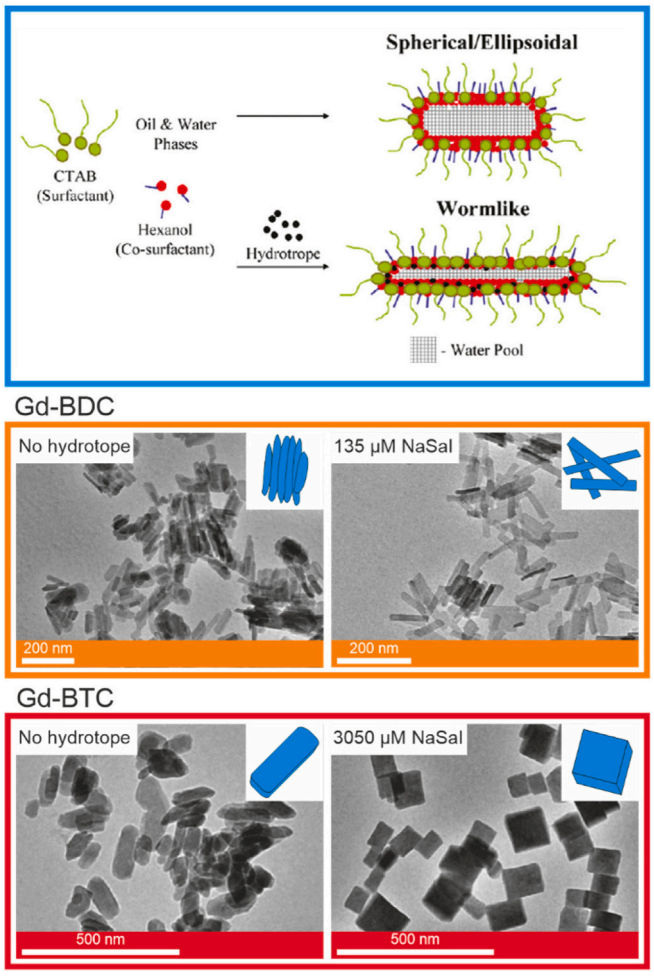

Fig. 25. Schematic effect of a hydrotrope on the shape of the reverse microemulsion stabilized by CTAB and used for Gd-MOF's preparation; change in size of Gd-BDC (rods) and Gd-BTC (ellipsoidal particles, cubes); (reproduced from [154]).

the square {100} facets. This results in perfect octahedrons composed solely of triangular {111} facets (Fig. 21) [143].

Another member of the same family, MOF-5 (IRMOF-1), also showed a similar change in morphology, however, the surfactant also induced a significant effect on crystal size. MOF-5, when prepared without any additives, crystallizes in a microsized cube-shape morphology with an average size of 5–200 μm (Fig. 22) [139,144]. Controlled nucleation and growth by CTAB adsorption gave regular or truncated octahedral crystals of nanometer size [145]. The opposite direction of morphology transformation, namely, from rhombic dodecahedrons to truncated cubes, was observed when the preparation of ZIF-8 was modulated with CTAB at increasing concentrations from 0.07 to 0.35 mM [138,146] (Fig. 22). It is worth mentioning that the morphology of ZIF-8 changes during crystal growth from cubes with 6 {100} facets to intermediate shapes and finally to rhombic dodecahedrons exposing 12 {110} facets as the most likely stable equilibrium morphology of this MOF [147]. In the presence of surfactant, the growth rate of the {100} direction in ZIF-8 is slowed due to the higher affinity of the CTAB cation for this facet (highest interaction energy) compared to the others (Fig. 22). Therefore, the development of {110} and {111} facets was promoted under the proposed conditions [138,146,148]. Analogous to MOF-5, the crystal size of ZIF-8 decreased from about 4 μm to about 100 nm when the highest modulator concentration was used [138].

The presence and increasing concentration of surfactant can also provide larger crystals as demonstrated by Umemura *et al.* for $[Cu_3(BTC)_2]_n$ [149]. The direction of coordination bonds between the copper cation and the -COOH groups in the BTC ligand determines the growth of the {111} facets, thus the octahedral morphology. As shown in Fig. 23, the addition of the small amount of lauric acid (LA) resulted in larger crystals with unchanged morphology. The morphological transition to cuboctahedron, truncated cube, and finally to cube (with exposed {100} facets) was observed due to modulation of the thermodynamic stability of the growing facets by larger amounts of LA [149]. Under these conditions, the crystal size increased slightly and then remained almost unchanged. This surfactant not only selectively interacts with the MOF's specific facets but also leads to the alteration of the crystal nucleation rate by forming competitive interactions with the metal precursor, thus additional coordination modulation.

The effect of the surfactant structure – the fact that they contain different "tails", "heads" and sometimes occur as ions – on the MOF's morphology has not been clearly indicated yet. Differences in alkyl chain length and counterion type had no particular effect on ZIF-8 morphology as demonstrated by using cetyltrimethylammonium chloride (CTAC) and trimethylstearylammonium chloride (STAC) were applied instead of CTAB [138]. Despite the use of a surfactant with a significantly different structure - polymeric polyvinylpyrrolidone (PVP) - for the synthesis of MOF-5, a similar effect was obtained as with cationic CTAB, namely, facilitating the growth of the {111} facets and evolved transformation of the morphology from cube to truncated cube, truncated octahedron, and octahedron as the surfactant concentration increased, as shown in Fig. 24 [150]. Moreover, the BET surface area of these structures was also not affected by the morphology, being on the level of 2566–2684 m^2/g for samples with the mentioned shapes[150]. Analogous observations were made for ZIF-8, regardless of morphology, BET surface area remained around 1200 m^2/g [138]. In the case of hierarchical porous framework of Cu-BTC the influence of three different surfactants was investigated [151]. Apart from cationic CTAB, anionic sodium dodecylbenzene sulfonate (SDBS) and non-ionic N, N–dimethyltetradecylamine (N,N) were also utilized. Although octahedral particles of Cu_xO_y@HP–Cu–BTC were obtained for all of three applied surfactants, the size of surface area and size of single crystals were divergent. The highest value of BET surface was reached for non-ionic surfactant (almost 1200 m^2/g), while the values decreased to 817 m^2/g and 620 m^2/g for cationic and anionic surfactants respectively.

In case of bismuth-based MOF – CAU-17 – addition of QAC have influenced the growth speed in different directions. Addition of 25 mg of CTAB to the reaction mixture resulted in the obtainment of 2 μm long solids with hexagonal base instead of plate-shaped morphology [142]. By increasing the amount of surfactant introduced into the reaction environment (keeping the same quantity of linker and metal precursor), the diameter of the particles was decreasing, while at the same time their length was increasing. Thin nanowires of CAU-17 were formed when the amount of CTAB reached 400 mg. Interestingly, no visible change in particle morphology was observed for two other surfactants, namely SDS and PVP, in comparison with the product obtained when no additives were added [142]. However, promotion of growth along different crystallographic axes was also achieved by using additive modulators along with surfactants. For example, the simultaneous application of CTAB and tris(hydroxymethyl)aminomethane (TRIS) to the preparation of ZIF-8 resulted in particles with irregular shapes and higher facet indices, with hexapod (lower concentration of TRIS) or burr puzzles (higher concentration of TRIS) morphology (Fig. 24). These structures reflect the combined interactions of modulators with specific ZIF-8 facets. Unlike CTAB (which, as mentioned above, preferentially adsorbs on {100}), TRIS molecules preferentially stabilize the {111} facet [146]. The BET surface area values of burr puzzles (1282 m^2/g) were only slightly higher compared to cubes (1193 m^2/g). The combination of CTAB and tetrabutylammonium bromide (TBAB) for the synthesis of ZIF-8, on the other hand, in contrast to the above mentioned examples, provided a 3D structure composed of stackable small nanoparticles with

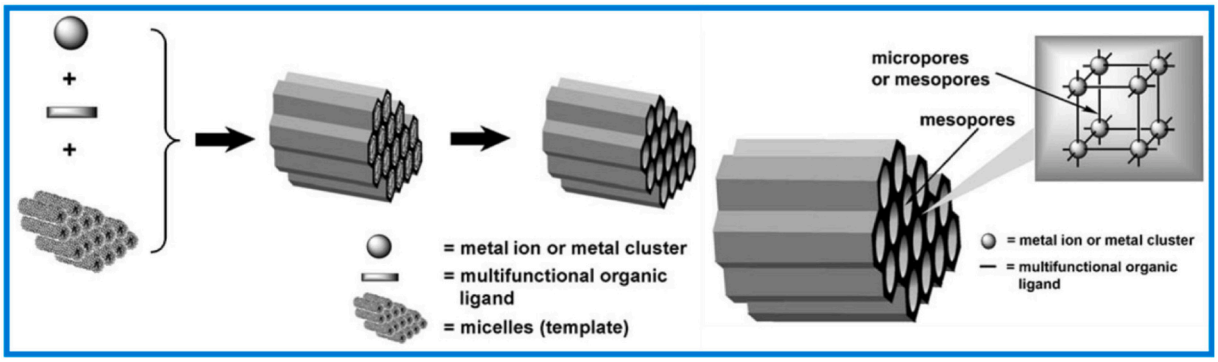

Fig. 26. Formation of mesostructured HKUST-1 by the CTAB templated method (reproduces from [140]).

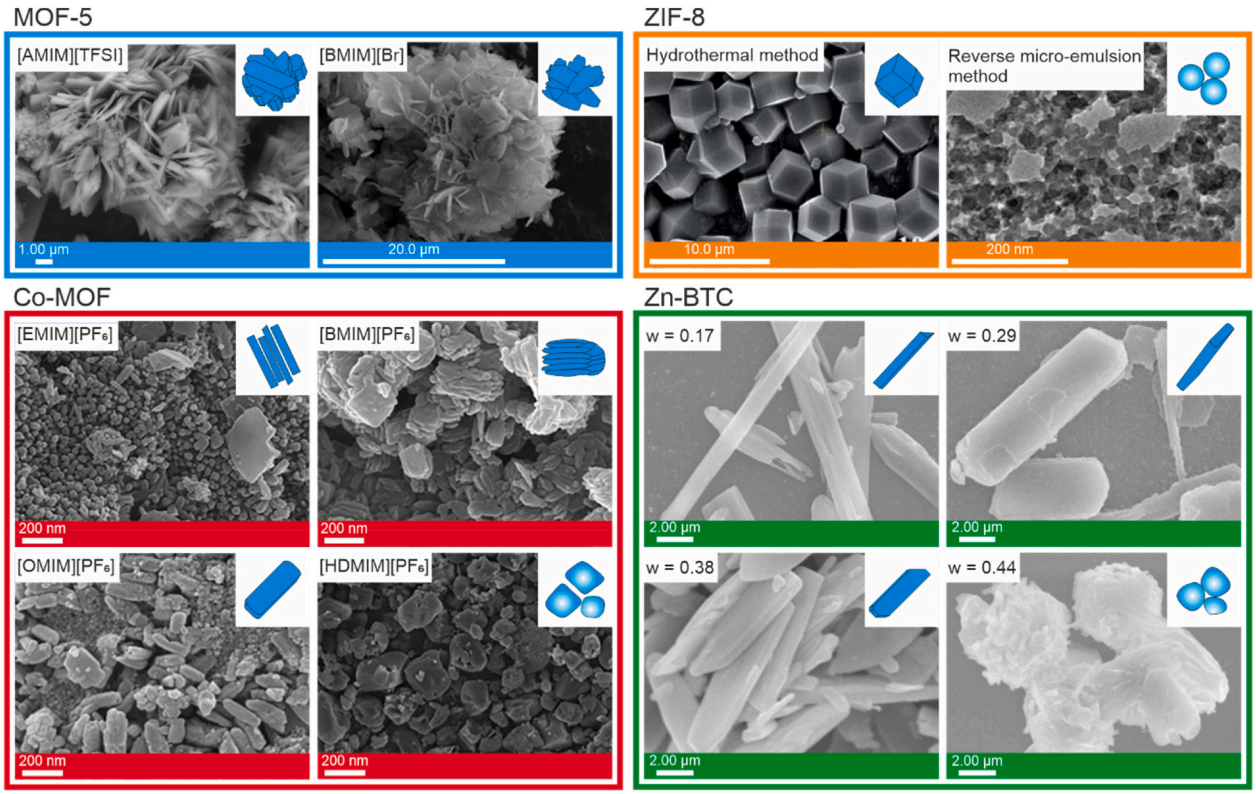

Fig. 27. SEM images of desert-rose like MOF-5 synthesized electrochemically using [AMIM][TFSI] (reproduced from [164]), and [BMIM][Br] as electrolytes (reproduced from [160]); SEM image of rhombic dodecahedron-shaped ZIF-8 synthesized by a hydrothermal method (reproduced from [138]) and TEM image of stackable particles by reverse micro-emulsion route (reproduced from [158]); SEM images of Co-MOFs synthesized with addition of ILs with increasing hydrophobicity (reproduced from [161]); [EMIM][PF_6]: rod-like particles, [BMIM][PF_6]: multilayer nanoplate crystals, [OMIM][PF_6]:rod-like particles, [HDMIM][PF_6]: nano-block crystals; SEM images of Zn-BTC synthesized with different mass fraction of $ZnCl_2$ in glycerol-[DDMIM][Cl] mixed solvents, w -mass fraction of $ZnCl_2$ in glycerol-[DDMIM][Cl] mixed solvents (reproduced from [165]), for increasing w value: needle-like, rod-like, sheet-like, spherical-like particles.

much lower BET surface area (814 m^2/g) [153].

In addition to the capping properties of the surfactants, their ability to selectively direct the structure growth has been also exploited in syntheses targeting the supramolecular template. For example, a CTAB-stabilized reverse microemulsion system was used to prepare Gd-MOF [93,154]. Taylor *et al.* [93] obtained block-like nanostructures of Gd-BHC ($Gd_2(BHC)(H_2O)_6$), that were approximately 25 by 50 by 100 nm in size. The tendency of the product to aggregate was negated by additional PVP coating. Hatakeyama *et al.* [154] also used a surfactant-assisted synthesis method, but, selected hydrotropes (sodium salicylate, 5-methylsalicylic acid, and salicylic acid) were additionally used to induce micelle shape change, thus affecting the morphology of Gd-MOF. According to the literature, incorporation of selected hydrotropes into a CTAB-based microemulsion system can induce a transition from spherical/ellipsoidal to worm-like micelles [155]. This approach was found as a straightforward way to control size of Gd-BDC ($Gd(BDC)_{1.5}(H_2O)_2$), yielding structures with increased length as a function of hydrotrope concentration (Fig. 25). However, the Gd-BTC crystals prepared with a ligand containing three carboxylic groups ($Gd(1,2,4\text{-}BTC)(H_2O)_3H_2O$) and sodium salicylate showed a decrease in the average length and width dimension (Fig. 25) [154].

The formation of hierarchical HKUST-1 structures ($[Cu_3(BTC)_2(H_2O)_3]$) with adjustable porosity was proposed by Qiu *et al.* [140] through MOF self-organization using cylindrical CTAB micelles as a template (Fig. 26). Electrostatic interactions between cationic micelles and deprotonated negatively charged BTC^{3-} ligands probably

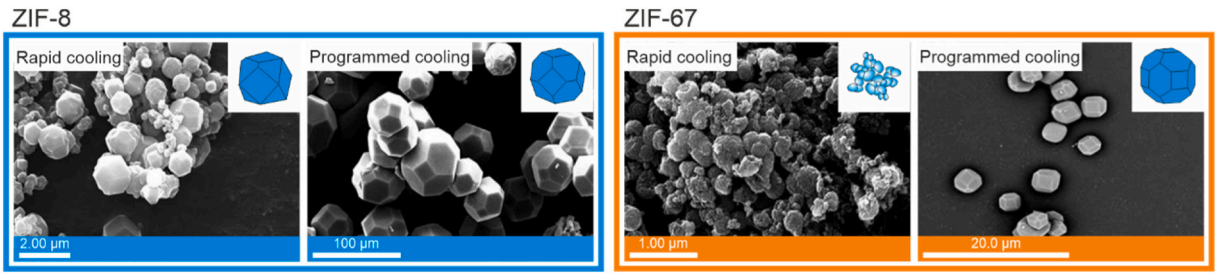

Fig. 28. SEM images of ZIF-8 (cuboctahedron, truncated rhombic dodecahedron) and ZIF-67 (aggregated spherical particles, truncated rhombic dodecahedron) synthesized in [EMIM][Br] (reproduced from [159]).

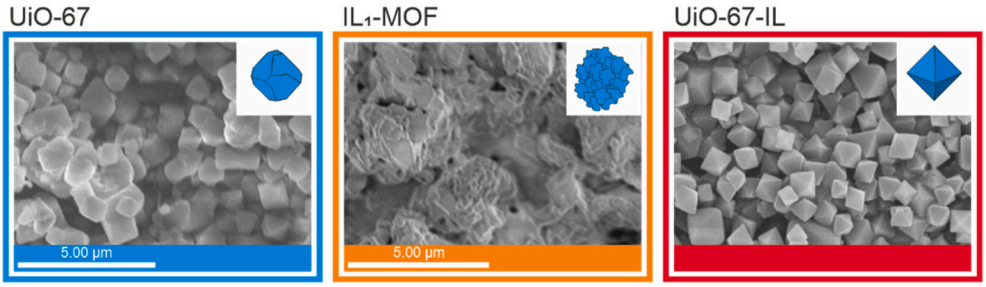

Fig. 29. SEM images of UiO-67-derived MOF obtained by using linkers modified by IL (reproduced from [166] and [155]), from left: distorted octahedrons, irregular structures, octahedrons.

determined the positioning of the MOF building blocks leading to the formation of hierarchical micro- and mesoporous structures. The mesopore walls of HKUST-1 were composed of a microporous framework of a 3D channel system with a pore diameter of 0.82 nm. Increasing the CTAB/Cu^{2+} molar ratio from 0.15 to 0.60 provided an increase in mesopores diameter (from 3.8 to 5.6 nm), which was further reflected in the lower BET specific surface area (decrease from 1225 to 905 m^2/g). Moreover, the expansion of mesopore diameter (even up to 31 nm) was achieved by using 1,3,5-trimethylbenzene (TMB) as a micelle swelling agent [140].

Numerous morphologies of MOFs can be obtained by introducing surfactants into the system and adjusting their amount [146]. The size, shape, porosity and aggregation tendency of the crystals can be altered. A surfactant can simultaneously promote the growth of a particular MOF's facet and inhibit another (*Mechanism III*) [138,143]. In this way, the MOF's morphology control can be realized. The effect of a surfactant type on the MOF's morphology has not yet been clearly determined. Differences in the alkyl chain length and surfactant counterion type had no specific effect. The type of hydrophilic "head" may be the difference due to the different energy of interaction with a particular facet. Long-chain carboxylic acids are a special type of surfactant because not only selectively interacts with specific MOF facets, but also lead to a change in crystal nucleation rates by forming competitive interactions with the metal precursor, thus additional coordination modulation (*Mechanism I*). Control of the morphology of MOF's can also be realized by using surfactants in the aggregated form as a soft template.

4.5. *Effect of ionic liquids*

Consisting of bulky organic cation, small organic or inorganic anion, and having peculiar properties, ionic liquids (ILs) have also found applications in the synthesis of metal-organic frameworks. The reported studies involving ILs as morphology-affecting agents mainly concern the influence on MOFs like UiO-67 [156], HKUST-1 [157], ZIF-8 [158], ZIF-67 [159], MOF-5 [160], MOF-74 [161]. The liquidity over a wide temperature range allows the use of ILs as a solvent or cosolvent in solvothermal/ionothermal synthesis or dispersion components in the (micro)emulsion method [158]. The ionic structure also allows their use as electrolytes in various electrochemical processes, thus replacing completely or partially the commonly used salts and solvents [160]. Post synthetic modification of MOF surfaces with ILs is also popular, especially in the context of modifying sorption properties [162].

During a typical solvothermal process, MOF-5 particles grow as regular cubes (see for example Fig. 22) [144]. Applying an electrochemical approach leads to the formation of spherical shaped particles when a small amount of 1 – butyl-3-methylimidazolium chloride [BMIM][Cl] was added to the reaction medium [163] or flower-shaped structures - shown in Fig. 27 - when 1 – butyl-3-methylimidazolium bromide [BMIM][Br] [160] or 1-allyl-3-methylimidazolium bis(trifluoromethylsulfonyl)imide [AMIM][TFSI] [164] acts as electrolytes. The movement of ions during the process is directed by the electric field mediated by ILs, affecting the morphology of MOF. Moreover, ILs also show structuring ability, a kind of template or the growth of structures that change the orientation of the attached molecules.

Solvent properties of 1-dodecyl-3-methylimidazolium chloride [DDMIM][Cl] in a mixture with glycerol, were analyzed in Zn-BTC synthesis [165]. This time, the morphology transition has been achieved by a change in the mass fraction of the precursor ($ZnCl_2$), thereby the amount of IL in the solvent mixture (Fig. 27). Long needle-like particles were formed when the mass fractionation of $ZnCl_2$ was 0.17. As the zinc salt content increased, and thus the amount of IL decreased, the MOFs expanded toward rod-like (0.29) and plate-like (0.38) shapes. In the presence of relatively least amount of [DDMIM][Cl] (mass fraction 0.44) - only spheres with a rough surface were observed. The higher IL content also resulted in an increase in the crystallinity of the samples. Furthermore, small-angle X-ray scattering (SAXS) analysis confirmed that the shapes of the formed Zn-BTC particles corresponded to those of the supramolecular domains formed by IL during the synthesis process, suggesting that [DDMIM][Cl] acts as a template.

The amphiphilic properties of ILs were utilized in reverse microemulsion system containing water, n-pentanol, n-dodecane, and stabilized by 1-tetradecyl-3-methylimidazole chloride [TDMIM][Cl] to obtain nanometric crystals of ZIF-8 [158]. This method allowed a narrowed range of particles between 15 and 35 nm instead of values

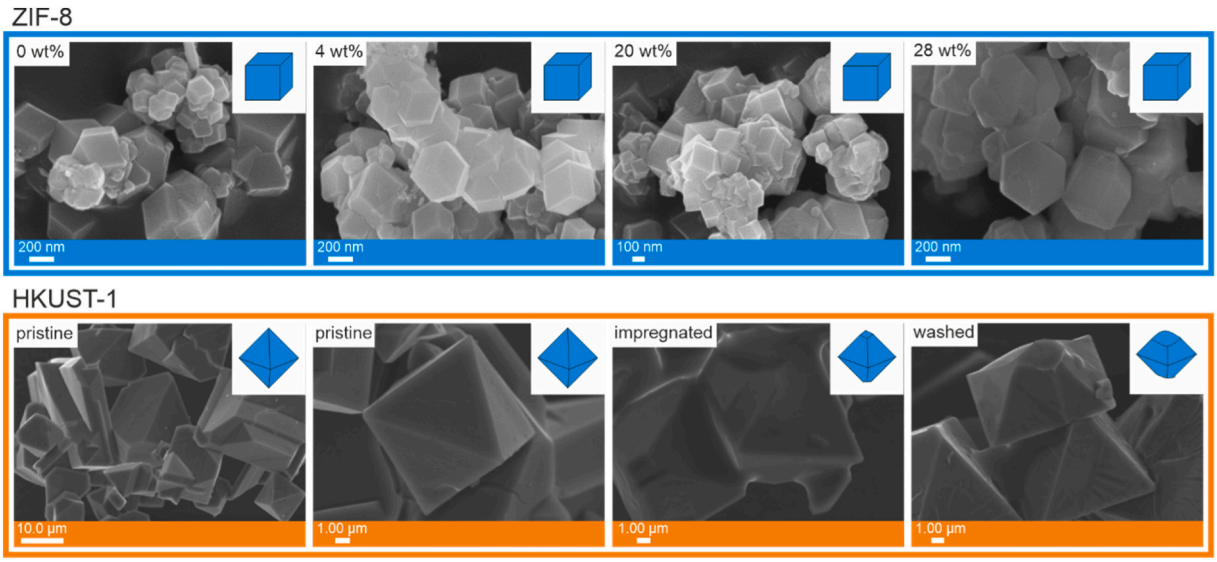

Fig. 30. SEM images of intergrown cubes of ZIF-8 samples impregnated with different amount of [BMIM][BF_4] (reproduced from [168]) and distorted octahedrons of HKUST-1 samples treated with [EMIM][Tf_2N] (reproduced from [157]).

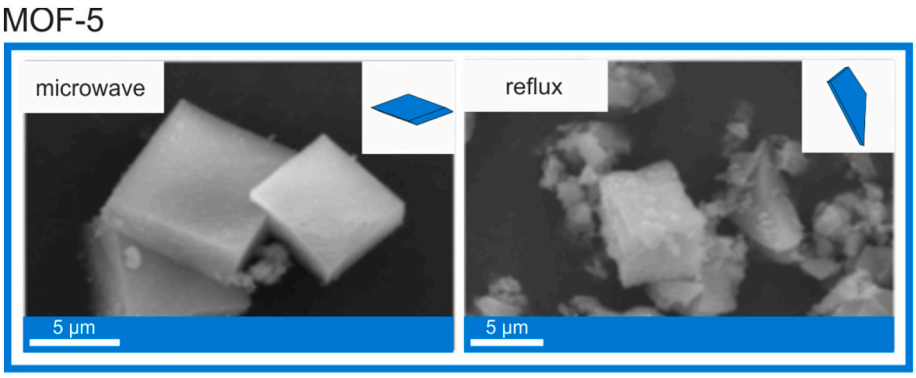

Fig. 31. Cubic morphology of the MOF-5 samples synthesized using microwave at 105 °C for 30 min, and synthesized via traditional reflux route at 105 °C for 4 h (reproduced from [172]).

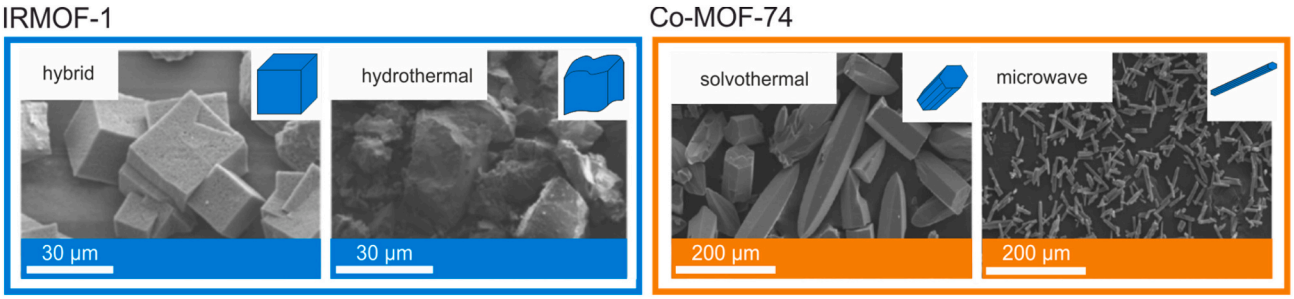

Fig. 32. SEM images of cubic shape of IRMOF-1 synthesized by hybrid (microwave + sonication) and hydrothermal methods (reproduced from [173]); SEM images of hexagonal column structured particles of Co-MOF-74 obtained under conventional solvothermal and microwave assisted solvothermal methods (reproduced from [176]).

exceeding 100 nm in case of typical hydrothermal (Fig. 27) [138] or solvothermal method (see previously shown Fig. 19) [130]. A notable rise of surface area and pore volume can be observed – from 816 m^2/g and 0.1754 cm^3/g for general ZIF-8 to 1477 m^2/g and 0.6181 cm^3/g for nano-ZIF-8 [158]. Moreover, as the alkyl side chain length of IL increases, the expansion of the Co-MOF crystals obtained in the water/DMF emulsion stabilized by Triton TX-100 and selected 1-alkyl-3-methylimidazolium hexafluorophosphates [AMIM][PF_6]) is revealed (Fig. 27). The use of 1-ethyl-3-methylimidazolium hexafluorophosphate [EMIM][PF_6], containing two C atoms, leads to the formation of aggregated, oblong nanoparticles of about 100 nm in length, while 1-hexadecyl-3-methylimidazolium derivative [HDMIM][PF_6] contributes to the formation of individual chunks over 200 nm in wide. It was concluded that ILs containing a short alkyl chain could more tightly surround around polar cores through electrostatic and steric stabilization, whereas ILs with longer substituent adhere less firmly to the crystal

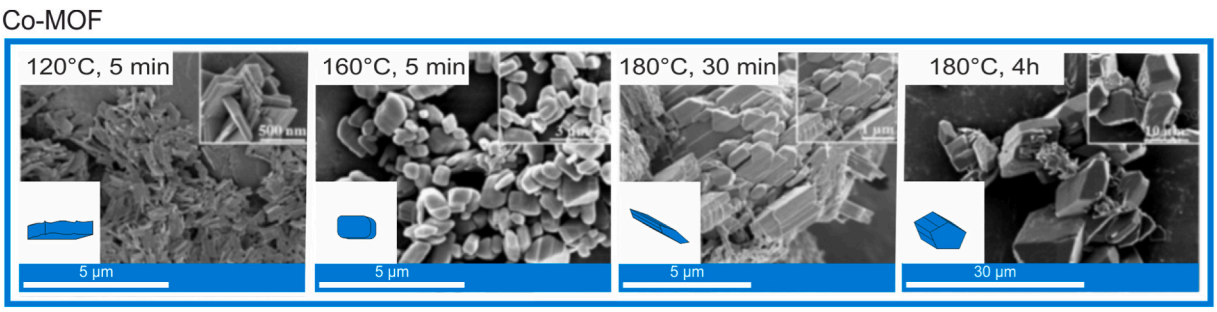

Fig. 33. SEM images of Co-MOF microcrystals obtained by microwave-assisted method in the presence of SDS surfactant (reproduced from [177]). Morphology from left: nanoplates, multilayered microcubes, aggregated nanorods and microrods.

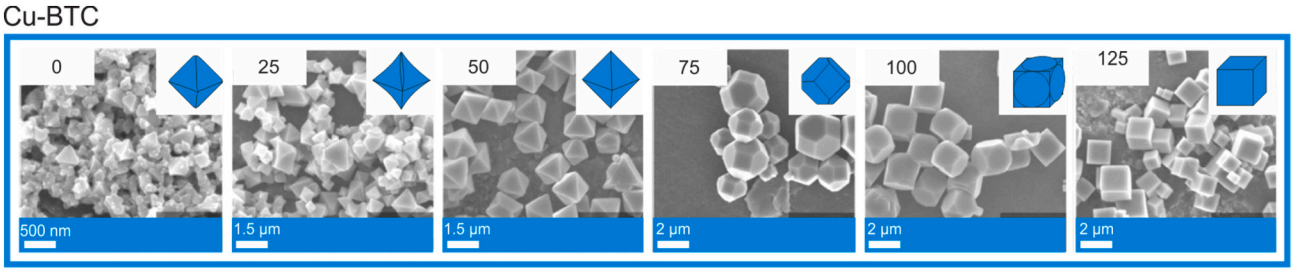

Fig. 34. FESEM images of $[Cu_3(BTC)_2]_n$ synthesized using copper nitrate and lauric acid/BTC different molar ratio; x = [lauric acid]/[BTC] molar ratio, x = 0, 25, 50, 75, 100, and 125 (reproduced from [149]). The first three images show different octahedron morphology, while the other three show different cubes morphology.

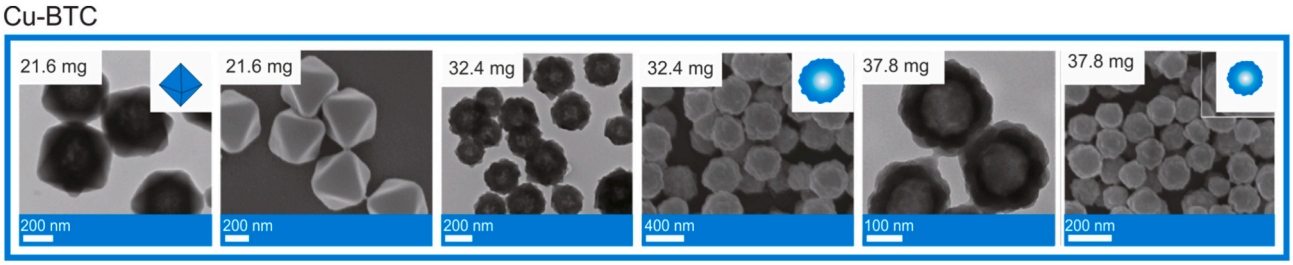

Fig. 35. Selected morphology of $[Cu_3(BTC)_2]_n$ controlled by addition of POM (reproduced from [178]). Morphology from left: octahedron, porous spheres and smaller porous spheres.

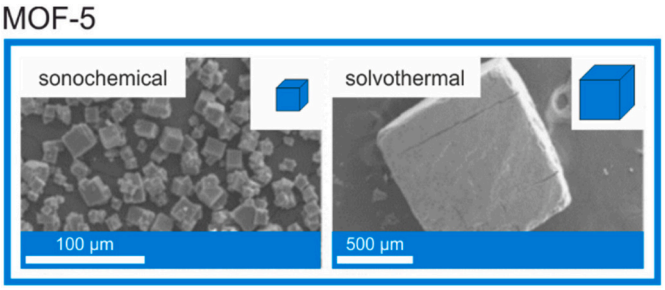

Fig. 36. Comparison of cubic morphology of MOF-5 obtained by sonochemical and solvothermal methods (reproduced from [184]).

surface (*Mechanism III* shown in Fig. 4). The decreasing tendency to form agglomerated structures was also attributed to an increase in the viscosity of the emulsion (caused by the concomitant elongation of IL side chain). Although nanoparticles were obtained by this method, the values of surface area and pores volume were relatively low within the range of 263–628 m^2/g and 0.22–0.31 cm^3/g respectively. This may be explained by residual ILs and surfactants that are difficult to remove from Co-MOF pores and contribute to channel occlusion.

The effect of reactor cooling procedure during formation of ZIF-8 and ZIF-67 by ionothermal method using 1-ethyl-3-methylimidazolium bromide ([EMIM][Br]) was analyzed by Wang *et al.* [159]. The rapid change of temperature resulted in the formation of crystal agglomerates consisting of uneven particle size (Fig. 28), which is the result of simultaneous rapid nucleation and slow crystal growth. Separate, clearly outlined truncated octahedra (typical morphology of these ZIFs) of similar dimensions were obtained when the cooling process was carried out at a certain rate due to the slowing of the nucleation rate and the acceleration of the growth rate. Reduced number of shaping particles reduces the risk of collisions and sticking in agglomerates. The BET surface area was 1428 m^2/g with rapid cooling and 1211 m^2/g with programmed cooling suggesting that no significant amount of IL remained in the pores of ZIF-8.

Syntheses of UiO-67-derived structures containing IL-modified linkers were reported by Xue *et al.* [166] and Ding *et al.* [155]. Shown in Fig. 29 IL_1MOF was obtained by bonding 1-(1-methyl-3-imidazolio)-propane-3-sulfonate zwitterion with 4,4′-biphenyl-dicarboxylate acid (H_2BPDC) and incorporation of this linker into MOF containing Zr^{4+} nodes during typical solvothermal reaction. The structure of IL_1MOF was confirmed by powder X-ray diffraction to be analogous with UiO-67 (a MOF with H_2BPDC linker), however the structure changed from individual UiO-67 crystals to intergrown aggregates of crystals with lower

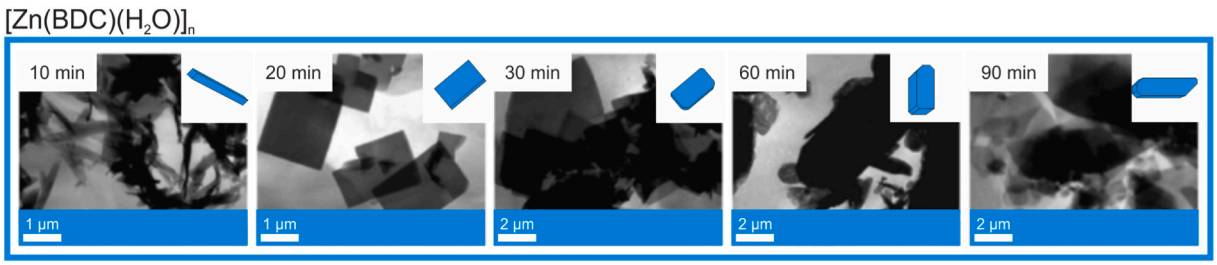

Fig. 37. Morphology changes of $[Zn(BDC)(H_2O)]_n$ structures synthesized for various reaction times (reproduced from [185]). Morphology from left: nanobelts, nanosheets, oval nanosheets, microcrystals and irregular nanosheets.

BET surface area. However, incorporation of an imidazolium-derived linker containing a shorter side chain, regular octahedral shape of IL-modified MOF particles was obtained [155].

With reference to the above examples, another approach can also be taken to use ILs in synthesizing MOFs, namely dipping and soaking the MOFs in a solution containing ILs (impregnation or encapsulation). IL simply penetrates the pores of the MOFs, as evidenced by the reduced surface area values. However, after subsequent washing procedures, only a thin layer or trace amounts of ILs remain on the surface of MOFs, which do not necessarily significantly reduce the surface development. This method affects properties such as ionic conductivity [167], gas separation abilities [162,168], adhesive abilities [157] or chemical and thermal stability [169], but is not supposed to significantly change the morphology of the structure (Fig. 30). However, de Trindade *et al.* reported that impregnation of UiO-66 with following ILs - 3-triethylammonium propane sulfonic hydrogensulfate TEA-[PS][HSO_4], 1-butylimidazole hydrogensulfate [BIM][HSO_4] and 1-butyl-3-methylimidazolium hydrogensulfate [BMIM][HSO_4] - results in partial separation of agglomerated particles and slight enlargement of single cubes [169]. It has been observed that an increase in the amount of these ILs is associated with a concomitant decrease in the pH of the reaction medium, allowing them to act as structural modulators.

The effect of ionic liquids based on 1-alkyl-3-methylimidazolium cations combined with halide anions on the structure and properties of MOFs is most commonly discussed in the literature [160,163,165]. The ILs can play an important role both during and after MOFs synthesis as summarized below. Primarily, ILs can be utilized as a reaction medium - individual or co-solvent [159,170], emulsion phase [158,161] or electrolyte [160,164]. Thereby, ionic liquids can significantly influence the shape of the product [163,165]. Their high viscosity makes particle movement much more difficult, and steric stabilization prevents aggregation, thus limiting the size of the MOF. Meanwhile, encapsulation [157,169] or linker's modification - performed pre- [155,166] or post-synthetically [166,171] - are reported to improve physicochemical properties of MOFs and influence the specific surface area without significant change of morphology. In many cases significantly decreased values of surface area can be observed for samples synthesized/treated with ILs because IL's ions occupy the open pores of MOF [161,166].

4.6. *Effect of microwave*

Microwave is an electromagnetic radiation with frequency shifting from 300 MHz to 600 GHz and could be combined with known synthesis strategy to shorter preparation time due to interaction of electromagnetic waves with polar solvents and/or ions in reaction environment. Lu *et al.* [172] reported microwave assisted solvothermal synthesis of MOF-5 and revealed that 30 min of reaction was sufficient to obtain the product. Obtained MOF-5 were cubic in shape with dimensions in the range of 5–10 μm and had more uniform and structured morphology (Fig. 31), than structures obtained by standard refluxing method, which required more than 4 h of conducting the reaction. In the work [30], the effect of various parameters of microwave synthesis of MOF-5 such as microwave power, irradiation time, temperature, solvent concentration, and substrate composition on the morphology of MOF-5 were examined. Using a microwave MOF-5 had morphology of single phase cubic crystals 20–25 μm in size, which was 20 times smaller than the same materials obtained using conventional convection heating (ca. 500 μm). The increase in temperature, power level and substrate concentration mainly promoted the reduction of synthesis time and improvement of crystal quality. With the lengthening of the reaction time, the quality of the crystals deteriorated and more surface defects were formed, but the cubic morphology was preserved.

Combination of microwave with sonification provided similar results [173]. MOF-5 structures were obtained with the morphology of typical cubic crystals (approximate dimensions of 5–15 μm), however, a more regulated cubic shape compared to those synthesized by classical hydrothermal synthesis (Fig. 32). Furthermore, approximately 10 times reduction in particle size was also observed for MOF-5 materials obtained by hybrid approach. Further reduction in particle size was possible through increasing ultrasonic bath temperature and sonication time. Such observation is common among crystals synthesized with the assistance of microwave or ultrasonic energy, where application of those methods promotes uniform and fast nucleation [174,175].

In other work [176], application of microwaves caused significantly smaller hexagonal column structured particles of Co-MOF-74 than the same materials obtained under conventional solvothermal method. Conventional solvothermal method enabled formation of particles with dimension such as approximately 300 μm long and 70 μm wide, while particles synthesized under microwave assisted solvothermal route were approximately 50 μm long and 8 μm wide (Fig. 32), which was observed due to limitation of particle growth by short reaction time, while nucleation is not hindered.

On the other hand, under the microwave conditions of synthesis, the addition of e.g. surfactants affected the morphology of MOFs. Microwaves and presence of surfactants had a pronounced effect on the size and morphology of MOFs. It was found that the surface layers of the crystals could incorporate the surfactants, provided that there was a degree of complementarity between the charge and size of the guest ions and interstices in the structure of the crystal boundary layers [177]. Furthermore, studying the microwave synthesis parameters (temperature and time) with the presence of surfactants enabled MOFs morphology transformation. With the increase of temperature from 120 to 160 °C and time from 5 to 30 min and presence of SDS, transformation of Co-MOF nanosheets/nanoplates into larger multilayered microcubes was observed (Fig. 33). When the temperature and reaction time reached 180 °C and 30 min growth of the microcubes into larger microcrystals was observed. The addition of the CTAB surfactant and changing temperature from 120 to 160 °C and time from 5 to 30 min caused differences in the size and morphology of the Co-MOFs, namely morphology varied from small nanosheets to the layered microrods. The application of P123 surfactant during this synthesis method yielded aggregated nanorods. Importantly, MOFs synthesized with the addition of a surfactant had highly porous nanostructures, whereas samples synthesized without a surfactant had less porous nanostructures.

Table 3
Summary of factors, their effect on the MOFs' morphology and correlation with the mechanisms responsible for morphology control.

Factor	MOFs feature	The most probable type of mechanism controlling morphology
Effect of pH of the reaction environment		
pH of reaction mixture (alkaline modulator)	size shape	deprotonation of the linker according to *Mechanism II*, acceleration of the crystal's nucleation rate, slowing the growth phase,
pH of reaction mixture (acidic modulator)	shape	protonation of the linker according to the protonation/deprotonation mechanism (*Mechanism II*),
appropriate acid–base equilibrium	crystals of the desired shape	adjusting the nucleation rate, formation of the thermodynamically favorable MOF crystals of the desired shape,
unsuitable alkalinity/acidity of the reaction system	reappearance of larger crystals, formation of amorphous materials, decrease of the crystal anisotropy, change of the specific MOF structure to other phase structures, formation of infinite coordination polymer particles,	affecting the crystallization rate,
small amount of alkaline modulator	size, morphology of the crystals not affected,	deprotonation of the linker according to *Mechanism II*, acceleration of the crystal's nucleation rate, prevention of aggregation,
too high pH of the system (too much alkaline modulator)	lower crystallinity, disordered structure, larger size	competition of the modulators and linkers for coordination to metal ions (*Mechanism I*), accompanied by an extremely fast nucleation rate,
pH of the etchant solution	surface area surface defects	wet chemical etching
alkaline modulator	change in the dimensions of the crystals (e.g. bigger crystals leading to narrower size distribution.)	due to changes in the supersaturation of the reaction solution after the addition of the alkaline modulator (e.g. relatively slow nucleation is followed by fast particle growth,
acidic modulator (organic)	size	capping ability (mode of action similar to *Mechanism III*)
Functionality of the additive		
modulator with the same functionality as linker	size – smaller particles shape	competition of the modulators and linkers for coordination to metal ions (*Mechanism I*), improvement of crystallinity, prevention of aggregation,
simultaneous modulation by additives with different functionalities (both acidic and basic)	shape	competition of the modulators and linkers for coordination to metal ions (*Mechanism I*) resulting in growth in certain direction,
Temperature		
changes of the temperature conditions	gradual/smooth or sudden change of shape, thickness, size, the surface area, or the porosity of the structure	changes in kinetics of particle nucleation and growth,
higher temperature	particle size; surface area; increase in the the amount of impurities; smoother the edges; smaller surface area; possible shape change;	faster nucleation (more and smaller crystallites); easier to exceed the activation energy of product formation; lowering of solution viscosity (faster diffusion);
too high temperature	shape deformation	smoothing the edges
lower temperature	size; surface area: polydisperse crystals;	slower nucleation; stimulation of crystal growth;
rate of cooling	shape	control of crystal growth kinetics;
Solvent		
solvent (general)	shape	solvent molecules can take part in the coordination of metal ions; different solubility of precursors in solvents or mixture of solvents; solvent can affect the way the linker is coordinated with the metal;
solvent (general)	size of channel, pore size/volume	solvent molecules can be guests in the pores;
solvent (general)	size	polarity
solvent concentration	size defects	rate of crystallization;
Specific solvent DMF		during heating, DMF decomposes into dimethylamine, and formic acid; dimethylamine deprotonates linker (*Mechanism II*), which interact with metal ions to form SBUs and bonds between these MOFs fragments; formic acid acts as a modulator (*Mechanism I*) of the resulting backbone;

(*continued on next page*)

Table 3 (*continued*)

Factor	MOFs feature	The most probable type of mechanism controlling morphology
Precursor		
type of precursor salt	shape, size of crystals	reactivity of these salts (soft acid M^{n+} and hard or soft base)
molar ratios of two metals' cations that form MOFs	shape of MOFs	affinity/competition to react with linker
Surfactant		
type of surfactants	size, shape, porosity and aggregation tendency of the crystals	*Mechanism III* stabilizing surface atoms and lowering their surface energy; formation of a physical barrier to atom deposition/diffusion which affects the kinetics of crystal growth; simultaneous promotion of growth of a particular MOF's facet and inhibition of another;
surfactant functionality (-COOH group)	size, shape	changing the crystal nucleation rate by forming competitive interactions with the metal precursor (*Mechanism I*);
concentration of surfactants	shape aspect ratio	*Mechanism III* modulation of the thermodynamic stability of the growing facets (selective interaction with the MOF's specific facets) different growth speed in different directions
concentration of surfactants	size shape	aggregation, formation of the soft templates (micelles, microemulsions) for MOF's growth
type and concentration of surfactants	hierarchical structure	through MOF self-organization using surfactant micelles
Ionic liquids		
ionic liquid type	shape	structuring activity, template for MOF's growth,
ionic liquid type	size shape	surface activity, thereby stabilization of microemulsion
ionic liquid concentration		template for MOF's growth,
ionic liquid	less agglomerated structures size	high viscosity of ILs makes particle movement much more difficult, steric stabilization, electrostatic stabilization,
Method of energy supply		
microwave	more uniform and structured morphology	uniform and fast nucleation
microwave	size	limitation of particle growth by short reaction time
prolonged application of microwave	defect formations morphology distortion	regulation of kinetics of nucleation and growing process (*Mechanism IV*);
ultrasounds	size	promoting fast nucleation; affecting nucleation due to extremely local temperature and pressure
ultrasound irradiation time	shape size	extended time causes one structure transformation into other structure due to weak binding interactions between 2D coordination polymers

In some cases, the modulator's effect is only visible under microwave assisted synthesis conditions. Umemura *et al.* [149] reported control over the morphology by applying different amounts of lauric acid (LA) playing the role of the modulator under microwave conditions. Increase in concentration of the modulator resulted in transformation of $[Cu_3(BTC)_2]n$ morphology from octahedron through cuboctahedron to cube as shown in Fig. 34. They also studied the mechanism of presented morphology transformation by coarse-grain modeling. It was proposed that modulator was acting as a growth-blocking agent on the site type FOUR, which led to the lowered crystal growth in the (100) directions, while preorganized SBU were controlled by the modulator concentration which influenced on the reaction kinetics in the form of creation of coordination bond between copper and BTC oriented in the (111) directions. As a result of faster reaction of BTC from copper complexes in comparison with copper nitrate the growth in the (111) directions was accelerated, which caused formation of (100) facets.

Xu et al. [178] proposed the method of controlling the morphology of $[Cu_3(BTC)_2]_n$ by using polyoxometalates as coordination modulators. It was found that without or low addition of polyoxometalates (POMs) to the reaction medium caused formation of ill-defined worm-like particles. With increasing amounts of sodium phosphotungstate (NaPW) morphology of $[Cu_3(BTC)_2]_n$ turned firstly to nanooctahedrons and through solid octahedral with different truncated degree to even hierarchical spheres (Fig. 35). They also studied the role of POM in morphology change. Without or small addition of POM caused poor kinetic control over large quantities of free metal cations and organic ligands in the reaction environment. With the proper amount of coordination modulator separation of nucleation and growth processes was achieved. During microwave-assisted synthesis, acidic modulators can also be used as modulators, such as formic, acetic, nitic, hydrochloric, citric, succinic, dichloroacetic and propionic acid, which also affect the shape and size of MOFs [179,180].

Ma et al. [181] proposed microwave synthesis of MIL-88B-Fe and NH_2-MIL-88B and by changing the reaction conditions, the morphology variation was achieved. They studied the influence of time, temperature and mother solution concentration on morphologies of MIL-88B-Fe. In this case, an increase of reaction time did have influence on the MIL-88B-Fe morphology while increasing the synthesis temperature improved yield and the crystallinity of MOFs. Small variations of crystal size and morphology were observed with changing $Fe^{3+}/H_2BDC/DMF$ molar.

Microwave assistance during MOFs synthesis can influence not only on mentioned above aspects but also on the yield of synthesis. Liu et al. [182] found that the yield of microwave synthesis of Zr-fum-fcu-MOF is higher compared with the yield of solvothermal synthesis (applying the same temperature and modulator amount while the microwave

synthesis time was reduced to 1 h).

Concluding, microwaves are employed mostly to shorten reaction time, since prolonged application of microwaves resulted in defect formations and morphology distortion of MOFs. Shape and size of MOFs could be controlled by jointly usage of microwave with other factors, e. g. surfactants or other additives.

4.7. Effect of ultrasounds

Ultrasounds are sound waves with frequencies greater than 20 kHz and inaudible for humans and could be another form of energy supplied to the reaction system to realize synthesis of materials including MOFs. Application of ultrasounds during synthesis resulted in extremely high local temperature and pressure generated in liquid phase (~5000 K and over 1000 atm) due to cavitation phenomena, thus synthesis could be realized in a short period of time but in extreme conditions. Ultrasonic power, reaction time and temperature could affect the morphology and size of the MOFs crystal [183]. Son et al. proposed synthesis of MOF-5 using a sonochemical method, which allowed the synthesis of this MOF in a shorter time (ca. 30 min) when compared with conventional solvothermal synthesis (24 h) [184]. More importantly, the use of the sonochemical method influenced the morphology of synthesized cubic crystals of MOF-5. Cubic crystals of MOF-5 obtained by sonochemical method had the size of 5–25 μm, which was approximately 60 times smaller than MOF-5 synthesized using solvothermal synthesis (ca. 900 μm) (Fig. 36).

Studying the ultrasound irradiation time by Li et al. [185] enabled to obtain MOF-1 $[Zn(BDC)(H_2O)]_n$ with different morphologies, i.e. nanobelts, nanosheets, and microcrystals as shown in Fig. 37. Nanobelts 150–300 nm wide and 2–5 μm long were obtained by running the reaction for 10 min. Increasing the reaction time to 20 min led to formation of nanosheets with a morphology of regular squares ranging in size from 500 nm to 2 μm. Further increasing the reaction time to 60 min caused the formation of microcrystals with up to 10 μm in size instead of nanosheets. Further extension of the reaction time to 90 min again allowed the formation of nanosheets, but of irregular size and shape. It has been proposed that prolonged ultrasonic time causes microcrystals to be destroyed and transformed into nanosheets due to weak binding interactions between 2D coordination polymers.

Khan and Jhung [122] studied the $Cu_3(BTC)_2(H_2O)_3$ morphology in relation to the environment and parameters of ultrasound synthesis. Small and homogeneous structures can be obtained in a short reaction time of 1 min. Further increase in synthesis time to 60 min caused aggregation of particles. They also reported about the role of DMF contents in the solvent system during the synthesis, where too much DMF addition influenced the aggregation of Cu-BTC crystals due to condensation of terminal functional group of Cu-BTC crystals while with too low DMF concentration formation of Cu-BTC is reduced due to surely low deprotonation rate. MOF obtained by ultrasonic radiation had higher surface area and pore volume, and smaller particles compared to conventional heating or microwave synthesis, even performed at higher temperature, but without addition of DMF. Jung et al. [186] also compared properties of MOF-177 synthesized by using sonochemical and microwave methods. Sonochemical route enabled formation of crystals in the size range of 5–20 μm while crystals from microwave synthesis under similar conditions had 5–50 μm and exhibited inferior crystallinity. The latest research also confirms the above-mentioned effects of ultrasound-assisted synthesis on the rate of synthesis, morphology and other properties (e.g. higher BET surface area, higher defect-site contents, smaller particle size and higher porosity) [187–190].

5. Conclusions

A constantly growing number of papers on the preparation of MOFs, both new MOFs, obtained by a new approach in synthesis route or just for new application, requires the organization of knowledge in the field of control of their morphology throughout the synthesis path. Mostly, MOFs are obtained using solvothermal synthesis or temperature-mediated synthesis in solvents and these access allows to affect shape, size, porosity through careful control of reaction mixture content (precursors types, amounts, ratio, solvent types and ratio, and other additives) and synthesis parameters (temperature, heating rate and duration, heating source, *etc*.). Table 3. organizes and summarizes mechanisms employed in the morphology control, as well as, factors affecting MOFs morphology, which are discussed in our manuscript and are evidenced in available literature. In the synthesized process, the morphologies of MOF materials were adjusted through synergistic effects of the solvents, surfactants and concentrations *etc*.

Concluding, the review presents main mechanisms describing formation of MOFs during synthesis and affecting their final morphology. We are convinced that better understanding of these mechanisms and synthesis of MOFs with desired morphology brings us closer to controlling other features – depending on the morphology- and will be useful for the design of MOFs.

Declaration of Competing Interest

None.

Acknowledgment

This research was supported by the Polish National Science Center under the grant 2021/41/B/ST4/00849.

References

[1] Yaghi OM, Kalmutzki MJ, Diercks CS. Introduction to reticular chemistry: metal-organic frameworks and covalent organic frameworks. Wiley 2019. https://doi.org/10.1002/9783527821099.
[2] Moghadam PZ, Li A, Wiggin SB, et al. Development of a Cambridge structural database subset: a collection of metal-organic frameworks for past, present, and future. Chem Mater 2017;29(7):2618–25. https://doi.org/10.1021/acs.chemmater.7b00441.
[3] Furukawa H, Ko N, Go YB, et al. Ultrahigh porosity in metal-organic frameworks. Science 2010;329(5990):424–8. https://doi.org/10.1126/science.1192160.
[4] Furukawa H, Go YB, Ko N, et al. Isoreticular expansion of metal-organic frameworks with triangular and square building units and the lowest calculated density for porous crystals. Inorg Chem 2011;50(18):9147–52. https://doi.org/10.1021/ic201376t.
[5] Hönicke IM, Senkovska I, Bon V, et al. Balancing mechanical stability and ultrahigh porosity in crystalline framework materials. Angew Chem Int Ed 2018;57(42):13780–3. https://doi.org/10.1002/anie.201808240.
[6] Healy C, Patil KM, Wilson BH, et al. The thermal stability of metal-organic frameworks. Coord Chem Rev 2020;419:213388. https://doi.org/10.1016/j.ccr.2020.213388.
[7] Sumida K, Rogow DL, Mason JA, et al. Carbon dioxide capture in metal-organic frameworks. Chem Rev 2012;112(2):724–81. https://doi.org/10.1021/cr2003272.
[8] Ghanbari T, Abnisa F, Wan Daud WMA. A review on production of metal organic frameworks (MOF) for CO2 adsorption. Sci Total Environ 2020;707:135090. https://doi.org/10.1016/j.scitotenv.2019.135090.
[9] Rogge SMJ, Bavykina A, Hajek J, et al. Metal-organic and covalent organic frameworks as single-site catalysts. Chem Soc Rev 2017;46(11):3134–84. https://doi.org/10.1039/c7cs00033b.
[10] Pascanu V, González Miera G, Inge AK, Martín-Matute B. Metal-organic frameworks as catalysts for organic synthesis: a critical perspective. J Am Chem Soc 2019;141(18):7223–34. https://doi.org/10.1021/jacs.9b00733.
[11] Wang Q, Astruc D. State of the art and prospects in metal-organic framework (MOF)-based and MOF-derived nanocatalysis. Chem Rev 2020;120(2):1438–511. https://doi.org/10.1021/acs.chemrev.9b00223.
[12] Yuan G, Tan L, Wang P, et al. MOF-COF composite Photocatalysts: design, synthesis, and mechanism. Cryst Growth Des 2022;22(1):893–908. https://doi.org/10.1021/acs.cgd.1c01071.
[13] Kang Z, Fan L, Sun D. Recent advances and challenges of metal-organic framework membranes for gas separation. J Mater Chem A 2017;5(21):10073–91. https://doi.org/10.1039/c7ta01142c.
[14] Li JR, Sculley J, Zhou HC. Metal-organic frameworks for separations. Chem Rev 2012;112(2):869–932. https://doi.org/10.1021/cr200190s.
[15] Kreno LE, Leong K, Farha OK, Allendorf M, Van Duyne RP, Hupp JT. Metal-organic framework materials as chemical sensors. Chem Rev 2012;112(2):1105–25. https://doi.org/10.1021/cr200324t.

[16] Li HY, Zhao SN, Zang SQ, Li J. Functional metal-organic frameworks as effective sensors of gases and volatile compounds. Chem Soc Rev 2020;49(17):6364–401. https://doi.org/10.1039/c9cs00778d.

[17] Han B, Ou X, Zhong Z, et al. Photoconversion of anthropogenic CO2 into tunable syngas over industrial wastes derived metal-organic frameworks. Appl Catal Environ 2021;283:119594. https://doi.org/10.1016/j.apcatb.2020.119594.

[18] So MC, Wiederrecht GP, Mondloch JE, Hupp JT, Farha OK. Metal-organic framework materials for light-harvesting and energy transfer. Chem Commun 2015;51(17):3501–10. https://doi.org/10.1039/c4cc09596k.

[19] Simon-Yarza T, Mielcarek A, Couvreur P, Serre C. Nanoparticles of metal-organic frameworks: on the road to in vivo efficacy in biomedicine. Adv Mater 2018;30 (37):1707365. https://doi.org/10.1002/adma.201707365.

[20] Sun Y, Zheng L, Yang Y, et al. Metal–organic framework nanocarriers for drug delivery in biomedical applications. Nano-Micro Lett 2020;12(1):103. https://doi.org/10.1007/s40820-020-00423-3.

[21] Work WJ, Horie K, Hess M, Stepto RFT. Definitions of terms related to polymer blends, composites, and multiphase polymeric materials (IUPAC recommendations 2004). Pure Appl Chem 2004;76(11):1985–2007. https://doi.org/10.1351/pac200476111985.

[22] Pokropivny VV, Skorokhod VV. Classification of nanostructures by dimensionality and concept of surface forms engineering in nanomaterial science. Mater Sci Eng C 2007;27(5-8 SPEC. ISS):990–3. https://doi.org/10.1016/j.msec.2006.09.023.

[23] McGuire CV, Forgan RS. The surface chemistry of metal-organic frameworks. Chem Commun 2015;51(25):5199–217. https://doi.org/10.1039/c4cc04458d.

[24] Lin Y, Wan H, Wu D, et al. Metal–organic framework hexagonal nanoplates: bottom-up synthesis, topotactic transformation, and efficient oxygen evolution reaction. J Am Chem Soc 2020;142(16):7317–21. https://doi.org/10.1021/jacs.0c01916.

[25] Man P, He B, Zhang Q, et al. A one-dimensional channel self-standing MOF cathode for ultrahigh-energy-density flexible Ni-Zn batteries. J Mater Chem A 2019;7(48):27217–24. https://doi.org/10.1039/c9ta11759h.

[26] Benoit V, Pillai RS, Orsi A, et al. MIL-91(Ti), a small pore metal-organic framework which fulfils several criteria: An upscaled green synthesis, excellent water stability, high CO2 selectivity and fast CO2 transport. J Mater Chem A 2016;4(4):1383–9. https://doi.org/10.1039/c5ta09349j.

[27] Cheng XM, Dao XY, Wang SQ, Zhao J, Sun WY. Enhanced photocatalytic CO2 reduction activity over NH2-MIL-125(Ti) by facet regulation. ACS Catal 2021;11 (2):650–8. https://doi.org/10.1021/acscatal.0c04426.

[28] Liu C, Lin L, Sun Q, et al. Site-specific growth of MOF-on-MOF heterostructures with controllable nano-architectures: beyond the combination of MOF analogues. Chem Sci 2020;11(14):3680–6. https://doi.org/10.1039/d0sc00417k.

[29] Kim JO, Min KI, Noh H, Kim DH, Park SY, Kim DP. Direct fabrication of free-standing MOF superstructures with desired shapes by micro-confined interfacial synthesis. Angew Chem Int Ed 2016;55(25):7116–20. https://doi.org/10.1002/anie.201601754.

[30] Choi JS, Son WJ, Kim J, Ahn WS. Metal-organic framework MOF-5 prepared by microwave heating: factors to be considered. Microporous Mesoporous Mater 2008;116(1–3):727–31. https://doi.org/10.1016/j.micromeso.2008.04.033.

[31] Zhao Y, Cai W, Chen J, Miao Y, Bu Y. A highly efficient composite catalyst constructed from NH2-MIL-125(Ti) and reduced graphene oxide for CO2 photoreduction. Front Chem 2019:7. https://doi.org/10.3389/fchem.2019.00789.

[32] Qin L, Zhao S, Fan C, Ye Q. A photosensitive metal–organic framework having a flower-like structure for effective visible light-driven photodegradation of rhodamine B. RSC Adv 2021;11(30):18565–75. https://doi.org/10.1039/D1RA02746H.

[33] Liseev T, Howe A, Hoque MA, Gimbert-Suriñach C, Llobet A, Ott S. Synthetic strategies to incorporate Ru-terpyridyl water oxidation catalysts into MOFs: direct synthesis: vs. post-synthetic approach. Dalton Trans 2020;49(39):13753–9. https://doi.org/10.1039/d0dt01890b.

[34] Huang C, Liu R, Yang W, Li Y, Huang J, Zhu H. Enhanced catalytic activity of MnCo-MOF-74 for highly selective aerobic oxidation of substituted toluene. Inorg Chem Front 2018;5(8):1923–32. https://doi.org/10.1039/c8qi00429c.

[35] Pang M, Cairns AJ, Liu Y, Belmabkhout Y, Zeng HC, Eddaoudi M. Synthesis and integration of Fe-soc-MOF cubes into colloidosomes via a single-step emulsion-based approach. J Am Chem Soc 2013;135(28):10234–7. https://doi.org/10.1021/ja403994u.

[36] Schoedel A, Li M, Li D, O'Keeffe M, Yaghi OM. Structures of metal-organic frameworks with rod secondary building units. Chem Rev 2016;116(19): 12466–535. https://doi.org/10.1021/acs.chemrev.6b00346.

[37] Bétard A, Fischer RA. Metal-organic framework thin films: from fundamentals to applications. Chem Rev 2012;112(2):1055–83. https://doi.org/10.1021/cr200167v.

[38] Mancuso JL, Mroz AM, Le KN, Hendon CH. Electronic structure modeling of metal-organic frameworks. Chem Rev 2020;120(16):8641–715. https://doi.org/10.1021/acs.chemrev.0c00148.

[39] Zhang W, Xiong RG. Ferroelectric metal-organic frameworks. Chem Rev 2012; 112(2):1163–95. https://doi.org/10.1021/cr200174w.

[40] Cui Y, Yue Y, Qian G, Chen B. Luminescent functional metal-organic frameworks. Chem Rev 2012;112(2):1126–62. https://doi.org/10.1021/cr200101d.

[41] Jiang J, Yaghi OM. Brønsted acidity in metal-organic frameworks. Chem Rev 2015;115(14):6966–97. https://doi.org/10.1021/acs.chemrev.5b00221.

[42] Lim DW, Kitagawa H. Proton transport in metal-organic frameworks. Chem Rev 2020;120(16):8416–67. https://doi.org/10.1021/acs.chemrev.9b00842.

[43] Xie LS, Skorupskii G, Dincă M. Electrically conductive metal-organic frameworks. Chem Rev 2020;120(16):8536–80. https://doi.org/10.1021/acs.chemrev.9b00766.

[44] Liu X, Wang X, Kapteijn F. Water and metal-organic frameworks: from interaction toward utilization. Chem Rev 2020;120(16):8303–77. https://doi.org/10.1021/acs.chemrev.9b00746.

[45] Terzopoulou A, Nicholas JD, Chen XZ, Nelson BJ, Pane S, Puigmartí-Luis J. Metal−organic frameworks in motion. Chem Rev 2020;120(20):11175–93. https://doi.org/10.1021/acs.chemrev.0c00535.

[46] Horcajada P, Gref R, Baati T, et al. Metal-organic frameworks in biomedicine. Chem Rev 2012;112(2):1232–68. https://doi.org/10.1021/cr200256v.

[47] Islamoglu T, Chen Z, Wasson MC, et al. Metal-organic frameworks against toxic chemicals. Chem Rev 2020;120(16):8130–60. https://doi.org/10.1021/acs.chemrev.9b00828.

[48] Rojas S, Horcajada P. Metal-organic frameworks for the removal of emerging organic contaminants in water. Chem Rev 2020;120(16):8378–415. https://doi.org/10.1021/acs.chemrev.9b00797.

[49] Sanz-Pérez ES, Murdock CR, Didas SA, Jones CW. Direct capture of CO2 from ambient air. Chem Rev 2016;116(19):11840–76. https://doi.org/10.1021/acs.chemrev.6b00173.

[50] Yu J, Xie LH, Li JR, Ma Y, Seminario JM, Balbuena PB. CO2 capture and separations using MOFs: computational and experimental studies. Chem Rev 2017;117(14):9674–754. https://doi.org/10.1021/acs.chemrev.6b00626.

[51] Suh MP, Park HJ, Prasad TK, Lim DW. Hydrogen storage in metal-organic frameworks. Chem Rev 2012;112(2):782–835. https://doi.org/10.1021/cr200274s.

[52] Rice AM, Martin CR, Galitskiy VA, Berseneva AA, Leith GA, Shustova NB. Photophysics modulation in photoswitchable metal-organic frameworks. Chem Rev 2020;120(16):8790–813. https://doi.org/10.1021/acs.chemrev.9b00350.

[53] Asselin P, Harvey PD. Visible-light-driven production of solar fuels catalyzed by nanosized porphyrin-based metal-organic frameworks and covalent-organic frameworks: a review. ACS Appl Nano Mater 2023. https://doi.org/10.1021/acsanm.2c00831. Published online 2022:acsanm.2c00831.

[54] Wang PL, Xie LH, Joseph EA, Li JR, Su XO, Zhou HC. Metal-organic frameworks for food safety. Chem Rev 2019;119(18):10638–90. https://doi.org/10.1021/acs.chemrev.9b00257.

[55] Wang Z, Liu L, Li Z, et al. Shaping of metal-organic frameworks: a review. Energy Fuel 2022;36(6):2927–44. https://doi.org/10.1021/acs.energyfuels.1c03426.

[56] Howarth AJ, Peters AW, Vermeulen NA, Wang TC, Hupp JT, Farha OK. Best practices for the synthesis, activation, and characterization of metal−organic frameworks. Chem Mater 2017;29(1):26–39. https://doi.org/10.1021/acs.chemmater.6b02626.

[57] Tsuruoka T, Furukawa S, Takashima Y, Yoshida K, Isoda S, Kitagawa S. Nanoporous nanorods fabricated by coordination modulation and oriented attachment growth. Angew Chem Int Ed 2009;48(26):4739–43. https://doi.org/10.1002/anie.200901177.

[58] Guo H, Zhu Y, Qiu S, Lercher AJ, Zhang H. Coordination modulation induced synthesis of nanoscale Eu 1-Tbxmetal-organic frameworks for luminescent thin films. Adv Mater 2010;22(37):4190–2. https://doi.org/10.1002/adma.201000844.

[59] Guo H, Zhu Y, Wang S, Su S, Zhou L, Zhang H. Combining coordination modulation with acid-base adjustment for the control over size of metal-organic frameworks. Chem Mater 2012;24(3):444–50. https://doi.org/10.1021/cm202593h.

[60] Wang F, Guo H, Chai Y, Li Y, Liu C. The controlled regulation of morphology and size of HKUST-1 by "coordination modulation method.". Microporous Mesoporous Mater 2013;173:181–8. https://doi.org/10.1016/j.micromeso.2013.02.023.

[61] LaMer VK, Dinegar RH. Theory, production and mechanism of formation of monodispersed hydrosols. J Am Chem Soc 1950;72(11):4847–54. https://doi.org/10.1021/ja01167a001.

[62] Ostwald W. Studien über die Bildung und Umwandlung fester Körper. Zeitschrift für Phys Chemie 1897;22U(1):289–330. https://doi.org/10.1515/zpch-1897-2233.

[63] Erdemir D, Lee AY, Myerson AS. Nucleation of crystals from solution: classical and two-step models. Acc Chem Res 2009;42(5):621–9. https://doi.org/10.1021/ar800217x.

[64] Zurek WH, Schieve WC. Multistep clustering and nucleation. J Phys Chem 1980; 84(12):1479–82. https://doi.org/10.1021/j100449a010.

[65] Millange F, Medina MI, Guillou N, Férey G, Golden KM, Walton RI. Time-resolved in situ diffraction study of the solvothermal crystallization of some prototypical metal-organic frameworks. Angew Chem Int Ed 2010;49(4):763–6. https://doi.org/10.1002/anie.200905627.

[66] Zacher D, Liu J, Huber K, Fischer RA. Nanocrystals of [Cu3(btc)2] (HKUST-1): a combined time-resolved light scattering and scanning electron microscopy study. Chem Commun 2009;9:1031. https://doi.org/10.1039/b819580c.

[67] Wang XG, Cheng Q, Yu Y, Zhang XZ. Controlled nucleation and controlled growth for size predicable synthesis of nanoscale metal-organic frameworks (MOFs): a general and scalable approach. Angew Chem Int Ed 2018;57(26):7836–40. https://doi.org/10.1002/anie.201803766.

[68] Férey G, Haouas M, Loiseau T, Taulelle F. Nanoporous solids: how do they form? An in situ approach. Chem Mater 2014;26(1):299–309. https://doi.org/10.1021/cm4019875.

[69] Cravillon J, Schröder CA, Nayuk R, Gummel J, Huber K, Wiebcke M. Fast nucleation and growth of ZIF-8 nanocrystals monitored by time-resolved in situ

small-angle and wide-angle X-ray scattering. Angew Chem Int Ed 2011;50(35):8067–71. https://doi.org/10.1002/anie.201102071.
[70] Liu X, Chee SW, Raj S, Sawczyk M, Král P, Mirsaidov U. Three-step nucleation of metal–organic framework nanocrystals. Proc Natl Acad Sci 2021;118(10). https://doi.org/10.1073/pnas.2008880118.
[71] Saha S, Springer S, Schweinefuß ME, Pontoni D, Wiebcke M, Huber K. Insight into fast nucleation and growth of zeolitic imidazolate framework-71 by in situ time-resolved light and X-ray scattering experiments. Cryst Growth Des 2016;16(4):2002–10. https://doi.org/10.1021/acs.cgd.5b01594.
[72] Lv Y, Wang S, Zhang R, Zhang D, Yu H, Lu G. PH-modulated formation of uniform MOF-5 sheets. Inorg Chem Commun 2018;97:30–3. https://doi.org/10.1016/j.inoche.2018.09.003.
[73] Cravillon J, Nayuk R, Springer S, Feldhoff A, Huber K, Wiebcke M. Controlling zeolitic imidazolate framework nano- and microcrystal formation: insight into crystal growth by time-resolved in situ static light scattering. Chem Mater 2011;23(8):2130–41. https://doi.org/10.1021/cm103571y.
[74] Pham MH, Vuong GT, Fontaine FG, Do TO. Rational synthesis of metal-organic framework nanocubes and nanosheets using selective modulators and their morphology-dependent gas-sorption properties. Cryst Growth Des 2012;12(6):3091–5. https://doi.org/10.1021/cg300297p.
[75] Seoane B, Dikhtiarenko A, Mayoral A, et al. Metal organic framework synthesis in the presence of surfactants: towards hierarchical MOFs? CrystEngComm. 2015;17(7):1693–700. https://doi.org/10.1039/c4ce02324b.
[76] Loiseau T, Lecroq L, Volkringer C, et al. MIL-96, a porous aluminum trimesate 3D structure constructed from a hexagonal network of 18-membered rings and μ3-oxo-centered trinuclear units. J Am Chem Soc 2006;128(31):10223–30. https://doi.org/10.1021/ja0621086.
[77] Volkringer C, Popov D, Loiseau T, et al. Synthesis, single-crystal X-ray microdiffraction, and NMR characterizations of the giant pore metal-organic framework aluminum trimesate MIL-100. Chem Mater 2009;21(24):5695–7. https://doi.org/10.1021/cm901983a.
[78] Haouas M, Volkringer C, Loiseau T, Férey G, Taulelle F. The extra-framework sublattice of the metal-organic framework MIL-110: a solid-state NMR investigation. Chem - A Eur J 2009;15(13):3139–46. https://doi.org/10.1002/chem.200801856.
[79] Zhao XY, Shi YS, Pang ML, Zhang WN, Li YH. Facile fabrication of Eu-1,4-NDC-fcu-MOF particles for sensing of benzidine. Main Gr Chem 2020;19(2):117–24. https://doi.org/10.3233/MGC-190848.
[80] Avci C, Ariñez-Soriano J, Carné-Sánchez A, et al. Post-synthetic anisotropic wet-chemical etching of colloidal sodalite ZIF crystals. Angew Chem Int Ed 2015;54(48):14417–21. https://doi.org/10.1002/anie.201507588.
[81] Spokoyny AM, Kim D, Sumrein A, Mirkin CA. Infinite coordination polymer nano- and microparticle structures. Chem Soc Rev 2009;38(5):1218–27. https://doi.org/10.1039/b807085g.
[82] Biemmi E, Christian S, Stock N, Bein T. High-throughput screening of synthesis parameters in the formation of the metal-organic frameworks MOF-5 and HKUST-1. Microporous Mesoporous Mater 2009;117(1–2):111–7. https://doi.org/10.1016/j.micromeso.2008.06.040.
[83] Wee LH, Bajpe SR, Janssens N, et al. Convenient synthesis of Cu3(BTC)2 encapsulated Keggin heteropolyacid nanomaterial for application in catalysis. Chem Commun 2010;46(43):8186–8. https://doi.org/10.1039/c0cc01447h.
[84] Seo YK, Hundal G, Jang IT, Hwang YK, Jun CH, Chang JS. Microwave synthesis of hybrid inorganic-organic materials including porous Cu3(BTC)2 from Cu(II)-trimesate mixture. Microporous Mesoporous Mater 2009;119(1–3):331–7. https://doi.org/10.1016/j.micromeso.2008.10.035.
[85] Campagnol N, Van Assche T, Boudewijns T, et al. High pressure, high temperature electrochemical synthesis of metal-organic frameworks: films of MIL-100 (Fe) and HKUST-1 in different morphologies. J Mater Chem A 2013;1(19):5827–30. https://doi.org/10.1039/c3ta10419b.
[86] Chowdhury P, Bikkina C, Meister D, Dreisbach F, Gumma S. Comparison of adsorption isotherms on Cu-BTC metal organic frameworks synthesized from different routes. Microporous Mesoporous Mater 2009;117(1–2):406–13. https://doi.org/10.1016/j.micromeso.2008.07.029.
[87] Yuan M, Wang R, Sun Z, et al. Morphology-controlled synthesis of Ni-MOFs with highly enhanced electrocatalytic performance for urea oxidation. Inorg Chem 2019;58(17):11449–57. https://doi.org/10.1021/acs.inorgchem.9b01124.
[88] Rodenas T, Luz I, Prieto G, et al. Metal-organic framework nanosheets in polymer composite materials for gas separation. Nat Mater 2015;14(1):48–55. https://doi.org/10.1038/nmat4113.
[89] Chui SSY, Lo SMF, Charmant JPH, Orpen AG, Williams ID. A chemically functionalizable nanoporous material [Cu3(TMA)2 (H2O)3](n). Science 1999;283(5405):1148–50. https://doi.org/10.1126/science.283.5405.1148.
[90] Alaerts L, Séguin E, Poelman H, Thibault-Starzyk F, Jacobs PA, De Vos DE. Probing the lewis acidity and catalytic activity of the metal-organic framework [Cu3(btc)2] (BTC = Benzene-1,3,5-tricarboxylate). Chem - A Eur J 2006;12(28):7353–63. https://doi.org/10.1002/chem.200600220.
[91] Vishnyakov A, Ravikovitch PI, Neimark AV, Bülow M, Wang QM. Nanopore structure and sorption properties of Cu-BTC metal-organic framework. Nano Lett 2003;3(6):713–8. https://doi.org/10.1021/nl0341281.
[92] Li X, Cheng F, Zhang S, Chen J. Shape-controlled synthesis and lithium-storage study of metal-organic frameworks Zn4O(1,3,5-benzenetribenzoate)2. J Power Sources 2006;160(1):542–7. https://doi.org/10.1016/j.jpowsour.2006.01.015.
[93] Taylor KML, Jin A, Lin W. Surfactant-assisted synthesis of nanoscale gadolinium metal-organic frameworks for potential multimodal imaging. Angew Chem Int Ed 2008;47(40):7722–5. https://doi.org/10.1002/anie.200802911.
[94] Hu Y, Dong X, Nan J, et al. Metal-organic framework membranes fabricated via reactive seeding. Chem Commun 2011;47(2):737–9. https://doi.org/10.1039/c0cc03927f.
[95] Meshram AA, Sontakke SM. Synthesis of highly stable nanoscale MIL-53 MOF and its application for the treatment of complex mixed dye solutions and real-time dye industry effluent. Sep Purif Technol 2021;274:119073. https://doi.org/10.1016/j.seppur.2021.119073.
[96] Jajko G, Gutiérrez-Sevillano JJ, Sławek A, et al. Water adsorption in ideal and defective UiO-66 structures. Microporous Mesoporous Mater 2022;330:111555. https://doi.org/10.1016/j.micromeso.2021.111555.
[97] Jajko G, Gryta P, Kozyra P, et al. Effect of synthesis temperature on water adsorption in UiO-66 derivatives: experiment, DFT+D modeling, and Monte Carlo simulations. J Phys Chem C 2022;126(21):9185–94. https://doi.org/10.1021/acs.jpcc.2c02315.
[98] Ali S, Zuhra Z, Abbas Y, Shu Y, Ahmad M, Wang Z. Tailoring defect density in UiO-66 frameworks for enhanced Pb(II) adsorption. Langmuir. 2021;37(46):13602–9. https://doi.org/10.1021/acs.langmuir.1c02032.
[99] Ma C, Guo Y, Liu H, Zhang X. Facile synthesis of bimetallic MOF crystals with controllable morphology and topology by the self-converted strategy of hydroxy double salts (HDSs). Microporous Mesoporous Mater 2021;322:111153. https://doi.org/10.1016/j.micromeso.2021.111153.
[100] Jia N, Zhang X, He W, et al. Property of YAG: Ce phosphors powder prepared by mixed solvothermal method. J Alloys Compd 2011;509(5):1848–53. https://doi.org/10.1016/j.jallcom.2010.10.071.
[101] Pichon A, Lazuen-Garay A, James SL. Solvent-free synthesis of a microporous metal-organic framework. CrystEngComm. 2006;8(3):211–4. https://doi.org/10.1039/b513750k.
[102] Kemnitz E, Mahn S, Krahl T. Nano metal fluorides: small particles with great properties. ChemTexts. 2020;6(3):19. https://doi.org/10.1007/s40828-020-00115-w.
[103] Qadir NU, Said SAM, Bahaidarah HM. Structural stability of metal organic frameworks in aqueous media - controlling factors and methods to improve hydrostability and hydrothermal cyclic stability. Microporous Mesoporous Mater 2015;201(C):61–90. https://doi.org/10.1016/j.micromeso.2014.09.034.
[104] Zhang B, Zhang J, Liu C, et al. Solvent determines the formation and properties of metal-organic frameworks. RSC Adv 2015;5(47):37691–6. https://doi.org/10.1039/c5ra02440d.
[105] Hu Z, Kundu T, Wang Y, Sun Y, Zeng K, Zhao D. Modulated hydrothermal synthesis of highly stable MOF-808(Hf) for methane storage. ACS Sustain Chem Eng 2020;8(46):17042–53. https://doi.org/10.1021/acssuschemeng.0c04486.
[106] Wang F, Zhu L, Wei Q, Wang Y. Research on the effects of hydrothermal synthesis conditions on the crystal habit of MIL-121. R Soc Open Sci 2020;7(11):201212. https://doi.org/10.1098/rsos.201212.
[107] Han Y, Fu L, Mafra L, Shi FN. Hydrothermal synthesis, crystal structures and photoluminescence properties of mixed europium-yttrium organic frameworks. J Solid State Chem 2012;186:165–70. https://doi.org/10.1016/j.jssc.2011.12.007.
[108] Rani R, Deep A, Mizaikoff B, Singh S. Enhanced hydrothermal stability of Cu MOF by post synthetic modification with amino acids. Vacuum. 2019;164:449–57. https://doi.org/10.1016/j.vacuum.2019.01.011.
[109] Haouas M, Volkringer C, Loiseau T, Férey G, Taulelle F. In situ NMR, ex situ XRD and SEM study of the hydrothermal crystallization of nanoporous aluminum trimesates MIL-96, MIL-100, and MIL-110. Chem Mater 2012;24(13):2462–71. https://doi.org/10.1021/cm300439e.
[110] Tambat SN, Sane PK, Suresh S, Varadan ON, Pandit AB, Sontakke SM. Hydrothermal synthesis of NH2-UiO-66 and its application for adsorptive removal of dye. Adv Powder Technol 2018;29(11):2626–32. https://doi.org/10.1016/j.apt.2018.07.010.
[111] Motegi H, Yano K, Setoyama N, Matsuoka Y, Ohmura T, Usuki A. A facile synthesis of UiO-66 systems and their hydrothermal stability. J Porous Mater 2017;24(5):1327–33. https://doi.org/10.1007/s10934-017-0374-5.
[112] McKinstry C, Cathcart RJ, Cussen EJ, Fletcher AJ, Patwardhan SV, Sefcik J. Scalable continuous solvothermal synthesis of metal organic framework (MOF-5) crystals. Chem Eng J 2016;285:718–25. https://doi.org/10.1016/j.cej.2015.10.023.
[113] Kamal K, Bustam MA, Ismail M, Grekov D, Shariff AM, Pré P. Optimization of washing processes in solvothermal synthesis of nickel-based mof-74. Materials (Basel) 2020;13(12):1–10. https://doi.org/10.3390/ma13122741.
[114] Hu S, Liu M, Li K, et al. Solvothermal synthesis of NH2-MIL-125(Ti) from circular plate to octahedron. CrystEngComm. 2014;16(41):9645–50. https://doi.org/10.1039/c4ce01545b.
[115] Wang CY, Gray JL, Gong Q, et al. Hydrogen storage with spectroscopic identification of chemisorption sites in Cu-TDPAT via spillover from a Pt/activated carbon catalyst. J Phys Chem C 2014;118(46):26750–63. https://doi.org/10.1021/jp507395p.
[116] Yakovenko AA, Wei Z, Wriedt M, Li JR, Halder GJ, Zhou HC. Study of guest molecules in metal-organic frameworks by powder X-ray diffraction: analysis of difference envelope density. Cryst Growth Des 2014;14(11):5397–407. https://doi.org/10.1021/cg500525g.
[117] Akhbari K, Morsali A. Effect of the guest solvent molecules on preparation of different morphologies of ZnO nanomaterials from the [Zn 2 (1,4-bdc) 2 (dabco)] metal-organic framework. J Coord Chem 2011;64(20):3521–30. https://doi.org/10.1080/00958972.2011.623778.
[118] Xiao Y, Song B, Chen Y, Cheng L, Ren Q. ZIF-67 with precursor concentration-dependence morphology for aerobic oxidation of toluene. J Organomet Chem 2020;930:121597. https://doi.org/10.1016/j.jorganchem.2020.121597.

[119] Gascon J, Aguado S, Kapteijn F. Manufacture of dense coatings of Cu3(BTC)2 (HKUST-1) on α-alumina. Microporous Mesoporous Mater 2008;113(1–3):132–8. https://doi.org/10.1016/j.micromeso.2007.11.014.
[120] Marx S, Kleist W, Baiker A. Synthesis, structural properties, and catalytic behavior of cu-BTC and mixed-linker Cu-BTC-PyDC in the oxidation of benzene derivatives. J Catal 2011;281(1):76–87. https://doi.org/10.1016/j.jcat.2011.04.004.
[121] Ameloot R, Vermoortele F, Vanhove W, Roeffaers MBJ, Sels BF, De Vos DE. Interfacial synthesis of hollow metal organic framework capsules demonstrating selective permeability. Nat Chem 2011;3(5):382–7. https://doi.org/10.1038/nchem.1026.
[122] Khan NA, Jhung SH. Facile syntheses of metal-organic framework Cu3(BTC)2 (H2O)3 under ultrasound. Bull Korean Chem Soc 2009;30(12):2921–6. https://doi.org/10.5012/bkcs.2009.30.12.2921.
[123] Liu J, Yang J, An S, et al. Synthesis and electromagnetic properties of NH2-MIL-88B(Fe) crystals with morphology and size controllable through synergistic effects of surfactant and water. J Mater Sci Mater Electron 2022;33(17):14228–39. https://doi.org/10.1007/s10854-022-08351-1.
[124] Mazaj M, Birsa Čelič T, Mali G, Rangus M, Kaučič V, Zabukovec Logar N. Control of the crystallization process and structure dimensionality of Mg-benzene-1,3,5-tricarboxylates by tuning solvent composition. Cryst Growth Des 2013;13(8):3825–34. https://doi.org/10.1021/cg400929z.
[125] Wang Z, Guo X, Dou W, et al. High supercapacitive performances of Cu-MOFs dominated by morphologies: effects of solvents, surfactants and concentrations. J Solid State Chem 2020;289:121452. https://doi.org/10.1016/j.jssc.2020.121452.
[126] Lee YR, Jang MS, Cho HY, Kwon HJ, Kim S, Ahn WS. ZIF-8: a comparison of synthesis methods. Chem Eng J 2015;271:276–80. https://doi.org/10.1016/j.cej.2015.02.094.
[127] Bustamante EL, Fernández JL, Zamaro JM. Influence of the solvent in the synthesis of zeolitic imidazolate framework-8 (ZIF-8) nanocrystals at room temperature. J Colloid Interface Sci 2014;424:37–43. https://doi.org/10.1016/j.jcis.2014.03.014.
[128] Zhou X, Liu P, Huang WH, Kang M, Wang YY, Shi QZ. Solvents influence on sizes of channels in three fry topological Mn(ii)-MOFs based on metal-carboxylate chains: syntheses, structures and magnetic properties. CrystEngComm. 2013;15(40):8125–32. https://doi.org/10.1039/c3ce41120f.
[129] Huang WH, Luan XJ, Zhou X, Chen J, Wang YY, Shi QZ. The influence of ligand configuration, solvent size and solvent polarity on the porous shape and void volume in a series of isomeric or isomorphic porous MOFs. CrystEngComm. 2013;15(47):10389–98. https://doi.org/10.1039/c3ce41801d.
[130] Schejn A, Balan L, Falk V, Aranda L, Medjahdi G, Schneider R. Controlling ZIF-8 nano- and microcrystal formation and reactivity through zinc salt variations. CrystEngComm. 2014;16(21):4493–500. https://doi.org/10.1039/c3ce42485e.
[131] Colwell KA, Jackson MN, Torres-Gavosto RM, et al. Buffered coordination modulation as a Means of controlling crystal morphology and molecular diffusion in an anisotropic metal–organic framework. J Am Chem Soc 2021;143(13):5044–52. https://doi.org/10.1021/jacs.1c00136.
[132] He S, Li Z, Wang J. Bimetallic MOFs with tunable morphology: synthesis and enhanced lithium storage properties. J Solid State Chem 2022;307:122726. https://doi.org/10.1016/j.jssc.2021.122726.
[133] Suresh K, Aulakh D, Purewal J, Siegel DJ, Veenstra M, Matzger AJ. Optimizing hydrogen storage in MOFs through engineering of crystal morphology and control of crystal size. J Am Chem Soc 2021;143(28):10727–34. https://doi.org/10.1021/jacs.1c04926.
[134] Suresh K, Kalenak AP, Sotuyo A, Matzger AJ. Metal-organic framework (MOF) morphology control by design. Chem – A Eur J 2022;28(18). https://doi.org/10.1002/chem.202200334.
[135] Gao R, Zhang G, Ru X, et al. Morphology control of metal-organic frameworks by co-competitive coordination strategy for low-temperature selective catalytic reduction of NO with NH3. J Solid State Chem 2021;297:122031. https://doi.org/10.1016/j.jssc.2021.122031.
[136] Song T, Gao F, Guo S, et al. A review of the role and mechanism of surfactants in the morphology control of metal nanoparticles. Nanoscale. 2021;13(7):3895–910. https://doi.org/10.1039/d0nr07339c.
[137] Yang TH, Shi Y, Janssen A, Xia Y. Surface capping agents and their roles in shape-controlled synthesis of colloidal metal nanocrystals. Angew Chem Int Ed 2020;59(36):15378–401. https://doi.org/10.1002/anie.201911135.
[138] Pan Y, Heryadi D, Zhou F, et al. Tuning the crystal morphology and size of zeolitic imidazolate framework-8 in aqueous solution by surfactants. CrystEngComm. 2011;13(23):6937–40. https://doi.org/10.1039/c1ce05780d.
[139] Phan NTS, Le KKA, Phan TD. MOF-5 as an efficient heterogeneous catalyst for Friedel-Crafts alkylation reactions. Appl Catal Gen 2010;382(2):246–53. https://doi.org/10.1016/j.apcata.2010.04.053.
[140] Qiu LG, Xu T, Li ZQ, et al. Hierarchically micro- and mesoporous metal-organic frameworks with tunable porosity. Angew Chem Int Ed 2008;47(49):9487–91. https://doi.org/10.1002/anie.200803640.
[141] Cai X, Lin J, Pang M. Facile synthesis of highly uniform Fe-MIL-88B particles. Cryst Growth Des 2016;16(7):3565–8. https://doi.org/10.1021/acs.cgd.6b00313.
[142] Ying Y, Khezri B, Kosina J, Pumera M. Reconstructed bismuth-based metal−organic framework nanofibers for selective CO2-to-formate conversion: morphology engineering. ChemSusChem. 2021;14(16):3402–12. https://doi.org/10.1002/cssc.202101122.
[143] Yang JM, Liu Q, Kang YS, Sun WY. Controlled growth and gas sorption properties of IRMOF-3 nano/microcrystals. Dalton Trans 2014;43(44):16707–12. https://doi.org/10.1039/c4dt02429j.
[144] Kukulka W, Cendrowski K, Michalkiewicz B, Mijowska E. MOF-5 derived carbon as material for CO2 absorption. RSC Adv 2019;9(32):18527–37. https://doi.org/10.1039/c9ra01786k.
[145] Ma M, Zacher D, Zhang X, Fischer RA, Metzler-Nolte N. A method for the preparation of highly porous, nanosized crystals of isoreticular metal-organic frameworks. Cryst Growth Des 2011;11(1):185–9. https://doi.org/10.1021/cg101130m.
[146] Zheng G, Chen Z, Sentosun K, et al. Shape control in ZIF-8 nanocrystals and metal nanoparticles@ZIF-8 heterostructures. Nanoscale. 2017;9(43):16645–51. https://doi.org/10.1039/c7nr03739b.
[147] Cravillon J, Schröder CA, Bux H, Rothkirch A, Caro J, Wiebcke M. Formate modulated solvothermal synthesis of ZIF-8 investigated using time-resolved in situ X-ray diffraction and scanning electron microscopy. CrystEngComm. 2012;14(2):492–8. https://doi.org/10.1039/c1ce06002c.
[148] Zhang Y, Sun T, Zhang P, Liu K, Li F, Xu L. Synthesizing MOF-derived Ni N C catalyst via surfactant modified strategy for efficient electrocatalytic CO2 to CO. J Colloid Interface Sci 2023;631:96–101. https://doi.org/10.1016/j.jcis.2022.10.146.
[149] Umemura A, Diring S, Furukawa S, Uehara H, Tsuruoka T, Kitagawa S. Morphology design of porous coordination polymer crystals by coordination modulation. J Am Chem Soc 2011;133(39):15506–13. https://doi.org/10.1021/ja204233q.
[150] Wang S, Lv Y, Yao Y, Yu H, Lu G. Modulated synthesis of monodisperse MOF-5 crystals with tunable sizes and shapes. Inorg Chem Commun 2018;93:56–60. https://doi.org/10.1016/j.inoche.2018.05.010.
[151] Yang P, Meng X, Guo P, et al. Highly selective separation of C3H6/C3H8 within hierarchical metal–organic CuxOy@HP–Cu–BTCs. Mater Chem Phys 2023;294:127024. https://doi.org/10.1016/j.matchemphys.2022.127024.
[152] Wu YN, Zhou M, Zhang B, et al. Amino acid assisted templating synthesis of hierarchical zeolitic imidazolate framework-8 for efficient arsenate removal. Nanoscale. 2014;6(2):1105–12. https://doi.org/10.1039/c3nr04390h.
[153] Hu L, Yan Z, Mo X, Peng X, Chen L. Morphology control synthesis of ZIF-8 as highly efficient catalyst for the cycloaddition of CO2 to cyclic carbonate. ChemCatChem. 2019;11(14):3212–9. https://doi.org/10.1002/cctc.201900735.
[154] Hatakeyama W, Sanchez TJ, Rowe MD, Serkova NJ, Liberatore MW, Boyes SG. Synthesis of gadolinium nanoscale metal-organic framework with hydrotropes: manipulation of particle size and magnetic resonance imaging capability. ACS Appl Mater Interfaces 2011;3(5):1502–10. https://doi.org/10.1021/am200075q.
[155] Ding LG, Yao BJ, Jiang WL, et al. Bifunctional imidazolium-based ionic liquid decorated UiO-67 type MOF for selective CO2 adsorption and catalytic property for CO2 cycloaddition with epoxides. Inorg Chem 2017;56(4):2337–44. https://doi.org/10.1021/acs.inorgchem.6b03169.
[156] Rodrigues RK, Da Silva MA, Sabadini E. Worm-like micelles of CTAB and sodium salicylate under turbulent flow. Langmuir. 2008;24(24):13875–9. https://doi.org/10.1021/la802890x.
[157] Lin R, Ge L, Diao H, Rudolph V, Zhu Z. Ionic liquids as the MOFs/polymer interfacial binder for efficient membrane separation. ACS Appl Mater Interfaces 2016;8(46):32041–9. https://doi.org/10.1021/acsami.6b11074.
[158] Cao X, qiang, Wang X, Chen M, Xiao F, Huang Y meng, Lyu X jun.. Synthesis of nanoscale zeolitic imidazolate framework-8 (ZIF-8) using reverse micro-emulsion for Congo red adsorption. Sep Purif Technol 2021;260:118062. https://doi.org/10.1016/j.seppur.2020.118062.
[159] Wang Y, Xu Y, Li D, et al. Ionothermal synthesis of zeolitic imidazolate frameworks and the synthesis dissolution-crystallization mechanism. Chin J Catal 2015;36(6):855–65. https://doi.org/10.1016/S1872-2067(14)60278-3.
[160] Yang HM, Song XL, Yang TL, Liang ZH, Fan CM, Hao XG. Electrochemical synthesis of flower shaped morphology MOFs in an ionic liquid system and their electrocatalytic application to the hydrogen evolution reaction. RSC Adv 2014;4(30):15720–6. https://doi.org/10.1039/c3ra47744d.
[161] Huang C, Su X, Zhang D, Gu X, Liu R, Zhu H. Co-MOF nanocatalysts of tunable shape and size for selective aerobic oxidation of toluene. Inorg Chim Acta 2020;510:119737. https://doi.org/10.1016/j.ica.2020.119737.
[162] Sezginel KB, Keskin S, Uzun A. Tuning the gas separation performance of CuBTC by ionic liquid incorporation. Langmuir. 2016;32(4):1139–47. https://doi.org/10.1021/acs.langmuir.5b04123.
[163] Yang HM, Liu X, Song XL, Yang TL, Liang ZH, Fan CM. In situ electrochemical synthesis of MOF-5 and its application in improving photocatalytic activity of BiOBr. Trans Nonferrous Met Soc China (English Ed) 2015;25(12):3987–94. https://doi.org/10.1016/S1003-6326(15)64047-X.
[164] Singh A, Vedarajan R, Matsumi N. Modified metal organic frameworks (MOFs)/ionic liquid matrices for efficient charge storage. J Electrochem Soc 2017;164(8):H5169–74. https://doi.org/10.1149/2.0191708jes.
[165] Kang X, Zhu Q, Sun X, et al. Highly efficient electrochemical reduction of CO_2 to CH_4 in an ionic liquid using a metal-organic framework cathode. Chem Sci 2016;7(1):266–73. https://doi.org/10.1039/c5sc03291a.
[166] Xue WL, Deng WH, Chen H, et al. MOF-directed synthesis of crystalline ionic liquids with enhanced proton conduction. Angew Chem Int Ed 2021;60(3):1290–7. https://doi.org/10.1002/anie.202010783.
[167] Xu Q, Zhang X, Zeng S, Bai L, Zhang S. Ionic liquid incorporated metal organic framework for high ionic conductivity over extended temperature range. ACS Sustain Chem Eng 2019;7(8):7892–9. https://doi.org/10.1021/acssuschemeng.9b00543.
[168] Koyuturk B, Altintas C, Kinik FP, Keskin S, Uzun A. Improving gas separation performance of ZIF-8 by [BMIM][BF4] incorporation: interactions and their consequences on performance. J Phys Chem C 2017;121(19):10370–81. https://doi.org/10.1021/acs.jpcc.7b00848.

[169] da Trindade LG, Borba KMN, Zanchet L, et al. SPEEK-based proton exchange membranes modified with MOF-encapsulated ionic liquid. Mater Chem Phys 2019;236:121792. https://doi.org/10.1016/j.matchemphys.2019.121792.
[170] Liu C, Zhang B, Zhang J, et al. Gas promotes the crystallization of nano-sized metal-organic frameworks in ionic liquid. Chem Commun 2015;51(57):11445–8. https://doi.org/10.1039/c5cc02503f.
[171] Xu Z, Zhao G, Ullah L, et al. Acidic ionic liquid based UiO-67 type MOFs: a stable and efficient heterogeneous catalyst for esterification. RSC Adv 2018;8(18): 10009–16. https://doi.org/10.1039/c8ra01119b.
[172] Lu CM, Liu J, Xiao K, Harris AT. Microwave enhanced synthesis of MOF-5 and its CO2 capture ability at moderate temperatures across multiple capture and release cycles. Chem Eng J 2010;156(2):465–70. https://doi.org/10.1016/j.cej.2009.10.067.
[173] Sabouni R, Kazemian H, Rohani S. A novel combined manufacturing technique for rapid production of IRMOF-1 using ultrasound and microwave energies. Chem Eng J 2010;165(3):966–73. https://doi.org/10.1016/j.cej.2010.09.036.
[174] Gedanken A. Using sonochemistry for the fabrication of nanomaterials. Ultrason Sonochem 2004;11(2):47–55. https://doi.org/10.1016/j.ultsonch.2004.01.037.
[175] Hwang YK, Chang JS, Park SE, et al. Microwave fabrication of MFI zeolite crystals with a fibrous morphology and their applications. Angew Chem Int Ed 2005;44 (4):556–60. https://doi.org/10.1002/anie.200461403.
[176] Cho HY, Yang DA, Kim J, Jeong SY, Ahn WS. CO 2 adsorption and catalytic application of Co-MOF-74 synthesized by microwave heating. Catal Today 2012; 185(1):35–40. https://doi.org/10.1016/j.cattod.2011.08.019.
[177] Sarawade P, Tan H, Polshettiwar V. Shape- and morphology-controlled sustainable synthesis of Cu, Co, and in metal organic frameworks with high CO2 capture capacity. ACS Sustain Chem Eng 2013;1(1):66–74. https://doi.org/10.1021/sc300036p.
[178] Xu X, Lu Y, Yang Y, Nosheen F, Wang X. Tuning the growth of metal-organic framework nanocrystals by using polyoxometalates as coordination modulators. Sci China Mater 2015;58(5):370–7. https://doi.org/10.1007/s40843-015-0053-2.
[179] Tajnšek TK, Zabukovec Logar N, Mazaj M. Tuning size and properties of zinc ascorbate metal-organic framework via acid modulation. Molecules. 2022;28(1): 253. https://doi.org/10.3390/molecules28010253.
[180] Mao W, Huang R, Xu H, et al. Effects of acid modulators on the microwave-assisted synthesis of Cr/Sn metal-organic frameworks. Polymers (Basel) 2022;14 (18):3826. https://doi.org/10.3390/polym14183826.
[181] Ma M, Bétard A, Weber I, Al-Hokbany NS, Fischer RA, Metzler-Nolte N. Iron-based metal-organic frameworks MIL-88B and NH2-MIL-88B: high quality microwave synthesis and solvent-induced lattice "breathing.". Cryst Growth Des 2013;13(6):2286–91. https://doi.org/10.1021/cg301738p.
[182] Liu H, Zhao Y, Zhou C, Mu B, Chen L. Microwave-assisted synthesis of Zr-based metal–organic framework (Zr-fum-fcu-MOF) for gas adsorption separation. Chem Phys Lett 2021;780:138906. https://doi.org/10.1016/j.cplett.2021.138906.
[183] Shen M, Zhou J, Elhadidy M, et al. Cyclodextrin metal–organic framework by ultrasound-assisted rapid synthesis for caffeic acid loading and antibacterial application. Ultrason Sonochem 2022;86:106003. https://doi.org/10.1016/j.ultsonch.2022.106003.
[184] Son WJ, Kim J, Kim J, Ahn WS. Sonochemical synthesis of MOF-5. Chem Commun 2008;47:6336–8. https://doi.org/10.1039/b814740j.
[185] Li ZQ, Qiu LG, Wang W, Xu T, Wu Y, Jiang X. Fabrication of nanosheets of a fluorescent metal-organic framework [Zn(BDC)(H2O)]n (BDC = 1,4-benzenedicarboxylate): ultrasonic synthesis and sensing of ethylamine. Inorg Chem Commun 2008;11(11):1375–7. https://doi.org/10.1016/j.inoche.2008.09.010.
[186] Jung DW, Yang DA, Kim J, Kim J, Ahn WS. Facile synthesis of MOF-177 by a sonochemical method using 1-methyl-2-pyrrolidinone as a solvent. Dalton Trans 2010;39(11):2883–7. https://doi.org/10.1039/b925088c.
[187] Al-Attri R, Halladj R, Askari S. Green route of flexible Al-MOF synthesis with superior properties at low energy consumption assisted by ultrasound waves. Solid State Sci 2022;123:106782. https://doi.org/10.1016/j.solidstatesciences.2021.106782.
[188] Abdolalian P, Morsali A, Tizhoush SK. Sono-synthesis of basic metal-organic framework for reusable catalysis of organic reactions in the eco-friendly conditions. J Solid State Chem 2021;303:122525. https://doi.org/10.1016/j.jssc.2021.122525.
[189] Vaitsis C, Kanellou E, Pandis PK, et al. Sonochemical synthesis of zinc adipate metal-organic framework (MOF) for the electrochemical reduction of CO2: MOF and circular economy potential. Sustain Chem Pharm 2022;29:100786. https://doi.org/10.1016/j.scp.2022.100786.
[190] Ahmed I, Lee HJ, Jhung SH. A Tb-based-metal–organic framework prepared under ultrasound for detection of organic amines in aqueous solution through fluorescence quenching. J Mol Liq 2021;344:117765. https://doi.org/10.1016/j.molliq.2021.117765.